Available online at www.sciencedirect.com

SciVerse ScienceDirect

Geochimica et Cosmochimica Acta 84 (2012) 459–491

Geochimica et Cosmochimica Acta

www.elsevier.com/locate/gca

# Along and across arc geochemical variations in NW Central America: Evidence for involvement of lithospheric pyroxenite

Ken Heydolph [a,*], Kaj Hoernle [a,b], Folkmar Hauff [b], Paul van den Bogaard [a,b], Maxim Portnyagin [b], Ilya Bindeman [c], Dieter Garbe-Schönberg [d]

[a] *Sonderforschungsbereich 574, University of Kiel, Wischhofstr. 1-3, D-24148 Kiel, Germany*
[b] *Leibniz-Institut für Meereswissenschaften IFM-GEOMAR, Wischhofstr. 1-3, D-24148 Kiel, Germany*
[c] *Department of Geological Sciences, 1272 University of Oregon, Eugene, OR 97403, USA*
[d] *Institut für Geowissenschaften der Universität Kiel, Olshausenstrasse 40, 24148 Kiel, Germany*

Received 29 March 2011; accepted in revised form 23 January 2012; available online 4 February 2012

**Abstract**

The Central American Volcanic Arc (CAVA) has been the subject of intensive research over the past few years, leading to a variety of distinct models for the origin of CAVA lavas with various source components. We present a new model for the NW Central American Volcanic Arc based on a comprehensive new geochemical data set (major and trace element and Sr–Nd–Pb–Hf–O isotope ratios) of mafic volcanic front (VF), behind the volcanic front (BVF) and back-arc (BA) lava and tephra samples from NW Nicaragua, Honduras, El Salvador and Guatemala. Additionally we present data on subducting Cocos Plate sediments (from DSDP Leg 67 Sites 495 and 499) and igneous oceanic crust (from DSDP Leg 67 Site 495), and Guatemalan (Chortis Block) granitic and metamorphic continental basement. We observe systematic variations in trace element and isotopic compositions both along and across the arc. The data require at least three different endmembers for the volcanism in NW Central America. (1) The NW Nicaragua VF lavas require an endmember with very high Ba/(La, Th) and U/Th, relatively radiogenic Sr, Nd and Hf but unradiogenic Pb and low $\delta^{18}O$, reflecting a largely serpentinite-derived fluid/hydrous melt flux from the subducting slab into a depleted N-MORB type of mantle wedge. (2) The Guatemala VF and BVF mafic lavas require an enriched endmember with low Ba/(La, Th), U/Th, high $\delta^{18}O$ and radiogenic Sr and Pb but unradiogenic Nd and Hf isotope ratios. Correlations of Hf with both Nd and Pb isotopic compositions are not consistent with this endmember being subducted sediments. Granitic samples from the Chiquimula Plutonic Complex in Guatemala have the appropriate isotopic composition to serve as this endmember, but the large amounts of assimilation required to explain the isotope data are not consistent with the basaltic compositions of the volcanic rocks. In addition, mixing regressions on Nd vs. Hf and the Sr and O isotope plots do not go through the data. Therefore, we propose that this endmember could represent pyroxenites in the lithosphere (mantle and possibly lower crust), derived from parental magmas for the plutonic rocks. (3) The Honduras and Caribbean BA lavas define an isotopically depleted endmember (with unradiogenic Sr but radiogenic Nd, Hf and Pb isotope ratios), having OIB-like major and trace element compositions (e.g. low Ba/(La, Th) and U/Th, high La/Yb). This endmember is possibly derived from melting of young, recycled oceanic crust in the asthenosphere upwelling in the back-arc. Mixing between these three endmember types of magmas can explain the observed systematic geochemical variations along and across the NW Central American Arc.


* Corresponding author.
*E-mail address:* kheydolph@geomar.de (K. Heydolph).

0016-7037/$ - see front matter © 2012 Elsevier Ltd. All rights reserved.
doi:10.1016/j.gca.2012.01.035

## 1. INTRODUCTION

Subduction zones mark the sites where an oceanic plate is subducted beneath an oceanic or continental plate, transferring lithospheric material back into the Earth's mantle. The release of fluids or hydrous melts from the subducting slab causes partial melting in the mantle wedge resulting in arc volcanism. Therefore samples from arc volcanoes provide detailed information on various geochemically distinct source components contributing to subduction-related arc volcanism (e.g. subducting plate, mantle wedge and overlying crust).

Along the Central American subduction zone, where the Cocos Plate subducts beneath the Caribbean Plate, there are systematic variations in tectonic parameters, such as the subduction angle, thickness of the lithosphere and crust of the over-riding plate and the composition of both the subducting Cocos Plate and the crust of the over-riding Caribbean Plate (e.g. Carr, 1984; Patino et al., 2000; Carr and Feigenson, 2003; Rüpke et al., 2004; Auger et al., 2006; Syracuse and Abers, 2006; Abers et al., 2007; Hoernle et al., 2008; MacKenzie et al., 2008). An exceptionally broad geochemical database for Central American volcanism has led to a large number of, in some cases conflicting, models for the generation of Central American arc volcanism, invoking a combination of diverse tectonic parameters, varying crustal compositions and potential source components.

### 1.1. Overview of previous work

Below we summarize the previous work and models proposed to explain geochemical variations along and across the arc in Central America.

Carr et al. (1990) argued that Sr and Nd isotopic ratios of Central American volcanic rocks can be explained by mixing of four components: marine sediments from DSDP Site 495, MORB-source mantle (DM), EMORB-source mantle (EM) and continental crust. Mixing between DM and less than 0.5% marine sediments or fluids, form a modified mantle (MM) component. Most of the isotopic data form a trend between EM and MM, which is also well defined in the incompatible-element data e.g. Ba/La vs. La/Yb.

Feigenson and Carr (1993) used inverse modeling to calculate rare earth element patterns of Central American lava sources. Guatemalan and Costa Rican sources display high modal garnet contents and moderate-to-strong light rare earth element (LREE) enrichment, whereas Nicaraguan sources are defined by a slight LREE depletion and little to no modal garnet in the residuum. They propose that a broadly homogeneous but locally heterogeneous mantle wedge could contain relatively enriched small-sized garnet-bearing veins surrounded by an isotopically depleted mantle peridotite matrix. Melting of distinct sources can be explained by the varying dip of the subducting lithosphere beneath the volcanic arc, which causes varying amounts of flux melting beneath the different arc segments.

Leeman (1996) and Leeman et al. (1994) showed systematic along-arc variations in B/La ratio and strong correlations between B/La and $^{10}Be/^{9}Be$ ratios. They proposed that a decrease in B/La and $^{10}Be/^{9}Be$ ratios along the volcanic front from Nicaragua to Guatemala reflect a decreasing subduction (sediments and igneous crust) contribution to arc magma sources toward Guatemala. Using lithium concentrations and isotopic compositions and their strong correlations with other fluid–mobile elements (e.g. B, $^{10}Be$, U, $^{87}Sr/^{86}Sr$, LILE) from basaltic Central American Volcanic Arc lavas, Chan and Kastner (2000) and Chan et al. (1999, 2002, 2006) provided more evidence for subduction-related modification of subarc mantle by slab-derived fluids. They argued that the low $\delta^{6}Li$ values for the fluids overlap with altered oceanic crust and marine sediment compositions and that Li and Sr isotopic systematics can be explained by small additions of fluids from these sources to depleted or enriched mantle sources for the CAVA magmas.

Patino et al. (2000) used incompatible trace element ratios to demonstrate the role of two different Cocos Plate sediment units (i.e. carbonate and hemipelagic) on both local and regional geochemical variations in Central American arc lavas. Local geochemical variations in all arc segments, defined by trace element ratios with large differences between the stratigraphic units (e.g. Ba/Th and U/La), are a result of the relative variation in the amount of hemipelagic to carbonate sediment input into the magma generation process and in the flux of hydrous fluids (e.g. Ba/La and U/Th) from the altered oceanic crust and sediments of the subducting slab. In summary, the slab signal is strongest in the Nicaragua volcanic front lavas and decreases to the northwest and southeast along the volcanic arc and into the back arc.

Based on Sr–Nd–Pb isotope data, Feigenson et al. (2004) suggested that a combination of crustal contamination and subducted Cocos Plate sediments contribute to the Guatemalan and Honduran magmas. Using oxygen isotope data, Eiler et al. (2005) also argued that partial melts of subducted Cocos Plate sediments contribute to Guatemalan magma sources, whereas dehydration of hydrothermally-altered rocks and/or serpentinites contribute to central Nicaraguan magma sources. Walker et al. (2007) linked variations in uranium and thorium disequilibria to crustal contamination of mafic central Guatemalan lavas but proposed that Nicaraguan magmas contain a maximum contribution of subducted Cocos Plate sediments, consistent with the high $^{10}Be/^{9}Be$ isotope ratios in the central Nicaraguan lavas (Morris et al., 1990).

Sadofsky et al. (2008) reported large heterogeneity of CAVA magma sources on local and regional scales using olivine melt inclusion compositions (i.e. major and trace elements and volatile components) from CAVA samples from Guatemala to Costa Rica. They relate these variations to variable contributions of various crustal and mantle components involved in magma genesis. Correlations of water and major and trace elements (e.g. Ti, Y and Na) and trace element ratios (e.g. Ba/La, B/La) indicate melting in the mantle wedge, fluxed by Ba-, B- and $H_2O$-rich, possibly serpentinite-derived, fluids, in particular beneath the central (Nicaraguan) part of the arc. On the other hand, components with melt-like properties, e.g. high Cl, S, F,

LREE and La/Nb seem to control Guatemalan and Costa Rican magma generation.

Hoernle et al. (2008) argued, based on Pb and Nd isotopic and incompatible trace element (Ba/La and La/Yb), that a component with melt-like properties, derived from the subducting seamount province of the Galapagos hotspot track, is being added to the mantle wedge beneath Central Costa Rica. Systematic variations in isotopic composition of volcanic front volcanoes and arc-parallel seismic velocity anisotropy in the mantle wedge were interpreted to reflect northwestward flow of mantle from beneath Central Costa Rica to northwesternmost Nicaragua. Transfer of material from the slab beneath Nicaragua was interpreted to occur primarily through hydrous fluids derived from the subducting oceanic crust and/or serpentinites in the down-going slab ± small amounts of sediment melting. Using trace element modeling, Gazel et al. (2009) also demonstrated that the Galapagos hotspot contribution decreases systematically along the volcanic front from central Costa Rica to NW Nicaragua and that small amounts of sediment melts ($\leqslant$0.6 wt.%) also contribute to the trace element signatures.

In this study, we present a comprehensive, new geochemical (major and trace elements and Sr–Nd–Pb–Hf–O isotope ratios) data set, in order to evaluate the different models for the origin of mafic VF and BVF lava and tephra samples from volcanic centers along and across the Central American Volcanic Arc in Guatemala through El Salvador and Honduras to NW-Nicaragua. We note that our study is the first to present Hf isotope data from Central America. Our data confirm systematic along- and across-arc variations in isotopic compositions and major and trace elements (e.g. Carr et al., 1990; Feigenson and Carr, 1993; Carr and Feigenson, 2003; Feigenson et al., 2004; Sadofsky et al., 2008). We also present new geochemical data from potential geochemical endmembers in the Central American subduction system: subducting Cocos Plate sediments (from DSDP Leg 67 Sites 495 and 499), igneous oceanic crust (from DSDP Leg 67 Site 495) and Guatemalan (Chortis Block) continental basement (granitic and metamorphic). Combined, our extensive new geochemical datasets for volcanic rocks and subduction zone endmembers allow us to place further strong constraints on the sources involved in magma generation beneath northwestern Central America, allowing us to rule out some of the previous models and to propose some new models for the origin of the here suggested endmembers.

### 1.2. Geological overview

Subduction of the Cocos Plate beneath the Central America (Caribbean Plate) creates a chain of volcanoes extending for more than 1400 km from Tacaná Volcano near the Guatemalan–Mexican border to western Panama (Fig. 1). These subduction-related volcanic centers can be divided according to their relative location at the volcanic arc into volcanic front (VF) centers – making up the main chain of volcanoes – and generally smaller behind the volcanic front (BVF) volcanic centers (Carr, 1984), up to 350 km from the trench. Several back-arc volcanic centers (BA) occur in Honduras (e.g. Yojoa and Utila Island) at a distance of 350–520 km from the trench. An extensive overview of the Central American geology can be found in e.g. Auboin et al. (1982), Carr et al. (1990, 2003), and Protti et al. (1995). Below we summarize the Central American geology pertinent to this study.

In this paper, we concentrate on Quaternary subduction-related volcanism in the northwestern part of Central America, extending along the volcanic front from Momotombo Volcano in northwest Nicaragua to Santa Maria Volcano in northwest Guatemala to Utila Island (Caribbean) in the back-arc (Fig. 1). The Cocos Plate, generated at the East Pacific Rise, is subducting at a rate of $74 \pm 5$ mm/y and has a dip angle of ~48° offshore Guatemala. The rate of subduction increases to $84 \pm 5$ mm/y and the dip of the slab increases to ~64° offshore Nicaragua (Fig. 1) (DeMets, 2001). The age (~25 Ma; Protti et al., 1995) of the subducting Cocos Plate outboard of NW Nicaragua to Guatemala is similar, suggesting a similar subduction input for this part of the subduction system. The sediment input, which has been well-defined at Deep Sea Drilling Project (DSDP) Site 495 (Fig. 1), can be divided into a lower, ~250 m thick, unit of carbonate ooze and an overlying, ~200 m thick, unit of hemipelagic clay (Auboin et al., 1982; Plank and Langmuir, 1998; Patino et al., 2000; Sadofsky et al., 2008). The composition of the igneous portion of the Cocos Plate outboard of Guatemala is characterized by samples from Site 495 (in this study and Geldmacher et al., 2008) and outboard of Nicaragua by drill (Site 1256; Sadofsky et al., 2009) and dredge samples (from an off-axis seamount; Werner et al., 2003). The upper oceanic lithospheric mantle appears to be extensively serpentinized, most likely due to the presence of bend faults cutting through the entire crust into the upper mantle (Abers et al., 2003; Ranero et al., 2003; Rüpke et al., 2004; Grevemeyer et al., 2007; Ivandic et al., 2008; Syracuse et al., 2008). The subduction margin along the Pacific margin of Central America has been shown to be erosional (Ranero and Huene von, 2000; Vanucchi et al., 2001; Vannucchi et al., 2004). The forearc from Guatemala to NW Costa Rica consists of accreted intraplate and older arc assemblages (Hauff et al., 2000; Hoernle and Hauff, 2007; Geldmacher et al., 2008).

The composition of the overlying Caribbean Plate beneath the volcanic arc (Chortis Block) is variable, ranging from accreted oceanic igneous complexes beneath the VF in Nicaragua to continental crust beneath the Guatemala VF and the BVF regions in El Salvador, Honduras and Guatemala (Fig. 1). In Central Guatemala, the Motagua-Polochic transform fault system, a 110 Ma old convergence zone, marks the transition from the Caribbean Plate (Chortis Block) to the North-American Plate (Maya Block) (Fig. 1) (e.g. Donnelly et al., 1990; Meschede, 1998). The overlying crustal thickness increases from ~25 km beneath the Nicaraguan VF to ~46 km beneath the Guatemalan VF and with increasing distance behind the VF, for example to ~46 km in the Nicaragua back-arc (e.g. Ligorria and Molina, 1997; Narcía-Lopez et al., 2004; Auger et al., 2006; MacKenzie et al., 2008).

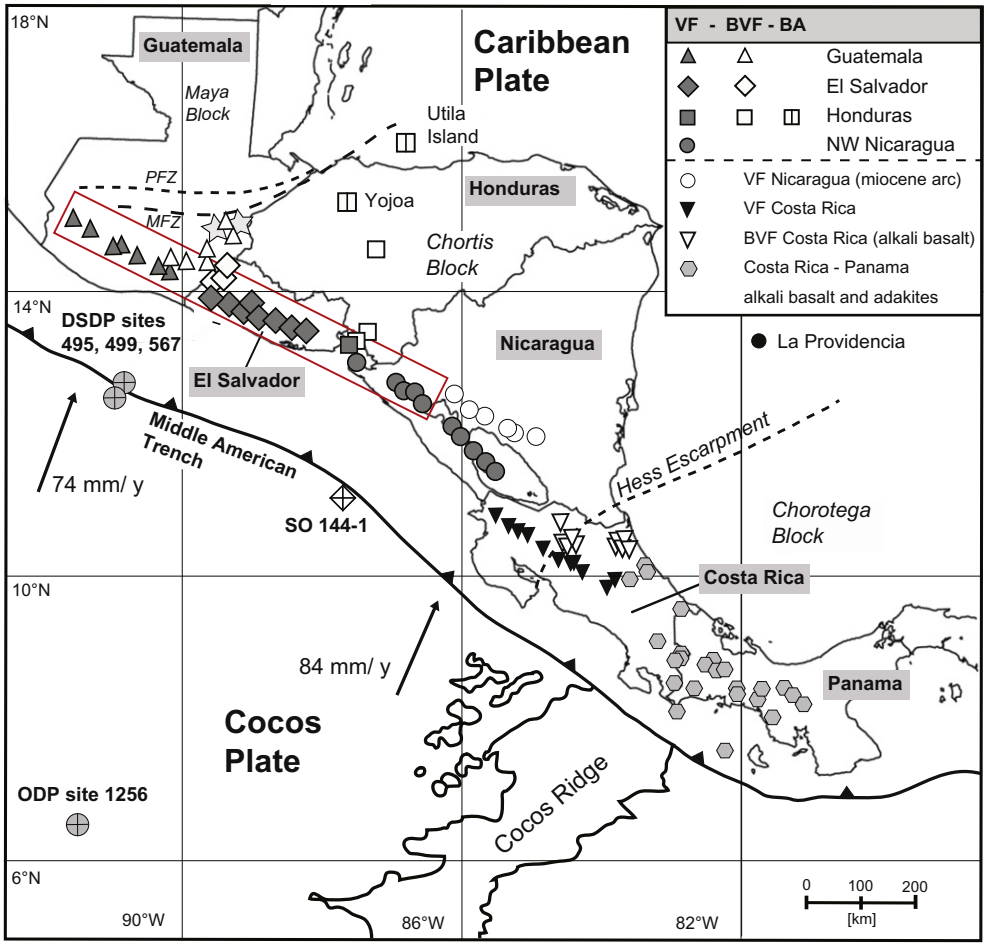


Fig. 1. Overview map of Central America, showing the subduction of the Cocos Plate beneath the Caribbean Plate. Black arrows indicate direction of Cocos Plate motion and relative velocities to the Caribbean Plate (in mm per year) after DeMets (2001). Solid/shaded symbols mark volcanic front (VF) volcanoes (rectangle encloses the studied part of the VF), open symbols mark behind the volcanic front volcanoes (BVF) and divided squares the Back-arc (BA) samples from Lake Yojoa and Utila Island (both Honduras) that were studied. Guatemala basement samples from the Chiquimula pluton (unfilled stars). DSDP leg 67 and 84 drill sites (495, 499 and 567) and ODP leg 206 drill site 1256, marked with gray circles with a "+" in them, provide samples for the subduction input (subducting sediments and altered oceanic crust and Guatemalan forearc basement). Data for samples from a seamount on the incoming plate outboard of Nicaragua obtained during the SO144 cruise are from Werner et al. (2003).

## 2. ANALYTICAL METHODS

We collected the freshest mafic lava and tephra samples from the youngest volcanic events, historic when possible, from volcanic centers along and across the volcanic arc from Nicaragua to Guatemala, including the back-arc in Honduras. After removal of the altered outer surfaces, the samples were crushed to small rock/glass chips using a steel jaw crusher. The chips were then washed in distilled water in an ultrasonic bath, dried in a drying cabinet at 50 °C, hand-picked under a binocular microscope and ground to powder (<63 μm) using an agate mill.

Major oxides of whole rock samples ($SiO_2$, $Al_2O_3$, MgO, $Fe_2O_3$, CaO, $Na_2O$, $K_2O$, $TiO_2$, MnO and $P_2O_5$) were measured on fused glass beads using a Phillips X'Unique PW 1480 X-ray fluorescence spectrometer (XRF) with an Rh-tube at the Leibniz Institute of Marine Sciences, IFM-GEOMAR. Volatiles ($H_2O$ and $CO_2$) were analyzed using an infrared photometer Rosemount CSA 5003. Analytical accuracy for major oxide concentrations for international reference standards (JA-2, JB-2, and JB-3) is generally better than 5%, except for MnO (5–12%) and $P_2O_5$ (4–10%), of the suggested values by Govindaraju (1994).

Trace elements (V, Cr, Co, Ni, Zn, Ga, Rb, Sr, Y, Zr, Nb, Mo, Sn, Sb, Cs, Ba, rare earth elements (REE), Hf, Ta, W, Tl, Pb, Th and U) were measured with a VG-Plasmaquad PQ1 inductively coupled plasma-mass spectrometer (ICP-MS) at the Institute of Geosciences, University of Kiel after the methods of Garbe-Schönberg (1993). Analytical accuracy for the standard material BHVO-1 for all trace elements is better than 5.5%, except

Table 1
Major (wt.%) and trace elements (ppm) and isotopic ratios of selected Central American Arc volcanics from volcanic front (VF), behind the volcanic front (BVF) and back-arc (BA) samples. Volcanics major and trace element data for samples marked with (*) from Sadofsky et al. (2008). Note Guatemalan basement sample G3K is sample G3 from Feigenson et al. (2004) reanalyzed for this study.

| Sample # | Sample Location | Sample Type | Rock Classification | Lat (N) | Long (W) | DAA | $SiO_2$ | $TiO_2$ | $AL_2O_3$ | $Fe_2O_3$ | MnO | MgO | CaO | $Na_2O$ | $K_2O$ | $P_2O_5$ | $H_2O$ | $CO_2$ | SUM |
|---|---|---|---|---|---|---|---|---|---|---|---|---|---|---|---|---|---|---|---|
| | | | | | | | wt% | wt% | wt% | wt% | wt% | wt% | wt% | wt% | wt% | wt% | wt% | wt% | wt% |
| *Guatemala volcanic front* | | | | | | | | | | | | | | | | | | | |
| GU2A | Pacaya complex | tephra | calc-alkaline basalt | 14.4090 | -90.6153 | 198.80 | 48.12 | 1.05 | 17.89 | 12.00 | 0.18 | 6.76 | 9.54 | 2.54 | 0.59 | 0.21 | 0.32 | 0.00 | 98.88 |
| GU4 | Acatenango | bomb | calc-alkaline basaltic andesite | 14.5398 | -90.8452 | 170.60 | 55.87 | 0.72 | 18.94 | 8.21 | 0.14 | 3.23 | 7.49 | 3.86 | 1.18 | 0.21 | 0.62 | 0.01 | 99.85 |
| GU5 | Acatenango (NW-flank) | bomb | calc-alkaline basaltic andesite | 14.5335 | -90.9022 | 165.70 | 57.99 | 0.81 | 18.76 | 7.19 | 0.14 | 2.40 | 6.50 | 4.43 | 1.55 | 0.28 | 0.55 | 0.02 | 100.05 |
| GU6 | Acatenango (NW-flank) | tephra | calc-alkaline basaltic andesite | 14.5235 | -90.9307 | 163.60 | 52.89 | 1.02 | 18.70 | 9.44 | 0.14 | 3.92 | 8.11 | 3.64 | 1.12 | 0.24 | 0.50 | 0.07 | 99.22 |
| GU8A | Pacaya | lava flow | calc-alkaline basalt | 14.3821 | -90.6023 | 201.40 | 51.62 | 1.31 | 17.83 | 11.52 | 0.19 | 4.39 | 8.62 | 3.81 | 1.09 | 0.35 | 0.10 | 0.01 | 100.73 |
| GU15A | Santa Maria (N-flank) | lava flow | calc-alkaline basaltic andesite | 14.7528 | -91.5242 | 96.60 | 56.37 | 0.75 | 19.15 | 8.21 | 0.14 | 3.56 | 7.64 | 3.91 | 1.08 | 0.25 | 0.18 | 0.01 | 101.06 |
| GU17A | Santa Maria (N-flank) | block and ash flow | calc-alkaline basaltic andesite | 14.7546 | -91.5239 | 96.60 | 53.85 | 0.81 | 17.74 | 8.72 | 0.15 | 4.70 | 7.63 | 3.67 | 1.03 | 0.21 | 0.62 | 0.03 | 98.51 |
| GU22 | Toliman Volcano (NW-flank) | lava flow | calc-alkaline basaltic andesite | 14.6501 | -91.2248 | 129.70 | 57.50 | 0.78 | 16.78 | 7.62 | 0.12 | 3.90 | 6.53 | 3.67 | 2.05 | 0.17 | 0.71 | 0.02 | 99.12 |
| GU23A | Atitlan Volcano (NW-flank) | bomb | calc-alkaline basalt | 14.6016 | -91.2251 | 132.30 | 51.31 | 1.00 | 18.38 | 9.51 | 0.13 | 4.94 | 8.82 | 3.37 | 0.98 | 0.22 | 0.41 | 0.05 | 98.66 |
| GU26 | San Pedro complex | lava flow | calc-alkaline basaltic andesite | 14.6540 | -91.2976 | 122.80 | 52.83 | 0.81 | 17.09 | 9.19 | 0.15 | 5.18 | 8.80 | 3.21 | 1.22 | 0.17 | 0.66 | 0.05 | 98.65 |
| OTO I | Fuego Volcano | lava flow | calc-alkaline basaltic andesite | 14.4830 | -90.8830 | 170.10 | 54.18 | 0.94 | 20.88 | 8.36 | 0.14 | 2.95 | 8.84 | 3.99 | 0.91 | 0.21 | 0.10 | 0.00 | 101.40 |
| OTO II | Fuego Volcano | lava flow | calc-alkaline basaltic andesite | 14.4830 | -90.8830 | 170.10 | 53.83 | 0.94 | 20.79 | 8.65 | 0.14 | 3.21 | 8.87 | 3.84 | 0.89 | 0.21 | 0.13 | 0.01 | 101.37 |
| *Guatemala behind the volcanic front* | | | | | | | | | | | | | | | | | | | |
| GU14A | Barberena-Cuilapa | lava flow | calc-alkaline basalt | 14.2942 | -90.3410 | 230.20 | 49.89 | 1.34 | 18.45 | 10.36 | 0.16 | 6.08 | 9.94 | 3.60 | 0.60 | 0.26 | 0.26 | 0.01 | 100.68 |
| GU29 | Conacaste town | lava flow | calc-alkaline basalt | 14.8566 | -89.5960 | 268.30 | 50.49 | 1.33 | 17.48 | 9.57 | 0.16 | 6.23 | 8.82 | 3.56 | 1.04 | 0.32 | 0.25 | 0.02 | 99.00 |
| GU30 | Conacaste town (SSE) | lava flow | calc-alkaline basaltic andesite | 14.8245 | -89.5639 | 273.00 | 52.95 | 1.39 | 17.30 | 9.99 | 0.17 | 5.20 | 7.29 | 4.01 | 1.47 | 0.43 | 0.43 | 0.01 | 100.20 |
| GU32 | Quezaltepeque (SSE) | lahar deposit | calc-alkaline basaltic andesite | 14.7447 | -89.5461 | 278.90 | 52.39 | 1.43 | 16.72 | 9.69 | 0.15 | 4.14 | 7.81 | 3.04 | 1.93 | 0.56 | 1.71 | 0.15 | 97.86 |
| GU35B | Los Gemeloz | lava flow | calc-alkaline basalt | 14.5953 | -89.6460 | 277.90 | 49.67 | 1.21 | 17.92 | 10.17 | 0.16 | 7.23 | 9.58 | 3.23 | 0.83 | 0.35 | 0.50 | 0.03 | 100.35 |
| GU38 | Cerro Gordo (W cone) | lava flow | calc-alkaline basalt | 14.4427 | -89.6110 | 289.30 | 50.41 | 1.12 | 17.54 | 10.23 | 0.17 | 6.92 | 9.69 | 2.94 | 1.49 | 0.39 | 0.30 | 0.01 | 100.90 |
| GU39 | San Miguel Chapron Graben | bomb | calc-alkaline basalt | 14.5113 | -89.7499 | 272.90 | 50.71 | 1.32 | 18.54 | 11.08 | 0.17 | 5.11 | 8.83 | 3.56 | 0.89 | 0.29 | 0.61 | 0.03 | 100.50 |
| *El Salvador volcanic front* | | | | | | | | | | | | | | | | | | | |
| ES002 | Siguatepeque Volcano (E) | scoria | calc-alkaline basaltic andesite | 13.6150 | -88.5556 | 431.30 | 54.72 | 1.23 | 15.75 | 11.96 | 0.22 | 3.46 | 7.36 | 3.45 | 1.76 | 0.37 | 0.86 | 0.03 | 100.28 |
| ES003 | Siguatepeque Volcano (E) | lava flow | calc-alkaline basaltic andesite | 13.6200 | -88.5600 | 431.30 | 54.00 | 1.21 | 15.30 | 11.56 | 0.22 | 3.33 | 7.03 | 3.49 | 1.92 | 0.38 | 1.14 | 0.03 | 98.44 |
| ES005 | Santa Ana Volcano | tephra | calc-alkaline basaltic andesite | 13.8451 | -89.6291 | 320.00 | 52.89 | 0.94 | 17.59 | 10.39 | 0.17 | 3.97 | 7.72 | 3.32 | 1.64 | 0.27 | 0.74 | 0.08 | 98.90 |
| ES009 | Laguna Caldera | bomb | calc-alkaline basaltic andesite | 13.8399 | -89.3609 | 345.00 | 54.88 | 1.22 | 15.99 | 11.46 | 0.21 | 2.76 | 6.99 | 3.67 | 1.68 | 0.32 | 0.36 | 0.01 | 99.18 |
| ES019 | Coujutepeque, Cerro de Las Pavas | bomb | calc-alkaline basalt | 13.7124 | -88.9365 | 391.00 | 49.92 | 1.20 | 17.90 | 9.97 | 0.16 | 5.52 | 8.96 | 3.31 | 1.01 | 0.36 | 0.96 | 0.03 | 98.31 |
| ES027B | San Miguel Volcano | lava flow | calc-alkaline basalt | 13.5028 | -88.2217 | 468.10 | 50.19 | 0.81 | 18.62 | 11.03 | 0.18 | 6.22 | 10.10 | 2.47 | 0.53 | 0.15 | 0.46 | 0.01 | 100.30 |
| ES028B | San Miguel Volcano (NW) | lava flow | calc-alkaline basalt | 13.5112 | -88.2478 | 465.30 | 50.93 | 0.98 | 18.93 | 10.99 | 0.18 | 4.19 | 10.23 | 2.75 | 0.73 | 0.18 | 0.33 | 0.03 | 100.09 |
| ES 031 | San Miguel Volcano | lava flow | calc-alkaline basalt | 13.4180 | -88.3142 | 464.30 | 51.21 | 1.03 | 18.74 | 11.03 | 0.18 | 4.17 | 10.13 | 2.84 | 0.82 | 0.21 | 0.35 | 0.02 | 100.36 |
| ES035A | Usulutan Complex | bomb | calc-alkaline basaltic andesite | 13.5538 | -88.4314 | 446.10 | 58.37 | 0.89 | 17.09 | 7.89 | 0.22 | 2.49 | 5.59 | 4.57 | 1.51 | 0.38 | 1.26 | 0.02 | 99.00 |
| ES036C | Izalco (northern flank) | tephra | calc-alkaline basaltic andesite | 13.8184 | -89.6312 | 321.30 | 54.02 | 0.85 | 18.49 | 9.53 | 0.16 | 4.22 | 8.20 | 3.72 | 1.19 | 0.16 | 0.20 | 0.01 | 100.54 |
| ES038 | Izalco (western flank) | lava flow | calc-alkaline basaltic andesite | 13.8168 | -89.6276 | 321.70 | 52.96 | 0.87 | 18.84 | 9.90 | 0.17 | 4.13 | 8.47 | 3.59 | 1.05 | 0.15 | 0.31 | 0.01 | 100.13 |
| ES SSI | San Salvador Volcano | lava flow | calc-alkaline basaltic andesite | 13.8045 | -89.3296 | 358.00 | 58.75 | 1.17 | 15.33 | 10.82 | 0.23 | 2.27 | 5.54 | 4.08 | 2.14 | 0.40 | 0.19 | 0.01 | 100.73 |
| ES SSII | San Salvador Volcano | lava flow | calc-alkaline basaltic andesite | 13.8045 | -89.3296 | 358.00 | 59.26 | 1.17 | 15.37 | 10.79 | 0.23 | 2.22 | 5.51 | 4.06 | 2.15 | 0.40 | 0.23 | 0.03 | 101.16 |
| *El Salvador behind the volcanic front* | | | | | | | | | | | | | | | | | | | |
| ES013 | cinder cone close to Cerrito Ojo de Agua | bomb | calc-alkaline basalt | 13.8572 | -89.2287 | 356.20 | 50.78 | 0.95 | 17.24 | 9.75 | 0.16 | 6.86 | 9.76 | 2.78 | 0.72 | 0.25 | 0.52 | 0.02 | 99.25 |
| ES014 | Cerrito Ojo de Agua | lava flow | calc-alkaline basaltic andesite | 13.8572 | -89.2287 | 356.20 | 53.85 | 1.01 | 17.61 | 9.13 | 0.16 | 4.48 | 7.83 | 3.51 | 1.59 | 0.39 | 0.72 | 0.02 | 99.56 |
| ES015 | Cerro Quemado | tephra | calc-alkaline basaltic andesite | 14.2422 | -89.4706 | 313.10 | 53.10 | 1.15 | 17.78 | 9.41 | 0.16 | 5.60 | 8.19 | 3.43 | 1.25 | 0.42 | 0.42 | 0.06 | 100.49 |
| ES016 | Cerro Quemado | bomb | calc-alkaline basaltic andesite | 14.2422 | -89.4706 | 313.10 | 52.70 | 1.18 | 17.50 | 9.36 | 0.16 | 5.33 | 8.13 | 3.71 | 1.28 | 0.42 | 0.38 | 0.01 | 99.77 |
| ES017 | Junquillo and Rio Ostija | lava flow | calc-alkaline basalt | 14.3180 | -89.5836 | 298.60 | 51.44 | 1.33 | 17.65 | 10.02 | 0.16 | 5.13 | 8.17 | 3.57 | 1.54 | 0.47 | 0.83 | 0.02 | 99.48 |
| ES018B | San Diego Volcano | lava flow | calc-alkaline basalt | 14.2750 | -89.4772 | 310.70 | 50.94 | 1.30 | 17.58 | 9.65 | 0.16 | 5.20 | 9.05 | 3.59 | 1.16 | 0.44 | 0.45 | 0.03 | 99.07 |
| ES024B | El Singüil | tephra | calc-alkaline basalt | 14.0488 | -89.6317 | 308.70 | 49.24 | 1.09 | 17.11 | 10.09 | 0.16 | 7.60 | 9.60 | 3.01 | 0.84 | 0.25 | 0.41 | 0.03 | 98.99 |
| *Honduras volcanic front* | | | | | | | | | | | | | | | | | | | |
| H3B | El Tigre Island (S) | bomb | trachybasalt | 13.2526 | -87.6304 | 536.20 | 57.93 | 0.83 | 18.20 | 7.88 | 0.21 | 2.58 | 6.55 | 4.51 | 0.92 | 0.28 | 0.47 | 0.01 | 99.89 |
| *Honduras behind the volcanic front* | | | | | | | | | | | | | | | | | | | |
| H1 | El Tigre Island (N) | bomb | calc-alkaline basalt | 13.2896 | -87.6418 | 533.10 | 49.64 | 0.87 | 18.22 | 10.66 | 0.18 | 5.21 | 9.51 | 3.05 | 0.85 | 0.26 | 1.11 | 0.07 | 98.45 |
| H4B | El Tigre Island (N) | bomb | calc-alkaline basaltic andesite | 13.2724 | -87.6561 | 532.80 | 52.43 | 0.90 | 19.15 | 10.58 | 0.18 | 3.33 | 9.23 | 3.24 | 0.86 | 0.19 | 0.51 | 0.01 | 100.09 |
| H5 | Sacate Grande - SE-flank | lava flow | calc-alkaline basalt | 13.3202 | -87.6171 | 533.70 | 51.46 | 0.94 | 18.33 | 11.33 | 0.19 | 3.79 | 9.23 | 3.31 | 0.64 | 0.18 | 0.59 | 0.02 | 99.40 |
| H9 | near Zambrano town | lava flow | calc-alkaline basalt | 14.2658 | -87.3960 | 501.90 | 51.21 | 1.13 | 17.91 | 10.17 | 0.16 | 5.41 | 8.96 | 3.03 | 1.14 | 0.42 | 0.86 | 0.01 | 99.54 |

(*continued on next page*)

Table 1 (*continued*)

| Sample # | Sample Location | Sample Type | Rock Classification | Lat (N) | Long (W) | DAA | $SiO_2$ | $TiO_2$ | $AL_2O_3$ | $Fe_2O_3$ | MnO | MgO | CaO | $Na_2O$ | $K_2O$ | $P_2O_5$ | $H_2O$ | $CO_2$ | SUM |
|---|---|---|---|---|---|---|---|---|---|---|---|---|---|---|---|---|---|---|---|
| | | | | | | | wt% | wt% | wt% | wt% | wt% | wt% | wt% | wt% | wt% | wt% | wt% | wt% | wt% |
| H13 | S of Pore Rios (Sula Graben) | lava flow | calc-alkaline basalt | 15.2066 | -87.9612 | 398.70 | 48.95 | 1.96 | 17.81 | 10.66 | 0.16 | 5.29 | 8.95 | 3.99 | 1.62 | 0.63 | 0.57 | 0.48 | 100.02 |
| H14 | Cerro Las Crucitas (W of Tegucigalpa) | lava flow | calc-alkaline basalt | 14.0168 | -87.3333 | 521.40 | 51.42 | 1.04 | 16.54 | 10.04 | 0.16 | 5.26 | 8.54 | 2.89 | 1.49 | 0.34 | 1.32 | 0.02 | 97.72 |
| H16 | SW of Tegucigalpa | lava flow | calc-alkaline basaltic andesite | 13.9551 | -87.2091 | 536.20 | 52.49 | 1.04 | 17.55 | 9.78 | 0.15 | 4.51 | 8.80 | 3.07 | 1.54 | 0.43 | 1.02 | 0.02 | 99.36 |
| *Honduras backarc* | | | | | | | | | | | | | | | | | | | |
| H10 | Laguna de Yojoa (N) | lava flow | Hawaiite | 14.9297 | -87.9801 | 412.10 | 48.92 | 2.50 | 16.34 | 11.77 | 0.21 | 3.96 | 7.12 | 4.55 | 2.41 | 0.93 | 1.01 | 0.05 | 98.71 |
| H17A | Utila Island | tuff | Hawaiite | 16.1207 | -86.8832 | 446.20 | 46.93 | 1.63 | 16.64 | 10.31 | 0.18 | 6.69 | 9.49 | 3.01 | 1.99 | 0.58 | 2.62 | 0.06 | 97.45 |
| H18A | Utila Island | clasts | Hawaiite | 16.1226 | -86.8815 | 446.30 | 48.20 | 1.65 | 17.25 | 10.14 | 0.16 | 6.14 | 8.44 | 3.79 | 2.31 | 0.59 | 1.71 | 0.09 | 98.67 |
| *NW Nicaragua volcanic front* | | | | | | | | | | | | | | | | | | | |
| P-60 | Cosigüina | lava block | calc-alkaline basaltic andesite | 12.8671 | -87.5551 | 564.40 | 56.63 | 0.68 | 19.43 | 7.42 | 0.12 | 1.82 | 8.05 | 3.26 | 1.39 | 0.17 | 1.11 | 0.05 | 98.97 |
| P-58A | Cosigüina | lava block | calc-alkaline basaltic andesite | 13.0336 | -87.5918 | 551.80 | 59.20 | 0.79 | 17.27 | 8.27 | 0.18 | 2.20 | 6.70 | 4.06 | 1.41 | 0.22 | 0.41 | 0.02 | 100.30 |
| P-27A | San Cristobal | block from lahar | calc-alkaline basalt | 12.6811 | -87.0278 | 623.10 | 49.82 | 0.97 | 18.20 | 12.10 | 0.21 | 4.55 | 10.45 | 2.83 | 0.71 | 0.20 | 0.32 | 0.02 | 100.24 |
| P-13 | Casitas | lava block | calc-alkaline basalt | 12.6857 | -86.9553 | 629.60 | 50.36 | 0.86 | 18.41 | 11.56 | 0.19 | 4.22 | 9.15 | 2.78 | 1.02 | 0.23 | 1.38 | 0.04 | 98.98 |
| P2-16 | Telica/ San Cristobal | tephra | calc-alkaline basalt | 12.5965 | -86.9322 | 636.60 | 48.57 | 0.72 | 18.21 | 10.27 | 0.17 | 5.71 | 12.21 | 1.83 | 0.73 | 0.13 | 0.57 | 0.09 | 98.55 |
| P-7A | Telica | bomb | calc-alkaline basalt | 12.6073 | -86.8332 | 645.10 | 51.52 | 0.84 | 17.93 | 10.90 | 0.18 | 4.48 | 10.04 | 2.67 | 1.20 | 0.16 | 0.31 | 0.02 | 100.15 |
| P-9 | Telica | lava flow | calc-alkaline basalt | 12.6051 | -86.8361 | 645.00 | 49.78 | 1.01 | 18.09 | 11.23 | 0.17 | 5.51 | 11.03 | 2.44 | 0.93 | 0.17 | 0.29 | 0.01 | 100.56 |
| P-43 | Cone3 | bomb | calc-alkaline basaltic andesite | 12.5334 | -86.6774 | 663.50 | 53.07 | 1.34 | 15.96 | 12.45 | 0.20 | 4.11 | 8.45 | 3.15 | 1.16 | 0.23 | 0.31 | 0.03 | 100.33 |
| P-51 | Cone2 | bomb | calc-alkaline basalt | 12.4696 | -86.7232 | 662.90 | 49.98 | 0.72 | 17.18 | 10.60 | 0.18 | 6.53 | 12.71 | 1.92 | 0.59 | 0.16 | 0.34 | 0.02 | 100.74 |
| P-56G | C. Las Palmitas | tuff | calc-alkaline basaltic andesite | 12.6072 | -86.7329 | 654.40 | 52.57 | 1.07 | 16.48 | 12.48 | 0.24 | 3.94 | 7.73 | 3.07 | 0.80 | 0.20 | 1.75 | 0.08 | 98.82 |
| P-4 | C. Negro | bomb | calc-alkaline basalt | 12.5076 | -86.7009 | 662.80 | 49.69 | 0.76 | 18.66 | 11.26 | 0.19 | 5.68 | 11.72 | 2.04 | 0.45 | 0.11 | 0.17 | 0.00 | 100.73 |
| P-6 | C. Negro | lava flow | calc-alkaline basalt | 12.5023 | -86.7005 | 663.10 | 49.91 | 0.79 | 19.59 | 10.93 | 0.18 | 4.58 | 11.37 | 2.26 | 0.50 | 0.12 | 0.22 | 0.01 | 100.41 |
| P2-3a | C. Negro | tephra | calc-alkaline basalt | 12.4987 | -86.7035 | 663.10 | 47.50 | 0.61 | 15.74 | 11.45 | 0.19 | 10.03 | 12.44 | 1.50 | 0.27 | 0.10 | 0.16 | 0.04 | 99.99 |
| P2-3b | C. Negro | tephra | calc-alkaline basalt | 12.4987 | -86.7035 | 663.10 | 48.86 | 0.68 | 21.26 | 9.84 | 0.16 | 4.10 | 12.45 | 2.12 | 0.40 | 0.13 | 0.19 | 0.03 | 100.15 |
| P2-3d | C. Negro | tephra | calc-alkaline basalt | 12.4987 | -86.7035 | 663.10 | 49.19 | 0.75 | 18.41 | 11.25 | 0.19 | 5.98 | 12.05 | 2.10 | 0.42 | 0.12 | 0.16 | 0.02 | 100.65 |
| P2-11 | C. Negro | lava flow | calc-alkaline basalt | 12.4984 | -86.7058 | 662.90 | 48.44 | 0.78 | 19.32 | 11.00 | 0.18 | 4.64 | 11.59 | 2.23 | 0.46 | 0.13 | 0.22 | 0.02 | 98.96 |
| P2-13 | C. Negro | lava flow | calc-alkaline basalt | 12.5105 | -86.7075 | 662.10 | 48.46 | 0.72 | 16.32 | 11.50 | 0.20 | 7.43 | 11.29 | 2.12 | 0.46 | 0.12 | 0.19 | 0.03 | 98.78 |
| P-50 | C. Diablo | bomb | calc-alkaline basalt | 12.4726 | -86.7236 | 662.70 | 49.90 | 0.71 | 17.33 | 10.62 | 0.18 | 6.41 | 12.64 | 1.93 | 0.60 | 0.16 | 0.30 | 0.02 | 100.66 |
| P-19 | Las Pilas | bomb | calc-alkaline basalt | 12.4933 | -86.6861 | 665.00 | 51.28 | 0.84 | 16.05 | 10.54 | 0.18 | 6.06 | 10.86 | 2.38 | 0.81 | 0.18 | 0.24 | 0.00 | 99.37 |
| P-40A | Cabeza de Vaca | bomb | calc-alkaline basalt | 12.5195 | -86.6815 | 663.90 | 47.39 | 0.71 | 17.55 | 12.39 | 0.19 | 7.81 | 12.25 | 1.63 | 0.36 | 0.09 | 0.26 | 0.04 | 100.55 |
| P-42 | Cabeza de Vaca | bomb | calc-alkaline basalt | 12.5198 | -86.6807 | 664.00 | 48.22 | 0.74 | 16.31 | 12.60 | 0.20 | 8.46 | 10.90 | 1.77 | 0.49 | 0.10 | 0.32 | 0.04 | 99.96 |
| P-23 | Ojo de Agua | lava flow | calc-alkaline basaltic andesite | 12.5145 | -86.6806 | 664.30 | 54.95 | 0.94 | 16.54 | 10.26 | 0.20 | 3.78 | 8.06 | 3.20 | 1.32 | 0.25 | 0.27 | 0.00 | 99.72 |
| P-46A | Laguna Asos | bomb | calc-alkaline basaltic andesite | 12.4402 | -86.6716 | 669.20 | 56.93 | 1.05 | 15.82 | 10.60 | 0.20 | 2.99 | 6.70 | 3.35 | 1.64 | 0.25 | 0.71 | 0.02 | 99.76 |
| P-47A | C. Buena vista | tephra | calc-alkaline basaltic andesite | 12.4005 | -86.6643 | 672.10 | 57.82 | 0.98 | 15.71 | 9.98 | 0.19 | 2.67 | 6.21 | 3.33 | 1.80 | 0.24 | 0.90 | 0.03 | 99.16 |
| P-48B | Cone4 | bomb | calc-alkaline basaltic andesite | 12.3727 | -86.6500 | 675.00 | 54.38 | 1.00 | 16.20 | 11.49 | 0.20 | 3.86 | 8.07 | 2.90 | 1.31 | 0.20 | 0.69 | 0.02 | 99.80 |
| P-32 | Momotombo | lava flow | calc-alkaline basaltic andesite | 12.4278 | -86.5808 | 678.30 | 52.57 | 0.76 | 17.69 | 10.64 | 0.18 | 5.04 | 9.85 | 2.52 | 0.79 | 0.15 | 0.21 | 0.02 | 100.40 |
| P-34 | Momotombo | lava flow | calc-alkaline basaltic andesite | 12.4565 | -86.5560 | 679.00 | 54.78 | 0.78 | 17.21 | 10.08 | 0.18 | 4.19 | 8.61 | 2.86 | 1.00 | 0.16 | 0.21 | 0.01 | 100.05 |
| *Guatemala basement* | | | | | | | | | | | | | | | | | | | |
| G 009 L1 | Santa Maria basement | basement | granodiorite | 14.7200 | -91.6200 | 89.50 | 52.87 | 1.11 | 16.58 | 11.05 | 0.17 | 5.02 | 7.97 | 3.43 | 1.69 | 0.15 | 1.09 | 0.04 | 100.26 |
| G 009 L2 | Santa Maria basement | basement | granodiorite | 14.7200 | -91.6200 | 89.50 | 57.60 | 2.04 | 16.22 | 8.88 | 0.14 | 2.42 | 4.08 | 4.98 | 3.14 | 0.47 | 0.79 | 0.03 | 100.32 |
| Chor 8A | Las Ovejas complex | basement | amphibolite/ diorite | 14.9150 | -89.7117 | 254.60 | 49.97 | 1.13 | 19.61 | 7.46 | 0.12 | 5.73 | 11.85 | 3.07 | 0.50 | 0.17 | 1.30 | 0.01 | 99.72 |
| P12 | Las Ovejas complex | basement | dirorite | 14.8896 | -89.8136 | 246.60 | 49.83 | 1.58 | 17.73 | 10.56 | 0.13 | 4.37 | 7.69 | 3.63 | 1.86 | 0.43 | 1.35 | 0.03 | 98.06 |
| G3K | near Chiquimula | basement | granitc | 14.9500 | -89.5400 | 268.40 | 76.27 | 0.14 | 12.95 | 1.17 | 0.03 | 0.11 | 0.45 | 3.95 | 4.70 | 0.03 | 0.35 | 0.01 | 99.80 |
| M1 | North of Jocotan Fault | basement | phyllite | 14.6900 | -89.6300 | 274.20 | 55.98 | 1.71 | 25.71 | 2.08 | 0.01 | 0.79 | 0.12 | 0.22 | 6.43 | 0.27 | 4.54 | 0.18 | 93.32 |
| M2 | North of Jocotan Fault | basement | phyllite | 14.7100 | -89.6200 | 274.00 | 81.46 | 0.95 | 10.65 | 0.38 | 0.00 | 0.24 | 0.00 | 0.03 | 2.36 | 0.03 | 2.15 | 0.02 | 96.10 |
| 619 | Rio Hondo (Maya Block) | basement | mylonitc gneiss | 15.0680 | -89.6020 | 256.30 | 68.46 | 0.46 | 14.79 | 4.24 | 0.06 | 1.56 | 3.03 | 3.22 | 2.93 | 0.16 | 1.23 | 0.05 | 98.91 |
| 714A | Concul (Maya Block) | basement | mylotinized orthogneiss | 15.0561 | -90.5190 | 172.90 | 57.33 | 2.51 | 15.43 | 8.52 | 0.12 | 1.54 | 5.23 | 1.84 | 5.65 | 0.65 | 1.65 | 0.06 | 98.82 |
| *Cocos plate sediments* | | | | | | | | | | | | | | | | | | | |
| 67_0495_009R_02W_73-75 | ODP site 495 | hemipelagic sediment | diatomaceous mud | 12.4963 | -91.0376 | 262.20 | 56.89 | 0.60 | 12.82 | 6.01 | 0.16 | 2.86 | 2.09 | 3.48 | 1.75 | 0.13 | 8.88 | 1.53 | 86.79 |
| 67_0499_019R_05W_80-82 | ODP site 499 | hemipelagic sediment | diatomaceous mud | 12.6705 | -90.9446 | 261.50 | 56.31 | 0.74 | 15.70 | 6.86 | 0.06 | 2.42 | 1.65 | 2.96 | 1.67 | 0.14 | 7.79 | 1.09 | 88.51 |
| *Cocos plate MORB* | | | | | | | | | | | | | | | | | | | |
| 67_0495_048R_04W_82-84 | ODP site 495 | MORB | tholeiite | 12.4963 | -91.0376 | 262.20 | 50.60 | 1.48 | 15.93 | 9.45 | 0.15 | 7.22 | 11.86 | 2.88 | 0.09 | 0.15 | 1.57 | 0.14 | 99.81 |
| 206_1256C_10R2_103-105 | IODP Site 1256C | MORB | tholeiite | 6.7360 | -91.9340 | 486.20 | 50.13 | 1.89 | 12.93 | 14.99 | 0.21 | 6.72 | 10.29 | 2.65 | 0.49 | 0.15 | 0.69 | 0.07 | 100.57 |
| 206_1256D_74R2_102-111 | IODP Site 1256D | MORB | tholeiite | 6.7360 | -91.9340 | 486.20 | 50.02 | 1.36 | 13.16 | 12.97 | 0.25 | 7.14 | 10.51 | 2.95 | 0.05 | 0.10 | 0.49 | 0.05 | 98.64 |

| Sample # | V ppm | Cr ppm | Co ppm | Ni ppm | Cu ppm | Zn ppm | Ga ppm | Rb ppm | Sr ppm | Y ppm | Zr ppm | Nb ppm | Mo ppm | Sn ppm | Sb ppm | Cs ppm | Ba ppm | La ppm | Ce ppm | Pr ppm | Nd ppm | Sm ppm | Eu ppm | Gd ppm | Tb ppm | Dy ppm | Ho ppm | Er ppm | Tm ppm | Yb ppm | Lu ppm | Hf ppm | T a ppm | W ppm | Tl ppm | Pb ppm | Th ppm | U ppm |
|---|---|---|---|---|---|---|---|---|---|---|---|---|---|---|---|---|---|---|---|---|---|---|---|---|---|---|---|---|---|---|---|---|---|---|---|---|---|
| *Guatemala volcanic front* | | | | | | | | | | | | | | | | | | | | | | | | | | | | | | | | | | | | | | |
| GU2A | 287 | 28.9 | 40.3 | 28.50 | 59.9 | 90.4 | 18.6 | 8.81 | 560 | 18.0 | 73.5 | 2.46 | 0.45 | 0.77 | 0.13 | 0.38 | 301 | 7.48 | 17.5 | 2.62 | 11.9 | 3.01 | 1.06 | 3.16 | 0.51 | 3.15 | 0.63 | 1.73 | 0.25 | 1.67 | 0.25 | 1.93 | 0.14 | 0.20 | 0.04 | 2.93 | 0.70 | 0.30 |
| GU4 | 143 | 1.87 | 20.1 | 4.22 | 47.6 | 85.6 | 20.0 | 24.0 | 584 | 18.2 | 110 | 2.89 | 1.12 | 0.86 | 0.31 | 1.21 | 519 | 10.1 | 22.3 | 3.28 | 14.5 | 3.40 | 1.05 | 3.37 | 0.51 | 2.97 | 0.58 | 1.59 | 0.24 | 1.56 | 0.24 | 2.85 | 0.15 | 0.38 | 0.05 | 4.80 | 1.67 | 0.66 |
| GU5 | 119 | 0.85 | 14.8 | 2.09 | 44.6 | 84.0 | 19.8 | 32.5 | 502 | 25.9 | 143 | 3.64 | 1.41 | 1.16 | 0.47 | 1.66 | 643 | 12.7 | 28.5 | 4.25 | 18.8 | 4.59 | 1.27 | 4.61 | 0.71 | 4.19 | 0.85 | 2.30 | 0.34 | 2.27 | 0.35 | 3.75 | 0.19 | 0.50 | 0.12 | 6.54 | 2.29 | 0.91 |
| GU6 | 245 | 13.7 | 25.3 | 10.69 | 74.7 | 93.4 | 20.6 | 21.3 | 579 | 18.0 | 130 | 3.46 | 0.88 | 1.00 | 0.19 | 0.79 | 547 | 13.2 | 29.7 | 4.03 | 16.8 | 3.72 | 1.15 | 3.54 | 0.55 | 3.20 | 0.63 | 1.72 | 0.25 | 1.64 | 0.24 | 3.22 | 0.21 | 0.41 | 0.07 | 5.70 | 1.58 | 0.59 |
| GU8A | 252 | 12.2 | 26.9 | 8.59 | 96.1 | 103 | 20.7 | 18.5 | 519 | 28.4 | 120 | 4.18 | 0.79 | 1.23 | 0.12 | 0.79 | 543 | 13.7 | 30.7 | 4.57 | 20.7 | 5.11 | 1.55 | 5.24 | 0.81 | 4.82 | 0.97 | 2.65 | 0.39 | 2.56 | 0.38 | 3.21 | 0.21 | 0.31 | 0.05 | 5.29 | 2.02 | 0.78 |
| GU15A | 155 | 34.7 | 21.2 | 19.60 | 40.6 | 95.2 | 19.9 | 17.4 | 542 | 20.9 | 135 | 3.12 | 0.95 | 0.94 | 0.21 | 0.49 | 521 | 10.1 | 22.8 | 3.38 | 15.3 | 3.67 | 1.09 | 3.74 | 0.59 | 3.61 | 0.73 | 2.05 | 0.31 | 2.08 | 0.32 | 3.41 | 0.18 | 0.38 | 0.06 | 5.52 | 0.92 | 0.42 |
| GU17A | 187 | 61.6 | 26.2 | 28.2 | 55.5 | 90.2 | 18.8 | 17.6 | 496 | 19.7 | 123 | 2.82 | 0.95 | 0.85 | 0.23 | 0.84 | 475 | 9.01 | 21.2 | 3.08 | 13.7 | 3.33 | 1.03 | 3.39 | 0.54 | 3.35 | 0.67 | 1.89 | 0.28 | 1.92 | 0.30 | 3.07 | 0.16 | 0.41 | 0.07 | 4.83 | 1.05 | 0.44 |
| GU22 | 153 | 35.7 | 19.7 | 14.1 | 33.1 | 69.4 | 16.9 | 47.3 | 424 | 19.9 | 140 | 3.96 | 1.85 | 1.19 | 0.31 | 1.92 | 665 | 13.5 | 28.9 | 3.92 | 16.5 | 3.74 | 0.97 | 3.73 | 0.58 | 3.44 | 0.70 | 1.95 | 0.29 | 1.98 | 0.30 | 3.95 | 0.24 | 0.75 | 0.17 | 7.39 | 4.55 | 1.66 |
| GU23A | 248 | 48.8 | 28.5 | 24.0 | 70.1 | 91.1 | 20.2 | 18.4 | 603 | 16.1 | 99.1 | 3.01 | 0.70 | 0.89 | 0.16 | 0.81 | 457 | 10.1 | 23.0 | 3.29 | 14.2 | 3.27 | 1.04 | 3.26 | 0.50 | 2.89 | 0.56 | 1.48 | 0.21 | 1.38 | 0.20 | 2.62 | 0.18 | 0.37 | 0.08 | 4.95 | 1.28 | 0.53 |
| GU26 | 236 | 68.1 | 29.5 | 18.1 | 55.2 | 87.6 | 19.1 | 23.0 | 581 | 18.3 | 104 | 2.44 | 0.73 | 0.88 | 0.11 | 0.87 | 458 | 9.96 | 22.1 | 3.20 | 13.8 | 3.27 | 0.99 | 3.24 | 0.52 | 3.13 | 0.64 | 1.77 | 0.26 | 1.73 | 0.26 | 2.74 | 0.15 | 0.31 | 0.08 | 5.15 | 2.29 | 0.78 |
| OTO I | 202 | 3.90 | 19.7 | 6.74 | 79.3 | 87.7 | 20.8 | 12.7 | 605 | 20.7 | 84.1 | 2.01 | 0.84 | 0.87 | 0.16 | 0.59 | 472 | 8.33 | 19.0 | 2.91 | 13.7 | 3.53 | 1.17 | 3.73 | 0.60 | 3.70 | 0.75 | 2.07 | 0.31 | 2.05 | 0.31 | 2.37 | 0.13 | 0.29 | 0.17 | 4.47 | 0.98 | 0.41 |
| OTO II | 208 | 4.01 | 21.2 | 7.84 | 81.0 | 87.9 | 20.6 | 11.5 | 605 | 19.8 | 81.0 | 1.93 | 0.78 | 0.85 | 0.15 | 0.57 | 453 | 7.91 | 18.1 | 2.77 | 13.2 | 3.37 | 1.13 | 3.56 | 0.58 | 3.54 | 0.72 | 1.97 | 0.29 | 1.95 | 0.29 | 2.27 | 0.13 | 0.29 | 0.05 | 4.20 | 0.93 | 0.38 |
| *Guatemala behind the volcanic front* | | | | | | | | | | | | | | | | | | | | | | | | | | | | | | | | | | | | | | |
| GU14A | 235 | 105 | 34.1 | 48.6 | 64.9 | 78.5 | 18.4 | 6.12 | 515 | 24.9 | 129 | 4.38 | 0.53 | 1.03 | 0.05 | 0.08 | 234 | 8.98 | 21.6 | 3.21 | 14.4 | 3.76 | 1.29 | 4.11 | 0.66 | 4.04 | 0.82 | 2.23 | 0.33 | 2.14 | 0.32 | 2.77 | 0.23 | 0.11 | 0.02 | 2.42 | 0.69 | 0.20 |
| GU29 | 199 | 160 | 33.3 | 76.6 | 39.7 | 82.2 | 17.6 | 10.8 | 509 | 27.3 | 155 | 8.97 | 1.02 | 1.12 | 0.06 | 0.30 | 405 | 13.8 | 30.2 | 4.25 | 18.9 | 4.55 | 1.52 | 4.87 | 0.79 | 4.77 | 0.97 | 2.68 | 0.40 | 2.64 | 0.40 | 3.55 | 0.57 | 0.29 | 0.06 | 3.91 | 1.21 | 0.48 |
| GU30 | 149 | 125 | 28.3 | 68.9 | 31.3 | 88.0 | 18.1 | 14.3 | 496 | 40.6 | 181 | 12.2 | 1.37 | 1.26 | 0.07 | 0.43 | 549 | 24.3 | 43.9 | 6.92 | 29.5 | 6.90 | 2.10 | 7.34 | 1.14 | 6.80 | 1.37 | 3.69 | 0.54 | 3.60 | 0.53 | 4.37 | 0.61 | 2.68 | 0.10 | 5.04 | 1.42 | 0.57 |
| GU32 | 215 | 90.5 | 28.8 | 41.3 | 43.7 | 107 | 19.2 | 43.6 | 589 | 32.6 | 230 | 11.2 | 1.32 | 1.37 | 0.07 | 0.81 | 719 | 25.1 | 54.8 | 7.60 | 32.0 | 6.91 | 2.01 | 6.58 | 1.01 | 5.87 | 1.15 | 3.11 | 0.45 | 2.97 | 0.44 | 5.38 | 0.58 | 0.52 | 0.27 | 7.90 | 2.16 | 0.71 |
| GU35B | 204 | 290 | 34.1 | 76.7 | 45.3 | 72.0 | 16.5 | 10.7 | 537 | 23.5 | 137 | 6.75 | 0.90 | 0.97 | 0.08 | 0.37 | 335 | 12.2 | 27.5 | 3.87 | 16.7 | 3.98 | 1.33 | 4.17 | 0.65 | 3.89 | 0.79 | 2.14 | 0.32 | 2.10 | 0.31 | 2.93 | 0.35 | 0.18 | 0.02 | 2.81 | 1.14 | 0.46 |
| GU38 | 232 | 238 | 34.1 | 65.9 | 42.0 | 77.3 | 16.8 | 39.6 | 585 | 28.4 | 139 | 5.43 | 0.87 | 0.97 | 0.12 | 1.03 | 476 | 15.9 | 34.3 | 5.09 | 22.3 | 5.25 | 1.65 | 5.35 | 0.79 | 4.55 | 0.91 | 2.44 | 0.36 | 2.34 | 0.35 | 3.22 | 0.25 | 0.39 | 0.13 | 3.83 | 1.38 | 0.75 |
| GU39 | 249 | 29.4 | 29.0 | 9.80 | 31.0 | 93.8 | 19.7 | 12.7 | 611 | 25.0 | 116 | 5.00 | 0.65 | 1.02 | 0.10 | 0.42 | 403 | 12.0 | 26.9 | 3.95 | 17.6 | 4.32 | 1.40 | 4.40 | 0.68 | 4.05 | 0.82 | 2.22 | 0.33 | 2.14 | 0.32 | 2.78 | 0.24 | 0.21 | 0.06 | 4.22 | 1.09 | 0.45 |
| *El Salvador volcanic front* | | | | | | | | | | | | | | | | | | | | | | | | | | | | | | | | | | | | | | |
| ES002 | 298 | 1.91 | 25.9 | 3.94 | 238 | 122 | 19.0 | 37.7 | 426 | 34.4 | 133 | 3.12 | 1.41 | 1.42 | 0.47 | 1.74 | 853 | 13.5 | 31.2 | 4.89 | 23.0 | 5.98 | 1.62 | 6.25 | 1.01 | 6.17 | 1.26 | 3.47 | 0.52 | 3.44 | 0.52 | 3.81 | 0.20 | 0.86 | 0.09 | 6.55 | 2.20 | 1.25 |
| ES003 | 281 | 1.20 | 25.6 | 3.55 | 246 | 122 | 20.2 | 43.6 | 417 | 38.3 | 147 | 3.68 | 1.48 | 1.32 | 0.52 | 1.84 | 834 | 13.9 | 32.5 | 5.00 | 23.2 | 5.98 | 1.62 | 6.25 | 0.98 | 5.99 | 1.22 | 3.42 | 0.50 | 3.33 | 0.50 | 3.80 | 0.17 | 0.56 | 0.09 | 5.96 | 2.55 | 1.36 |
| ES005 | 220 | 9.11 | 29.1 | 9.17 | 101 | 93.1 | 19.1 | 47.8 | 474 | 27.2 | 147 | 3.21 | 1.57 | 1.40 | 0.38 | 2.56 | 586 | 14.0 | 31.5 | 4.59 | 20.3 | 4.93 | 1.31 | 5.05 | 0.82 | 5.01 | 1.03 | 2.86 | 0.42 | 2.88 | 0.44 | 4.13 | 0.24 | 1.09 | 0.17 | 6.60 | 4.19 | 1.93 |
| ES009 | 211 | 1.92 | 23.2 | 2.24 | 183 | 115 | 19.1 | 38.9 | 377 | 42.9 | 170 | 3.22 | 1.49 | 1.71 | 0.37 | 1.97 | 799 | 14.1 | 33.9 | 5.28 | 25.0 | 6.63 | 1.78 | 7.33 | 1.24 | 7.81 | 1.63 | 4.54 | 0.68 | 4.57 | 0.68 | 5.11 | 0.22 | 0.75 | 0.17 | 6.69 | 2.57 | 1.26 |
| ES019 | 227 | 131 | 28.3 | 45.2 | 49.6 | 72.3 | 16.8 | 17.6 | 634 | 24.7 | 126 | 6.42 | 0.87 | 1.05 | 0.06 | 0.65 | 452 | 13.8 | 31.6 | 4.49 | 20.2 | 4.66 | 1.59 | 4.76 | 0.76 | 4.51 | 0.92 | 2.51 | 0.37 | 2.47 | 0.37 | 3.20 | 0.41 | 0.27 | 0.06 | 3.71 | 1.23 | 0.56 |
| ES027B | 309 | 35.8 | 38.3 | 27.8 | 148 | 91.4 | 19.0 | 8.16 | 450 | 20.1 | 56.0 | 1.47 | 0.49 | 0.60 | 0.18 | 0.38 | 384 | 5.55 | 12.9 | 2.08 | 10.0 | 2.78 | 0.90 | 3.05 | 0.49 | 3.07 | 0.64 | 1.77 | 0.27 | 1.76 | 0.26 | 1.51 | 0.07 | 0.18 | 0.07 | 2.39 | 0.71 | 0.37 |
| ES028B | 392 | 18.6 | 31.4 | 8.51 | 244 | 96.6 | 20.8 | 13.9 | 506 | 22.9 | 63.6 | 1.57 | 0.65 | 0.67 | 0.26 | 0.58 | 427 | 6.30 | 14.7 | 2.35 | 11.1 | 3.11 | 1.00 | 3.43 | 0.55 | 3.39 | 0.70 | 1.93 | 0.29 | 1.90 | 0.29 | 1.64 | 0.07 | 0.25 | 0.06 | 2.98 | 0.82 | 0.50 |
| ES 031 | 386 | 20.8 | 32.1 | 8.93 | 264 | 100 | 21.1 | 16.7 | 505 | 26.4 | 77.0 | 1.91 | 0.78 | 0.78 | 0.32 | 0.74 | 487 | 7.41 | 17.3 | 2.77 | 13.3 | 3.63 | 1.11 | 3.96 | 0.64 | 3.93 | 0.81 | 2.22 | 0.33 | 2.18 | 0.32 | 1.98 | 0.09 | 0.29 | 0.05 | 2.85 | 1.00 | 0.60 |
| ES035A | 104 | 3.54 | 13.0 | 2.15 | 19.6 | 104 | 19.7 | 30.3 | 526 | 34.8 | 115 | 2.74 | 1.21 | 1.52 | 0.40 | 1.33 | 809 | 11.4 | 27.0 | 4.20 | 19.8 | 5.20 | 1.57 | 5.56 | 0.88 | 5.34 | 1.10 | 3.03 | 0.45 | 3.00 | 0.45 | 3.04 | 0.13 | 0.44 | 0.07 | 5.48 | 1.97 | 1.05 |
| ES036C | 256 | 11.6 | 31.5 | 12.7 | 128 | 82.8 | 19.9 | 29.4 | 462 | 21.1 | 75.0 | 1.60 | 0.96 | 0.64 | 0.21 | 1.28 | 470 | 7.94 | 17.1 | 2.54 | 11.2 | 2.95 | 1.00 | 3.15 | 0.51 | 3.16 | 0.65 | 1.80 | 0.27 | 1.83 | 0.28 | 1.91 | 0.09 | 0.40 | 0.13 | 3.96 | 2.19 | 1.05 |
| ES038 | 264 | 9.92 | 29.4 | 10.8 | 111 | 76.6 | 18.1 | 23.5 | 467 | 18.0 | 59.9 | 1.24 | 0.84 | 0.59 | 0.17 | 1.24 | 456 | 7.42 | 16.5 | 2.41 | 11.1 | 2.86 | 1.05 | 3.14 | 0.53 | 3.28 | 0.68 | 1.91 | 0.28 | 1.94 | 0.30 | 1.93 | 0.10 | 0.47 | 0.06 | 3.83 | 1.97 | 0.95 |
| ES SSI | 108 | 0.34 | 18.3 | 1.03 | 61.8 | 123 | 18.7 | 47.8 | 353 | 48.6 | 195 | 3.80 | 1.70 | 1.68 | 0.41 | 2.17 | 939 | 16.4 | 38.7 | 6.00 | 28.3 | 7.48 | 1.86 | 8.16 | 1.35 | 8.45 | 1.76 | 4.91 | 0.74 | 4.95 | 0.74 | 5.55 | 0.25 | 0.83 | 0.17 | 7.79 | 2.92 | 1.49 |
| ES SSII | 103 | 0.36 | 17.8 | 0.91 | 55.9 | 121 | 18.6 | 47.1 | 353 | 48.6 | 197 | 3.15 | 1.64 | 0.85 | 0.38 | 1.84 | 951 | 16.5 | 38.9 | 6.00 | 28.3 | 7.50 | 1.85 | 8.15 | 1.35 | 8.44 | 1.76 | 4.91 | 0.74 | 4.95 | 0.75 | 5.54 | 0.16 | 0.69 | 0.18 | 7.84 | 2.92 | 1.49 |
| *El Salvador behind the volcanic front* | | | | | | | | | | | | | | | | | | | | | | | | | | | | | | | | | | | | | | |
| ES013 | 252 | 221 | 35.0 | 76.1 | 65.2 | 81.7 | 17.3 | 12.8 | 534 | 21.3 | 92.8 | 3.03 | 0.59 | 0.72 | 0.11 | 0.41 | 436 | 9.89 | 22.3 | 3.34 | 15.3 | 3.73 | 1.19 | 3.88 | 0.62 | 3.74 | 0.76 | 2.11 | 0.31 | 2.08 | 0.32 | 2.46 | 0.19 | 0.25 | 0.07 | 3.29 | 0.90 | 0.41 |
| ES014 | 206 | 68.6 | 28.0 | 32.0 | 69.7 | 93.7 | 19.6 | 23.7 | 548 | 39.1 | 205 | 6.88 | 1.26 | 1.11 | 0.10 | 0.49 | 653 | 20.4 | 41.0 | 6.02 | 25.7 | 5.59 | 1.59 | 5.73 | 0.86 | 5.13 | 1.07 | 2.99 | 0.44 | 2.91 | 0.46 | 4.42 | 0.29 | 0.31 | 0.13 | 6.53 | 1.23 | 0.54 |
| ES015 | 187 | 155 | 28.0 | 62.4 | 45.1 | 84.6 | 17.4 | 17.5 | 564 | 26.9 | 183 | 7.29 | 1.01 | 1.30 | 0.12 | 0.53 | 521 | 16.4 | 37.5 | 5.34 | 23.4 | 5.23 | 1.58 | 5.22 | 0.81 | 4.77 | 0.96 | 2.65 | 0.39 | 2.61 | 0.39 | 4.26 | 0.43 | 0.32 | 0.10 | 5.91 | 1.22 | 0.51 |
| ES016 | 198 | 143 | 27.8 | 53.5 | 48.2 | 84.7 | 18.4 | 19.3 | 555 | 29.6 | 194 | 8.43 | 1.08 | 1.26 | 0.13 | 0.53 | 494 | 16.8 | 38.1 | 5.38 | 23.1 | 5.23 | 1.56 | 5.20 | 0.79 | 4.66 | 0.93 | 2.57 | 0.38 | 2.55 | 0.38 | 4.21 | 0.38 | 0.28 | 0.09 | 5.60 | 1.37 | 0.56 |
| ES017 | 235 | 148 | 32.8 | 66.6 | 52.8 | 93.8 | 20.0 | 19.9 | 581 | 31.4 | 201 | 13.0 | 1.59 | 1.26 | 0.07 | 0.43 | 523 | 17.3 | 38.0 | 5.33 | 22.8 | 5.28 | 1.65 | 5.31 | 0.81 | 4.79 | 0.96 | 2.62 | 0.39 | 2.56 | 0.39 | 4.04 | 0.58 | 0.26 | 0.10 | 5.08 | 1.48 | 0.64 |
| ES018B | 213 | 94.2 | 26.6 | 36.0 | 47.6 | 80.5 | 17.7 | 15.6 | 580 | 27.9 | 189 | 7.95 | 0.99 | 1.24 | 0.10 | 0.45 | 450 | 16.7 | 39.4 | 5.64 | 24.7 | 5.51 | 1.76 | 5.49 | 0.87 | 5.19 | 1.05 | 2.86 | 0.42 | 2.80 | 0.42 | 4.54 | 0.48 | 0.28 | 0.07 | 4.96 | 1.08 | 0.45 |
| ES024B | 243 | 232 | 36.8 | 98.4 | 55.7 | 73.8 | 16.5 | 12.0 | 518 | 21.1 | 95.2 | 3.96 | 0.64 | 0.78 | 0.07 | 0.45 | 390 | 9.64 | 22.1 | 3.25 | 14.9 | 3.65 | 1.26 | 3.86 | 0.64 | 3.93 | 0.81 | 2.21 | 0.32 | 2.18 | 0.33 | 2.63 | 0.27 | 0.19 | 0.02 | 2.48 | 1.17 | 0.48 |
| *Honduras volcanic front* | | | | | | | | | | | | | | | | | | | | | | | | | | | | | | | | | | | | | | |
| H3B | 87.72 | 0.86 | 12.2 | 2.12 | 23.8 | 98.5 | 19.3 | 12.6 | 541 | 29.1 | 90.0 | 3.47 | 0.76 | 0.91 | 0.26 | 0.45 | 636 | 9.71 | 21.8 | 3.44 | 16.3 | 4.30 | 1.42 | 4.62 | 0.73 | 4.48 | 0.93 | 2.60 | 0.39 | 2.65 | 0.40 | 2.28 | 0.15 | 1.01 | 0.06 | 3.69 | 0.82 | 0.51 |
| *Honduras behind the volcanic front* | | | | | | | | | | | | | | | | | | | | | | | | | | | | | | | | | | | | | | |
| H1 | 257 | 45.8 | 30.6 | 22.1 | 95.6 | 82.7 | 18.0 | 19.6 | 584 | 18.5 | 69.6 | 14.8 | 1.16 | 0.78 | 0.15 | 0.52 | 481 | 13.2 | 24.2 | 3.15 | 13.6 | 3.21 | 1.11 | 3.33 | 0.53 | 3.23 | 0.66 | 1.83 | 0.27 | 1.82 | 0.27 | 1.87 | 0.75 | 1.19 | 0.03 | 2.60 | 2.75 | 0.75 |
| H4B | 312 | 3.05 | 26.2 | 4.64 | 173 | 104.9 | 22.0 | 13.2 | 544 | 22.6 | 77.8 | 2.77 | 0.67 | 0.71 | 0.17 | 0.43 | 564 | 7.84 | 17.3 | 2.63 | 12.3 | 3.25 | 1.09 | 3.49 | 0.55 | 3.43 | 0.71 | 1.98 | 0.30 | 1.99 | 0.30 | 1.94 | 0.13 | 0.19 | 0.05 | 3.17 | 0.84 | 0.51 |
| H5 | 325 | 4.44 | 27.7 | 5.64 | 148 | 93.7 | 20.2 | 7.81 | 527 | 39.4 | 58.9 | 2.19 | 0.50 | 0.62 | 0.11 | 0.20 | 462 | 9.70 | 15.2 | 3.05 | 14.6 | 3.87 | 1.42 | 4.73 | 0.73 | 4.51 | 0.98 | 2.69 | 0.38 | 2.44 | 0.37 | 1.48 | 0.10 | 0.18 | 0.03 | 2.24 | 0.51 | 0.37 |
| H9 | 227 | 108 | 31.7 | 45.1 | 66.7 | 99.4 | 19.4 | 16.4 | 605 | 26.4 | 147 | 6.97 | 0.91 | 1.00 | 0.09 | 0.40 | 554 | 16.5 | 34.2 | 5.05 | 22.1 | 4.89 | 1.52 | 4.84 | 0.71 | 4.11 | 0.83 | 2.22 | 0.33 | 2.11 | 0.32 | 3.29 | 0.29 | 0.25 | 0.07 | 5.02 | 1.07 | 0.38 |
| H13 | 201 | 93.3 | 30.9 | 44.8 | 29.0 | 86.5 | 19.3 | 18.4 | 586 | 35.1 | 278 | 29.5 | 2.29 | 1.70 | 0.05 | 0.24 | 336 | 24.3 | 50.5 | 6.67 | 27.4 | 6.15 | 1.94 | 6.25 | 0.96 | 5.62 | 1.13 | 3.06 | 0.45 | 2.94 | 0.44 | 5.30 | 1.42 | 0.27 | 0.07 | 3.35 | 1.91 | 0.81 |
| H14 | 231 | 174 | 33.8 | 61.7 | 71.1 | 93.4 | 18.2 | 27.6 | 535 | 73.6 | 149 | 6.52 | 0.67 | 0.95 | 0.08 | 0.38 | 721 | 38.1 | 59.9 | 11.5 | 50.1 | 11.9 | 3.70 | 12.4 | 1.91 | 11.2 | 2.21 | 5.88 | 0.86 | 5.58 | 0.81 | 3.42 | 0.35 | 0.35 | 0.08 | 5.45 | 1.62 | 0.57 |
| H16 | 238 | 64.5 | 26.6 | 28.5 | 74.8 | 94.5 | 18.6 | 27.2 | 652 | 22.3 | 167 | 7.61 | 1.06 | 1.17 | 0.06 | 0.58 | 685 | 20.9 | 44.7 | 6.14 | 26.1 | 5.55 | 1.54 | 5.09 | 0.74 | 4.29 | 0.84 | 2.26 | 0.33 | 2.14 | 0.33 | 3.94 | 0.42 | 0.25 | 0.12 | 6.38 | 1.46 | 0.52 |

(*continued on next page*)

Table 1 (*continued*)

| Sample # | V ppm | Cr ppm | Co ppm | Ni ppm | Cu ppm | Zn ppm | Ga ppm | Rb ppm | Sr ppm | Y ppm | Zr ppm | Nb ppm | Mo ppm | Sn ppm | Sb ppm | Cs ppm | Ba ppm | La ppm | Ce ppm | Pr ppm | Nd ppm | Sm ppm | Eu ppm | Gd ppm | Tb ppm | Dy ppm | Ho ppm | Er ppm | Tm ppm | Yb ppm | Lu ppm | Hf ppm | T a ppm | W ppm | Tl ppm | Pb ppm | Th ppm | U ppm |
|---|---|---|---|---|---|---|---|---|---|---|---|---|---|---|---|---|---|---|---|---|---|---|---|---|---|---|---|---|---|---|---|---|---|---|---|---|
| *Honduras backarc* | | | | | | | | | | | | | | | | | | | | | | | | | | | | | | | | | | | | |
| H10 | 164 | 15.1 | 23.3 | 11.2 | 18.7 | 109 | 21.6 | 22.7 | 505 | 41.7 | 275 | 47.1 | 3.41 | 1.82 | 0.07 | 0.30 | 408 | 31.2 | 66.3 | 8.75 | 37.0 | 8.33 | 3.08 | 8.38 | 1.30 | 7.62 | 1.49 | 3.97 | 0.56 | 3.69 | 0.54 | 5.62 | 2.73 | 0.58 | 0.06 | 3.03 | 2.98 | 1.05 |
| H17A | 213 | 242 | 34.5 | 90.3 | 56.4 | 72.9 | 17.0 | 30.4 | 603 | 27.5 | 185 | 61.3 | 2.33 | 1.36 | 0.05 | 0.29 | 545 | 33.2 | 60.8 | 7.06 | 26.4 | 5.25 | 1.80 | 5.15 | 0.81 | 4.79 | 0.95 | 2.56 | 0.37 | 2.48 | 0.37 | 3.54 | 3.15 | 0.87 | 0.10 | 1.98 | 4.45 | 1.09 |
| H18A | 163 | 175 | 28.7 | 58.5 | 47.8 | 70.8 | 17.4 | 39.3 | 528 | 25.8 | 196 | 64.5 | 3.42 | 1.43 | 0.06 | 0.31 | 482 | 35.3 | 64.1 | 7.12 | 27.3 | 5.43 | 1.76 | 5.36 | 0.83 | 4.93 | 0.98 | 2.67 | 0.39 | 2.56 | 0.38 | 3.83 | 3.37 | 0.44 | 0.07 | 2.16 | 4.93 | 1.20 |
| *NW Nicaragua volcanic front* | | | | | | | | | | | | | | | | | | | | | | | | | | | | | | | | | | | | |
| P-60 | 165 | 1.32 | 15.0 | 3.06 | 144 | 67.3 | 18.9 | 30.5 | 422 | 32.3 | 92.0 | 1.16 | 1.01 | 0.65 | 0.77 | 1.10 | 984 | 11.0 | 19.1 | 3.54 | 16.7 | 4.25 | 1.24 | 4.89 | 0.78 | 4.89 | 1.04 | 2.90 | 0.43 | 2.85 | 0.44 | 2.70 | 0.08 | 0.45 | n.d. | 3.84 | 1.39 | 1.07 |
| P-58A | 140 | 1.22 | 15.9 | 2.06 | 86.6 | 89.8 | 19.2 | 29.6 | 406 | 31.9 | 105 | 1.68 | 1.11 | 1.00 | 0.81 | 1.48 | 897 | 9.34 | 21.8 | 3.52 | 17.0 | 4.65 | 1.33 | 5.17 | 0.86 | 5.49 | 1.15 | 3.21 | 0.49 | 3.29 | 0.50 | 3.11 | 0.11 | 0.39 | n.d. | 4.25 | 1.49 | 1.22 |
| P-27A | n.d. | n.d. | n.d. | n.d. | 214 | n.d. | n.d. | 12.8 | 531 | 21.5 | 52.1 | 0.99 | 0.50 | 0.69 | 0.07 | 0.45 | 536 | 6.17 | 14.4 | 2.40 | 12.1 | 3.46 | 1.21 | 3.96 | 0.66 | 4.19 | 0.88 | 2.35 | 0.37 | 2.45 | 0.37 | 1.81 | 0.06 | 0.16 | 0.03 | 2.05 | 0.62 | 0.61 |
| P-13 | 271 | 4.28 | 27.6 | 6.93 | 117 | 91.1 | 18.7 | 19.6 | 499 | 24.9 | 66.4 | 1.41 | 0.59 | 0.68 | 0.11 | 0.21 | 704 | 7.86 | 18.4 | 2.97 | 14.3 | 3.87 | 1.17 | 4.09 | 0.68 | 4.25 | 0.88 | 2.50 | 0.37 | 2.47 | 0.37 | 2.01 | 0.08 | 0.18 | 0.24 | 3.16 | 1.08 | 0.92 |
| P2-16 (*) | 310 | 24.0 | 34.8 | 22.6 | 134 | 67.8 | 16.2 | 15.4 | 495 | 16.7 | 48.3 | 1.58 | 0.56 | 0.52 | 0.32 | 0.66 | 462 | 4.37 | 11.0 | 1.81 | 8.68 | 2.50 | 0.82 | 2.93 | 0.48 | 3.04 | 0.62 | 1.71 | 0.25 | 1.69 | 0.25 | 1.58 | 0.10 | 0.27 | 0.07 | 2.05 | 0.75 | 0.64 |
| P-7A | n.d. | n.d. | n.d. | n.d. | 183 | n.d. | n.d. | 25.8 | 489 | 20.4 | 77.0 | 1.86 | 0.92 | 0.77 | 0.49 | 1.12 | 743 | 6.45 | 14.8 | 2.38 | 11.5 | 3.27 | 1.09 | 3.74 | 0.62 | 3.90 | 0.81 | 2.19 | 0.34 | 2.31 | 0.34 | 2.52 | 0.13 | 0.37 | 0.12 | 2.74 | 1.15 | 1.12 |
| P-9 | 318 | 31.4 | 34.5 | 25.6 | 151 | 78.2 | 18.2 | 19.5 | 490 | 20.5 | 78.5 | 5.01 | 0.84 | 0.79 | 0.32 | 0.78 | 555 | 6.34 | 14.6 | 2.32 | 11.3 | 3.23 | 1.06 | 3.48 | 0.58 | 3.57 | 0.73 | 2.00 | 0.29 | 1.92 | 0.29 | 2.19 | 0.31 | 0.23 | 0.06 | 2.42 | 0.95 | 0.79 |
| P-43 | n.d. | n.d. | n.d. | n.d. | 185 | n.d. | n.d. | 22.1 | 410 | 26.4 | 108 | 6.45 | 1.19 | 1.07 | 0.40 | 0.99 | 680 | 8.30 | 19.4 | 2.97 | 14.5 | 4.15 | 1.42 | 4.85 | 0.82 | 5.16 | 1.08 | 2.87 | 0.45 | 2.99 | 0.45 | 3.29 | 0.40 | 0.36 | 0.11 | 2.70 | 1.05 | 0.93 |
| P-51 | n.d. | n.d. | n.d. | n.d. | 122 | n.d. | n.d. | 12.0 | 490 | 16.3 | 51.4 | 1.49 | 0.53 | 0.60 | 0.14 | 0.42 | 362 | 5.55 | 12.8 | 2.05 | 9.95 | 2.75 | 0.95 | 3.15 | 0.51 | 3.24 | 0.67 | 1.79 | 0.28 | 1.84 | 0.28 | 1.69 | 0.10 | 0.15 | 0.07 | 1.56 | 0.52 | 0.48 |
| P-56G | n.d. | n.d. | n.d. | n.d. | 168 | n.d. | n.d. | 12.0 | 595 | 22.6 | 49.9 | 0.86 | 0.54 | 0.70 | 0.09 | 0.48 | 764 | 6.93 | 15.7 | 2.59 | 12.9 | 3.70 | 1.48 | 4.23 | 0.70 | 4.44 | 0.92 | 2.47 | 0.39 | 2.60 | 0.40 | 1.78 | 0.06 | 0.15 | 0.11 | 2.66 | 0.59 | 0.58 |
| P-4 | n.d. | n.d. | n.d. | n.d. | 141 | n.d. | n.d. | 7.19 | 429 | 14.2 | 32.8 | 0.98 | 0.45 | 0.41 | 0.17 | 0.37 | 365 | 3.23 | 7.43 | 1.22 | 6.28 | 1.96 | 0.81 | 2.43 | 0.42 | 2.77 | 0.58 | 1.57 | 0.24 | 1.64 | 0.25 | 1.13 | 0.07 | 0.15 | 0.04 | 1.30 | 0.31 | 0.31 |
| P-6 | 334 | 18.7 | 31.1 | 15.3 | 174 | 81.0 | 19.5 | 7.37 | 478 | 16.6 | 39.8 | 1.30 | 0.54 | 0.50 | 0.19 | 0.35 | 436 | 3.61 | 8.60 | 1.40 | 7.12 | 2.17 | 0.83 | 2.52 | 0.44 | 2.87 | 0.60 | 1.70 | 0.25 | 1.69 | 0.25 | 1.22 | 0.11 | 0.13 | 0.04 | 2.02 | 0.40 | 0.36 |
| P2-3a (*) | 287 | 142 | 49.7 | 65.0 | 112 | 67.4 | 14.1 | 4.31 | 375 | 11.2 | 20.5 | 0.69 | 0.27 | 0.28 | 0.12 | 0.23 | 247 | 1.93 | 4.90 | 0.86 | 4.38 | 1.40 | 0.46 | 1.74 | 0.31 | 1.99 | 0.41 | 1.16 | 0.17 | 1.14 | 0.17 | 0.65 | 0.05 | 0.09 | 0.02 | 1.06 | 0.19 | 0.17 |
| P2-3b (*) | 279 | 11.0 | 26.1 | 11.5 | 126 | 67.1 | 17.8 | 6.35 | 505 | 13.2 | 28.2 | 0.93 | 0.37 | 0.40 | 0.15 | 0.32 | 344 | 2.67 | 6.52 | 1.13 | 5.61 | 1.70 | 0.52 | 2.06 | 0.35 | 2.30 | 0.48 | 1.35 | 0.20 | 1.37 | 0.20 | 0.85 | 0.06 | 0.11 | 0.03 | 1.49 | 0.30 | 0.27 |
| P2-3d (*) | 323 | 49.6 | 34.6 | 24.5 | 153 | 74.7 | 16.9 | 7.08 | 439 | 14.6 | 31.0 | 0.95 | 0.41 | 0.37 | 0.17 | 0.36 | 362 | 2.79 | 6.85 | 1.18 | 5.96 | 1.84 | 0.55 | 2.26 | 0.39 | 2.54 | 0.53 | 1.51 | 0.22 | 1.51 | 0.23 | 0.93 | 0.06 | 0.13 | 0.04 | 1.56 | 0.34 | 0.30 |
| P2-11 | 350 | 11.3 | 31.9 | 13.0 | 163 | 85.7 | 18.1 | 7.28 | 481 | 15.1 | 32.5 | 1.15 | 0.46 | 0.45 | 0.19 | 0.37 | 395 | 3.35 | 7.77 | 1.28 | 6.50 | 1.98 | 0.78 | 2.37 | 0.41 | 2.65 | 0.56 | 1.56 | 0.23 | 1.55 | 0.24 | 1.02 | 0.07 | 0.10 | 0.04 | 1.64 | 0.33 | 0.30 |
| P2-13 | 326 | 75.3 | 44.3 | 40.4 | 146 | 85.3 | 16.0 | 7.31 | 402 | 14.6 | 32.1 | 1.10 | 0.48 | 0.43 | 0.19 | 0.37 | 376 | 3.20 | 7.45 | 1.24 | 6.22 | 1.92 | 0.75 | 2.30 | 0.40 | 2.58 | 0.54 | 1.53 | 0.23 | 1.52 | 0.23 | 1.02 | 0.07 | 0.10 | 0.03 | 1.75 | 0.33 | 0.29 |
| P-50 | 277 | 102 | 35.1 | 30.8 | 142 | 69.4 | 15.8 | 11.7 | 477 | 17.6 | 53.3 | 1.57 | 0.53 | 0.58 | 0.14 | 0.41 | 369 | 5.42 | 12.6 | 2.03 | 9.69 | 2.63 | 0.87 | 2.86 | 0.48 | 3.00 | 0.61 | 1.72 | 0.25 | 1.70 | 0.25 | 1.51 | 0.10 | 0.14 | 0.05 | 1.90 | 0.57 | 0.47 |
| P-19 | n.d. | n.d. | n.d. | n.d. | 113 | n.d. | n.d. | 16.3 | 442 | 20.4 | 73.9 | 2.52 | 0.66 | 0.75 | 0.23 | 0.68 | 493 | 6.67 | 15.5 | 2.44 | 11.8 | 3.26 | 1.10 | 3.80 | 0.64 | 3.98 | 0.82 | 2.20 | 0.34 | 2.30 | 0.34 | 2.33 | 0.16 | 0.24 | 0.05 | 1.92 | 0.77 | 0.65 |
| P-40A | n.d. | n.d. | n.d. | n.d. | 165 | n.d. | n.d. | 5.70 | 437 | 12.4 | 27.0 | 0.72 | 0.24 | 0.43 | 0.10 | 0.25 | 311 | 3.05 | 6.80 | 1.13 | 5.79 | 1.78 | 0.72 | 2.17 | 0.38 | 2.46 | 0.51 | 1.37 | 0.21 | 1.42 | 0.22 | 0.95 | 0.05 | 0.09 | 0.04 | 0.99 | 0.26 | 0.27 |
| P-42 | 317 | 63.1 | 47.9 | 38.4 | 130 | 78.6 | 16.0 | 6.96 | 380 | 15.1 | 35.4 | 1.10 | 0.42 | 0.45 | 0.17 | 0.33 | 391 | 3.20 | 7.46 | 1.25 | 6.28 | 1.91 | 0.71 | 2.24 | 0.39 | 2.56 | 0.54 | 1.53 | 0.23 | 1.53 | 0.23 | 1.07 | 0.06 | 0.11 | 0.05 | 1.76 | 0.35 | 0.32 |
| P-23 | n.d. | n.d. | n.d. | n.d. | 90.3 | n.d. | n.d. | 23.7 | 399 | 25.6 | 105 | 4.46 | 1.15 | 0.98 | 0.37 | 1.05 | 778 | 9.19 | 20.9 | 3.27 | 15.4 | 4.18 | 1.33 | 4.74 | 0.78 | 4.88 | 1.02 | 2.74 | 0.42 | 2.84 | 0.44 | 3.21 | 0.28 | 0.35 | 0.14 | 3.00 | 1.13 | 0.98 |
| P-46A | n.d. | n.d. | n.d. | n.d. | 60.7 | n.d. | n.d. | 33.6 | 406 | 29.2 | 127 | 4.99 | 1.53 | 1.17 | 0.67 | 1.63 | 1005 | 9.83 | 22.5 | 3.47 | 16.4 | 4.60 | 1.47 | 5.28 | 0.88 | 5.59 | 1.16 | 3.17 | 0.50 | 3.34 | 0.51 | 3.97 | 0.32 | 0.51 | 0.10 | 3.87 | 1.54 | 1.43 |
| P-47A | n.d. | n.d. | n.d. | n.d. | 52.8 | n.d. | n.d. | 36.4 | 400 | 30.0 | 133 | 4.78 | 1.64 | 1.14 | 0.73 | 1.76 | 1085 | 10.2 | 23.3 | 3.58 | 17.0 | 4.71 | 1.49 | 5.37 | 0.89 | 5.71 | 1.19 | 3.24 | 0.50 | 3.40 | 0.52 | 4.15 | 0.31 | 0.54 | 0.16 | 4.45 | 1.66 | 1.55 |
| P-48B | n.d. | n.d. | n.d. | n.d. | 173 | n.d. | n.d. | 26.3 | 413 | 24.5 | 98.3 | 3.56 | 1.30 | 0.93 | 0.56 | 1.29 | 830 | 7.91 | 18.0 | 2.80 | 13.4 | 3.80 | 1.25 | 4.38 | 0.74 | 4.72 | 0.99 | 2.69 | 0.42 | 2.82 | 0.43 | 3.14 | 0.23 | 0.41 | 0.16 | 3.45 | 1.21 | 1.12 |
| P-32 | n.d. | n.d. | n.d. | n.d. | 136 | n.d. | n.d. | 13.6 | 464 | 17.6 | 52.6 | 1.34 | 0.67 | 0.56 | 0.25 | 0.62 | 599 | 5.57 | 12.5 | 2.00 | 9.70 | 2.79 | 1.01 | 3.21 | 0.53 | 3.41 | 0.72 | 1.92 | 0.30 | 2.04 | 0.31 | 1.77 | 0.09 | 0.21 | 0.10 | 2.03 | 0.60 | 0.62 |
| P-34 | 259 | 10.4 | 26.3 | 8.70 | 153 | 76.1 | 17.4 | 17.9 | 464 | 22.8 | 71.6 | 1.76 | 0.84 | 0.65 | 0.34 | 0.83 | 781 | 6.70 | 15.2 | 2.41 | 11.5 | 3.24 | 1.01 | 3.52 | 0.60 | 3.80 | 0.79 | 2.28 | 0.33 | 2.26 | 0.34 | 2.09 | 0.11 | 0.23 | 0.10 | 3.02 | 0.87 | 0.79 |
| *Guatemala basement* | | | | | | | | | | | | | | | | | | | | | | | | | | | | | | | | | | | | |
| G 009 L1 | 249 | 95.8 | 30.6 | 42.0 | 98.7 | 105 | 17.9 | 38.7 | 346 | 24.3 | 5.43 | 4.00 | 0.51 | 0.94 | 0.24 | 2.46 | 590 | 9.88 | 20.8 | 3.15 | 14.4 | 3.84 | 1.26 | 4.20 | 0.71 | 4.47 | 0.93 | 2.59 | 0.40 | 2.65 | 0.40 | 0.40 | 0.25 | 0.62 | 0.07 | 5.36 | 1.51 | 0.47 |
| G 009 L2 | 148 | 13.5 | 19.0 | 15.3 | 100.0 | 101 | 20.2 | 63.1 | 367 | 27.0 | 10.8 | 13.7 | 2.85 | 1.15 | 0.11 | 0.83 | 1639 | 20.6 | 45.7 | 6.42 | 27.8 | 6.19 | 1.83 | 5.91 | 0.88 | 5.09 | 1.00 | 2.67 | 0.38 | 2.38 | 0.34 | 0.43 | 0.76 | 0.49 | 0.13 | 7.82 | 2.81 | 0.63 |
| Chor 8A | 196 | 107 | 29.2 | 77.3 | 3.18 | 60.9 | 17.6 | 11.9 | 303 | 19.2 | 8.63 | 6.50 | 0.37 | 2.34 | 0.07 | 1.44 | 85.8 | 6.07 | 14.9 | 2.21 | 10.4 | 2.84 | 1.06 | 3.29 | 0.56 | 3.47 | 0.72 | 1.96 | 0.29 | 1.89 | 0.28 | 0.50 | 0.37 | 0.32 | 0.08 | 5.04 | 0.44 | 0.20 |
| P12 | 251 | 22.7 | 28.5 | 12.7 | 164 | 109 | 23.6 | 35.7 | 582 | 17.8 | 21.5 | 10.1 | 1.13 | 1.16 | 0.03 | 0.42 | 721 | 20.8 | 41.3 | 5.38 | 22.5 | 4.77 | 1.38 | 4.47 | 0.64 | 3.50 | 0.66 | 1.70 | 0.23 | 1.48 | 0.21 | 1.16 | 0.52 | 0.15 | | 5.57 | 0.92 | 0.45 |
| G3K | 4.64 | 0.37 | 0.54 | 0.26 | 3.32 | 22.0 | 14.6 | 129 | 39.0 | 8.95 | 18.9 | 10.3 | 1.07 | 1.34 | 0.06 | 2.19 | 589 | 14.4 | 27.4 | 3.31 | 11.8 | 2.22 | 0.26 | 1.95 | 0.29 | 1.65 | 0.33 | 0.92 | 0.14 | 0.97 | 0.15 | 0.70 | 0.87 | 0.67 | 0.64 | 10.3 | 8.8 | 1.44 |
| M1 | | | | | | | | | | | | | | | | | | | | | | | | | | | | | | | | | | | | |
| M2 | 62.9 | 42.2 | 0.30 | 28.3 | 4.06 | 9.24 | 14.0 | 96.5 | 36.8 | 6.39 | 11.1 | 13.9 | 0.45 | 1.86 | 2.27 | 5.23 | 1321 | 24.9 | 51.9 | 6.05 | 22.1 | 3.92 | 0.76 | 2.96 | 0.38 | 1.71 | 0.28 | 0.70 | 0.09 | 0.62 | 0.08 | 0.39 | 0.86 | 4.43 | 1.09 | 3.12 | 5.20 | 1.47 |
| 619 | 81.7 | 14.9 | 7.50 | 5.21 | 7.14 | 55.5 | 18.5 | 137 | 178 | 14.9 | 3.42 | 12.6 | 0.32 | 4.59 | 0.01 | 3.84 | 432 | 31.8 | 64.0 | 7.50 | 27.6 | 5.47 | 0.96 | 4.96 | 0.70 | 3.52 | 0.59 | 1.35 | 0.16 | 0.92 | 0.12 | 0.14 | 0.87 | 0.32 | 0.89 | 14.1 | 13.6 | 1.78 |
| 714A | 61.6 | 1.58 | 9.45 | 2.13 | 7.64 | 179 | 37.0 | 260 | 392 | 206 | 17.0 | 86.7 | 4.07 | 10.4 | 0.03 | 0.48 | 906 | 180 | 401 | 55.2 | 215 | 46.4 | 6.79 | 42.8 | 6.93 | 41.2 | 7.96 | 21.8 | 3.33 | 21.9 | 2.98 | 0.98 | 5.63 | 0.62 | 1.54 | 22.4 | 51.9 | 16.7 |
| *Cocos plate sediments* | | | | | | | | | | | | | | | | | | | | | | | | | | | | | | | | | | | | |
| 67_0495_009R_02W_73-75 | 162 | 58.6 | 30.0 | 216 | 158 | 309 | 16.7 | 38.1 | 308 | 20.87 | 82.42 | 3.64 | 4.85 | 0.87 | 4.82 | 2.70 | 240 | 11.9 | 23.3 | 3.29 | 14.3 | 3.29 | 0.88 | 3.54 | 0.56 | 3.45 | 0.72 | 2.00 | 0.30 | 2.05 | 0.32 | 2.01 | 0.24 | 1.84 | 1.12 | 6.57 | 2.32 | 4.57 |
| 67_0499_019R_05W_80-82 | 169 | 57.1 | 19.9 | 128 | 142 | 217 | 17.8 | 43.7 | 334 | 18.51 | 92.50 | 4.40 | 4.59 | 1.07 | 3.38 | 3.29 | 1676 | 11.6 | 23.5 | 3.06 | 12.9 | 2.98 | 0.81 | 3.08 | 0.49 | 3.04 | 0.64 | 1.81 | 0.28 | 1.95 | 0.31 | 2.47 | 0.29 | 1.67 | 1.02 | 8.38 | 2.97 | 7.74 |
| *Cocos plate MORB* | | | | | | | | | | | | | | | | | | | | | | | | | | | | | | | | | | | | |
| 67_0495_048R_04W_82-84 | 281 | 338 | 41.4 | 115 | 72.4 | 81.0 | 16.4 | 0.88 | 123 | 34.08 | 108.09 | 1.77 | 0.22 | 1.00 | 0.01 | 0.03 | 4.52 | 3.36 | 11.1 | 1.98 | 10.9 | 3.67 | 1.32 | 4.74 | 0.88 | 5.87 | 1.25 | 3.49 | 0.53 | 3.47 | 0.52 | 2.72 | 0.13 | 0.07 | 0.47 | 0.50 | 0.12 | 0.24 |
| 206_1256C_10R2_103-105 | 432 | 90.8 | 44.9 | 60.6 | 86.5 | 101 | 18.6 | 4.00 | 83.8 | 43.62 | 107.06 | 3.65 | 0.44 | 1.17 | 0.01 | 0.05 | 13.5 | 4.28 | 12.8 | 2.25 | 11.9 | 4.19 | 1.55 | 5.77 | 1.08 | 7.34 | 1.58 | 4.51 | 0.68 | 4.60 | 0.68 | 2.96 | 0.24 | 0.10 | 0.01 | 0.20 | 0.27 | 0.09 |
| 206_1256D_74R2_102-111 | 354 | 44.8 | 47.0 | 49.9 | 80.0 | 98.8 | 16.9 | 0.20 | 74.6 | 32.93 | 70.15 | 1.90 | 0.22 | 0.70 | 0.00 | 0.01 | 6.08 | 2.30 | 7.58 | 1.41 | 7.77 | 2.92 | 1.15 | 4.18 | 0.79 | 5.52 | 1.20 | 3.48 | 0.53 | 3.61 | 0.55 | 2.03 | 0.13 | 0.05 | 0.00 | 0.24 | 0.15 | 0.05 |

| | Selected trace element ratios | | | | | |
|---|---|---|---|---|---|---|
| | Ba/La | Ba/Th | U/Th | Sr/Ce | La/Yb | Zr/Hf |
| *Guatemala volcanic front* | | | | | | |
| GU2A | 40.2 | 428 | 0.43 | 32.0 | 4.49 | 38.1 |
| GU4 | 51.3 | 311 | 0.40 | 26.2 | 6.47 | 38.6 |
| GU5 | 50.6 | 281 | 0.40 | 17.6 | 5.59 | 38.0 |
| GU6 | 41.4 | 347 | 0.38 | 19.5 | 8.08 | 40.3 |
| GU8A | 39.6 | 269 | 0.38 | 16.9 | 5.35 | 37.4 |
| GU15A | 51.6 | 565 | 0.45 | 23.7 | 4.84 | 39.6 |
| GU17A | 52.7 | 454 | 0.42 | 23.4 | 4.68 | 40.1 |
| GU22 | 49.2 | 146 | 0.37 | 14.7 | 6.84 | 35.5 |
| GU23A | 45.2 | 356 | 0.41 | 26.2 | 7.36 | 37.9 |
| GU26 | 46.0 | 200 | 0.34 | 26.3 | 5.75 | 37.7 |
| OTO I | 56.7 | 480 | 0.42 | 31.8 | 4.07 | 35.5 |
| OTO II | 57.3 | 489 | 0.41 | 33.4 | 4.06 | 35.6 |
| *Guatemala behind the volcanic front* | | | | | | |
| GU14A | 26.1 | 340 | 0.29 | 23.8 | 4.21 | 46.7 |
| GU29 | 29.4 | 334 | 0.39 | 16.9 | 5.23 | 43.8 |
| GU30 | 22.6 | 387 | 0.40 | 11.3 | 6.75 | 41.5 |
| GU32 | 28.7 | 332 | 0.33 | 10.7 | 8.44 | 42.8 |
| GU35B | 27.4 | 295 | 0.41 | 19.5 | 5.84 | 46.7 |
| GU38 | 30.0 | 344 | 0.54 | 17.0 | 6.80 | 43.3 |
| GU39 | 33.5 | 370 | 0.41 | 22.7 | 5.63 | 41.9 |
| *El Salvador volcanic front* | | | | | | |
| ES002 | 63.4 | 388 | 0.57 | 13.7 | 3.92 | 34.8 |
| ES003 | 60.2 | 327 | 0.53 | 12.8 | 4.16 | 38.7 |
| ES005 | 42.0 | 140 | 0.46 | 15.1 | 4.85 | 35.6 |
| ES009 | 56.6 | 310 | 0.49 | 11.1 | 3.09 | 33.2 |
| ES019 | 32.7 | 367 | 0.46 | 20.1 | 5.60 | 39.3 |
| ES027B | 69.3 | 538 | 0.51 | 34.9 | 3.14 | 37.0 |
| ES028B | 67.8 | 522 | 0.61 | 34.4 | 3.32 | 38.8 |
| ES 031 | 65.7 | 487 | 0.60 | 29.2 | 3.40 | 38.9 |
| ES035A | 70.8 | 410 | 0.53 | 19.5 | 3.81 | 37.8 |
| ES036C | 59.2 | 215 | 0.48 | 27.0 | 4.34 | 39.3 |
| ES038 | 61.4 | 232 | 0.48 | 28.3 | 3.82 | 30.9 |
| ES SSI | 57.2 | 322 | 0.51 | 9.11 | 3.31 | 35.2 |
| ES SSII | 57.7 | 326 | 0.51 | 9.08 | 3.33 | 35.4 |
| *El Salvador behind the volcanic front* | | | | | | |
| ES013 | 44.1 | 486 | 0.46 | 24.0 | 4.75 | 37.8 |
| ES014 | 32.0 | 529 | 0.44 | 13.3 | 7.01 | 46.4 |
| ES015 | 31.8 | 426 | 0.42 | 15.0 | 6.27 | 43.0 |
| ES016 | 29.4 | 360 | 0.41 | 14.6 | 6.60 | 46.0 |
| ES017 | 30.3 | 354 | 0.43 | 15.3 | 6.76 | 49.8 |
| ES018B | 27.0 | 418 | 0.41 | 14.7 | 5.95 | 41.6 |
| ES024B | 40.5 | 333 | 0.41 | 23.4 | 4.42 | 36.2 |
| *Honduras volcanic front* | | | | | | |
| H3B | 65.5 | 779 | 0.62 | 24.8 | 3.66 | 39.4 |
| *Honduras behind the volcanic front* | | | | | | |
| H1 | 36.4 | 175 | 0.27 | 24.2 | 7.26 | 37.3 |
| H4B | 71.9 | 670 | 0.60 | 31.4 | 3.95 | 40.0 |
| H5 | 47.6 | 913 | 0.74 | 34.8 | 3.97 | 39.7 |
| H9 | 33.5 | 518 | 0.36 | 17.7 | 7.85 | 44.7 |
| H13 | 13.8 | 176 | 0.43 | 11.6 | 8.25 | 52.5 |
| H14 | 18.9 | 445 | 0.35 | 8.9 | 6.83 | 43.5 |
| H16 | 32.8 | 468 | 0.36 | 14.6 | 9.74 | 42.3 |
| *Honduras backarc* | | | | | | |
| H10 | 13.1 | 137 | 0.35 | 7.6 | 8.45 | 49.0 |
| H17A | 16.4 | 123 | 0.24 | 9.9 | 13.4 | 52.4 |
| H18A | 13.7 | 97.9 | 0.24 | 8.2 | 13.8 | 51.2 |

(*continued on next page*)

Table 1 (*continued*)

| | Selected trace element ratios | | | | | |
|---|---|---|---|---|---|---|
| | Ba/La | Ba/Th | U/Th | Sr/Ce | La/Yb | Zr/Hf |
| *NW Nicaragua volcanic front* | | | | | | |
| P-60 | 89.1 | 708 | 0.77 | 22.1 | 3.87 | 34.1 |
| P-58A | 96.1 | 602 | 0.82 | 18.6 | 2.84 | 33.6 |
| P-27A | 86.9 | 861 | 0.98 | 36.8 | 2.52 | 28.8 |
| P-13 | 90 | 652 | 0.85 | 27.2 | 3.18 | 33.0 |
| P2-16 (*) | 106 | 616 | 0.85 | 45.0 | 2.58 | 30.6 |
| P-7A | 115.2 | 646 | 0.97 | 33.0 | 2.79 | 30.6 |
| P-9 | 87.5 | 582 | 0.83 | 33.7 | 3.30 | 35.8 |
| P-43 | 82.0 | 646 | 0.89 | 21.1 | 2.78 | 32.8 |
| P-51 | 65 | 693 | 0.92 | 38.2 | 3.02 | 30.4 |
| P-56G | 110 | 1305 | 0.99 | 37.8 | 2.67 | 28.0 |
| P-4 | 113 | 1180 | 1.00 | 57.7 | 1.97 | 29.1 |
| P-6 | 121 | 1097 | 0.91 | 55.6 | 2.14 | 32.7 |
| P2-3a (*) | 128 | 1279 | 0.89 | 76.5 | 1.70 | 31.7 |
| P2-3b (*) | 129 | 1156 | 0.91 | 77.5 | 1.94 | 33.2 |
| P2-3d (*) | 130 | 1080 | 0.91 | 64.1 | 1.84 | 33.2 |
| P2-11 | 118 | 1198 | 0.91 | 61.8 | 2.17 | 31.9 |
| P2-13 | 117.4 | 1127 | 0.86 | 54.0 | 2.11 | 31.6 |
| P-50 | 68.1 | 653 | 0.83 | 37.8 | 3.18 | 35.2 |
| P-19 | 74 | 644 | 0.85 | 28.6 | 2.90 | 31.8 |
| P-40A | 102 | 1213 | 1.06 | 64.3 | 2.15 | 28.3 |
| P-42 | 122.1 | 1126 | 0.93 | 50.9 | 2.10 | 33.0 |
| P-23 | 85 | 686 | 0.86 | 19.1 | 3.24 | 32.7 |
| P-46A | 102 | 651 | 0.93 | 18.1 | 2.94 | 32.0 |
| P-47A | 106 | 655 | 0.94 | 17.2 | 3.00 | 32.0 |
| P-48B | 105 | 687 | 0.93 | 23.0 | 2.80 | 31.3 |
| P-32 | 108 | 1002 | 1.04 | 37.3 | 2.73 | 29.7 |
| P-34 | 116.53 | 897.47 | 0.91 | 30.55 | 2.96 | 34.3 |
| *Guatemala basement* | | | | | | |
| G 009 L1 | 59.70 | 391 | 0.32 | 16.68 | 3.73 | 13.5 |
| G 009 L2 | 79.49 | 583 | 0.23 | 8.0 | 8.65 | 25.1 |
| Chor 8A | 14.14 | 194 | 0.45 | 20.3 | 3.2 | 17.3 |
| P12 | 34.62 | 787.4 | 0.49 | 14.11 | 14.1 | 18.6 |
| G3K | 41.00 | 67.22 | 0.16 | 1.42 | 14.85 | 26.9 |
| M1 | | | | | | |
| M2 | 53.01 | 254.0 | 0.28 | 0.71 | 40.4 | 28.5 |
| 619 | 13.58 | 31.8 | 0.13 | 2.77 | 34.48 | 23.6 |
| 714A | 5.02 | 17.46 | 0.32 | 0.98 | 8.24 | 17.3 |
| *Cocos Plate Sediments* | | | | | | |
| 67_0495_009R_02W_73-75 | 20.26 | 104 | 1.97 | 13.2 | 5.79 | 41.1 |
| 67_0499_019R_05W_80-82 | 144.17 | 564.45 | 2.61 | 14.21 | 5.96 | 37.5 |
| *Cocos Plate MORB* | | | | | | |
| 67_0495_048R_04W_82-84 | 1.35 | 38.8 | 2.06 | 11.08 | 0.97 | 39.7 |
| 206_1256C_10R2_103-105 | 3.15 | 49.4 | 0.33 | 6.56 | 0.93 | 36.1 |
| 206_1256D_74R2_102-111 | 2.64 | 41.4 | 0.31 | 9.85 | 0.64 | 34.6 |

for Sn and Pb (~12.5%) and Tl (33%). Analytical accuracy for standard material for AGV-1 is better than 10%, except for Cr, Tl and Th (11–13%) and Li, Nb, Mo and Tm (21–28%), based on the suggested reference values of Govindaraju (1994) and Jochum and Jenner (1994).

All isotope analyses were carried out at IFM-GEOMAR using a Thermo Finnigan TRITON (Sr, Nd isotopes) and Finnigan MAT 262-RPQ2+ (Pb, Sr isotopes) thermal ionization mass spectrometers and an AXIOM multiple collector ICP-MS (Hf isotopes), all operating in static mode. Sr–Nd–Pb isotope analyses were carried on ca. 100 mg whole rock powders in Class 1000 clean rooms. The powders were weighed in Teflon beakers and digested in a solution of conc. HF u.p. (ultra-pure) and conc. $HNO_3$ (5:1) at 150 °C for 60 h. Ion chromatography was carried out following the procedures of Hoernle and Tilton (1991), Hoernle et al. (2008) and Geldmacher et al. (2006). Within-run normalization factors were 0.1194 for $^{86}Sr/^{88}Sr$ and 0.7219 for $^{146}Nd/^{144}Nd$. All errors are reported as $2\sigma$ of the mean. NBS 987 values measured along with the samples were normalized for each analytical session to $^{87}Sr/^{88}Sr = 0.71025$ and the session specific normalization value applied to the sample data. Over the course of the study (2005 and 2007) NBS 987 reproduced with $2\sigma \pm 0.000021$ ($n = 22$) on the TRITON and $2\sigma \pm 0.000007$ ($n = 9$) on the MAT262. Similarly the in-house Nd-monitor SPEX yielded $^{143}Nd/^{144}Nd = 0.511715 \pm 0.000006$ ($N = 29$) corresponding to a La Jolla calibrated value of $^{143}Nd/^{144}Nd = 0.511850$. Lead isotope ratios are normalized to NBS 981 values from Todt et al. (1996). The long-term reproducibility of NBS 981 measured along with the samples is $^{206}Pb/^{204}Pb = 16.902 \pm 0.009$, $^{207}Pb/^{204}Pb = 15.441 \pm 0.012$ and $^{208}Pb/^{204}Pb = 36.537 \pm 0.038$ ($n = 22$). Total blanks for Pb chemistry were <100 pg and thus are considered negligible. Hafnium isotope ratios were determined on a subset of samples. 200–500 mg of rock chips were digested for 60 h at 130℃ in a HF-$HNO_3$ mixture and chemical separation followed the procedures outlined in Blichert-Toft and Albarède (1997). For detailed descriptions of MC-ICP-MS setup and analyzing modes see Geldmacher et al. (2006). The JMC 475 Hf-reference solution gave $^{176}Hf/^{177}Hf = 0.282132 \pm 0.000005$ ($2\sigma$, $n = 25$) and all measured Hf values were corrected to JMC 475 = 0.282163 (Blichert-Toft and Albarède, 1997). O isotope analyses were carried out in the stable isotope laboratory at the University of Oregon using a 35 W $CO_2$-laser for laser fluorination (Bindeman, 2008). Up to 2 mg of bulk monomineralic fractions (olivine, plagioclase) were reacted with purified $BrF_5$ reagent to liberate oxygen. The gases were purified to get rid of traces of fluorine gas. Oxygen was converted to $CO_2$ gas using a small platinum-graphite converter and subsequently analyzed on a Finnigan MAT 253 gas source mass spectrometer. San Carlos olivine (SCO-2, $\delta^{18}O = 5.35‰$) and Gore Mt garnet (UWG-2, $\delta^{18}O = 5.75‰$) standards (Valley et al., 1995; Eiler et al., 2000) were measured along with the samples. Day-to-day variability was corrected to standard working values with the variability better than $1\sigma \pm 0.1‰$. Duplicates ($n = 6$) deviate less than 0.2‰ from each other.

## 3. RESULTS

Seventy-six volcanic whole-rock samples (36 lava and 40 tephra samples; MgO > 2 wt.%) from major volcanic centers along and across the northwestern Central American Volcanic Arc from NW Nicaragua (Momotombo Volcano) through El Salvador and Honduras to NW Guatemala have been analyzed for major and trace element (Table 1) and Sr–Nd–Pb–Hf isotopic compositions (Table 2). Microprobe whole rock compositions of the matrix glass of the tephras and compositions of olivine-hosted melt inclusions are reported for the tephra samples in Sadofsky et al. (2008). Lead and Nd isotope data from the NW Nicaragua samples are reported in Hoernle et al. (2008). Tables 1 and 2 also include data from samples of the granitic (Chor 8A, P12, G3, G009 L1 and G009 L2) and metamorphic (GU M1, GU M2, 619 and 714A) Guatemalan basement and Cocos Plate sediments and oceanic crust from DSDP Leg 67 Site 495 and ODP Leg 206 Site 1256 offshore Guatemala (Fig. 1).

### 3.1. Major and trace element data

On the Total Alkali vs. Silica (TAS) diagram, the NW Nicaragua VF lavas form a tight array with a positive slope extending from tholeiitic basalts to andesites (Fig. 2a). The El Salvador and Guatemala VF lavas form a similar array shifted to slightly higher total alkali content at a given $SiO_2$ content. The BVF lavas from Honduras, El Salvador and Guatemala are shifted to still higher total alkalis and range from tholeiites and basaltic andesites to alkali basalts, hawaiites and mugearites. Backarc samples from Honduras are hawaiites with the highest alkali contents. On a $SiO_2$ vs. $K_2O$ classification diagram for subalkalic rocks (Fig. 2b), VF samples from NW Nicaragua through El Salvador and Honduras to NW Guatemala have compositions within the Medium-K or Calc-alkaline series and BVF samples overlap the VF samples and extend into the High K or High-K Calc-alkaline series, as do the BA samples.

The most mafic (MgO = 5–8 wt.%) Guatemalan VF whole-rock samples extend to lower $FeO_t$ (total iron as FeO), CaO, MnO and slightly higher $SiO_2$, $TiO_2$ and $Na_2O$ contents than samples from Nicaragua with similar MgO content (Fig. 3a–i), consistent with previous studies of major element concentrations of whole rocks (e.g. Carr et al., 1990; Patino et al., 2000; Carr and Feigenson, 2003) and olivine-hosted melt inclusions (Sadofsky et al., 2008). At a given MgO content, El Salvador and Honduras VF samples show major element concentrations between corresponding VF samples from NW Guatemala and Nicaragua. BVF samples generally show a broader range in major element concentrations at a given MgO content (Fig. 3a–i), overlapping with the VF samples and in general extending to lower CaO and $FeO_t$ and to higher $TiO_2$, $Na_2O$, $K_2O$ and $P_2O_5$ than VF samples. At a given MgO content, the BA samples have low $SiO_2$ and CaO and the

Table 2
Sr–Nd–Pb–Hf–O isotopic compositions for Central American Arc volcanics from volcanic front (VF), behind the volcanic front (BVF) and back-arc (BA) samples with MgO > 2 wt.%. Note Pb and Nd isotope data for Nicaraguan samples marked with (**) from Hoernle et al. (2008).

| Sample # | $^{87}Sr/^{86}Sr$ | 2σ | $^{143}Nd/^{144}Nd$ | 2σ | εNd | $^{206}Pb/^{204}Pb$ | 2σ | $^{207}Pb/^{204}Pb$ | 2σ | $^{208}Pb/^{204}Pb$ | 2σ | $^{176}Hf/^{177}Hf$ | 2σ | εHf | $\delta^{18}O_{olivine}$ | 1 σ |
|---|---|---|---|---|---|---|---|---|---|---|---|---|---|---|---|---|
| *Guatemala volcanic front* | | | | | | | | | | | | | | | | |
| GU2A | 0.703852 | 0.000002 | 0.512885 | 0.000003 | 4.82 | 18.625 | 0.007 | 15.564 | 0.006 | 38.321 | 0.014 | 0.283008 | 0.000005 | 8.35 | 5.53 | 0.46 |
| GU 4 | 0.703824 | 0.000003 | 0.512925 | 0.000002 | 5.59 | 18.620 | 0.001 | 15.547 | 0.001 | 38.268 | 0.003 | | | | | |
| GU 5 | 0.703812 | 0.000002 | 0.512932 | 0.000003 | 5.74 | | | | | | | | | | | |
| GU6 | 0.703951 | 0.000004 | 0.512860 | 0.000002 | 4.33 | 18.647 | 0.000 | 15.566 | 0.000 | 38.345 | 0.001 | 0.282985 | 0.000004 | 7.52 | 5.65 | 0.46 |
| GU 8A | 0.703823 | 0.000003 | 0.512908 | 0.000002 | 5.26 | 18.628 | 0.001 | 15.556 | 0.001 | 38.300 | 0.003 | 0.283016 | 0.000008 | 8.63 | 5.56 | |
| GU 15A | 0.703863 | 0.000002 | 0.512928 | 0.000002 | 5.66 | 18.665 | 0.001 | 15.554 | 0.001 | 38.313 | 0.002 | | | | | |
| GU17A | 0.703872 | 0.000003 | 0.512911 | 0.000002 | 5.32 | 18.666 | 0.001 | 15.554 | 0.001 | 38.319 | 0.002 | 0.283042 | 0.000009 | 9.56 | 5.44 | 0.46 |
| GU 22 | 0.703859 | 0.000005 | 0.512874 | 0.000003 | 4.61 | 18.664 | 0.001 | 15.575 | 0.001 | 38.381 | 0.001 | | | | | |
| GU23A | 0.704046 | 0.000003 | 0.512824 | 0.000003 | 3.63 | 18.681 | 0.001 | 15.579 | 0.001 | 38.412 | 0.002 | 0.282975 | 0.000009 | 7.18 | 5.40 | 0.46 |
| GU26 | 0.703643 | 0.000002 | 0.512917 | 0.000003 | 5.45 | 18.634 | 0.001 | 15.556 | 0.001 | 38.304 | 0.002 | | | | | |
| OTO I | 0.703790 | 0.000002 | 0.512959 | 0.000003 | 6.26 | 18.602 | 0.001 | 15.545 | 0.000 | 38.243 | 0.001 | | | | 5.60 | 0.46 |
| OTO II | 0.703824 | 0.000003 | 0.512949 | 0.000002 | 6.06 | 18.606 | 0.000 | 15.548 | 0.000 | 38.257 | 0.001 | 0.283074 | 0.000008 | 10.69 | 5.52 | 0.17 |
| Guatemala behind the volcanic front | | | | | | | | | | | | | | | | |
| GUA 14A | 0.703401 | 0.000002 | 0.512968 | 0.000003 | 6.45 | 18.612 | 0.002 | 15.547 | 0.001 | 38.244 | 0.003 | 0.283055 | 0.000007 | 10.01 | 5.47 | |
| GU 29 | 0.703604 | 0.000003 | 0.512917 | 0.000003 | 5.45 | 18.670 | 0.001 | 15.567 | 0.001 | 38.352 | 0.001 | 0.282999 | 0.000007 | 8.02 | 5.59 | 0.05 |
| GU 30 | 0.703697 | 0.000003 | 0.512881 | 0.000003 | 4.74 | 18.655 | 0.002 | 15.571 | 0.001 | 38.351 | 0.003 | | | | | |
| GU32 | 0.704071 | 0.000005 | 0.512813 | 0.000003 | 3.41 | 18.693 | 0.001 | 15.582 | 0.001 | 38.423 | 0.002 | 0.282937 | 0.000007 | 5.83 | | |
| GU 35B | 0.703633 | 0.000003 | 0.512930 | 0.000003 | 5.70 | 18.669 | 0.002 | 15.577 | 0.002 | 38.367 | 0.006 | 0.283031 | 0.000008 | 9.17 | 5.64 | 0.46 |
| GU 38 | 0.704154 | 0.000003 | 0.512880 | 0.000002 | 4.73 | 18.636 | 0.000 | 15.568 | 0.000 | 38.337 | 0.001 | | | | | |
| GU 39 | 0.704110 | 0.000003 | 0.512831 | 0.000002 | 3.77 | 18.672 | 0.000 | 15.579 | 0.000 | 38.404 | 0.001 | | | | | |
| *El Salvador volcanic front* | | | | | | | | | | | | | | | | |
| ES002 | 0.703886 | 0.000003 | 0.513009 | 0.000003 | 7.23 | 18.535 | 0.000 | 15.523 | 0.000 | 38.143 | 0.001 | 0.283126 | 0.000007 | 12.52 | | |
| ES003 | 0.703871 | 0.000002 | 0.512990 | 0.000003 | 6.87 | 18.536 | 0.001 | 15.526 | 0.001 | 38.157 | 0.003 | | | | | |
| ES005 | 0.703689 | 0.000002 | 0.512997 | 0.000003 | 6.99 | 18.638 | 0.001 | 15.561 | 0.001 | 38.313 | 0.002 | 0.283117 | 0.000006 | 12.19 | 5.91 | 0.11 |
| ES009 | 0.703788 | 0.000003 | 0.512996 | 0.000003 | 6.97 | 18.573 | 0.001 | 15.551 | 0.001 | 38.243 | 0.002 | 0.283117 | 0.000005 | 12.19 | 5.50 | |
| ES019 | 0.703871 | 0.000003 | 0.512944 | 0.000003 | 5.97 | 18.601 | 0.001 | 15.556 | 0.001 | 38.274 | 0.002 | 0.283059 | 0.000006 | 10.14 | 5.35 | 0.14 |
| ES 027B | 0.703846 | 0.000002 | 0.513006 | 0.000002 | 7.17 | 18.537 | 0.002 | 15.531 | 0.002 | 38.173 | 0.004 | | | | | |
| ES 028B | 0.703881 | 0.000003 | 0.513008 | 0.000003 | 7.23 | 18.516 | 0.002 | 15.521 | 0.001 | 38.126 | 0.003 | | | | | |
| ES 031 | 0.703816 | 0.000005 | 0.513009 | 0.000005 | 7.23 | 18.519 | 0.002 | 15.529 | 0.001 | 38.153 | 0.004 | | | | | |
| ES 035A | 0.703863 | 0.000005 | 0.513007 | 0.000002 | 7.20 | 18.502 | 0.001 | 15.531 | 0.001 | 38.139 | 0.001 | | | | 4.90 | 0.11 |
| ES 036C | 0.703643 | 0.000004 | 0.513005 | 0.000003 | 7.15 | 18.663 | 0.000 | 15.554 | 0.000 | 38.307 | 0.001 | | | | | |
| ES038 | 0.704154 | 0.000003 | 0.513001 | 0.000003 | 7.08 | 18.654 | 0.001 | 15.546 | 0.000 | 38.285 | 0.001 | 0.283122 | 0.000005 | 12.36 | 5.00 | 0.11 |
| ES SSI | 0.703824 | 0.000002 | 0.512998 | 0.000004 | 7.03 | 18.568 | 0.000 | 15.527 | 0.000 | 38.173 | 0.001 | | | | | |
| ES SSII | 0.703824 | 0.000003 | 0.513009 | 0.000002 | 7.23 | 18.569 | 0.000 | 15.529 | 0.000 | 38.176 | 0.001 | 0.283106 | 0.000008 | 11.80 | | |
| *El Salvador behind the volcanic front* | | | | | | | | | | | | | | | | |
| ES013 | 0.703708 | 0.000003 | 0.513002 | 0.000003 | 7.11 | 18.562 | 0.001 | 15.538 | 0.001 | 38.189 | 0.001 | | | | | |
| ES014 | 0.703844 | 0.000003 | 0.512900 | 0.000003 | 5.12 | 18.648 | 0.001 | 15.557 | 0.001 | 38.318 | 0.002 | | | | | |

| | | | | | | | | | | | | | | | | | |
|---|---|---|---|---|---|---|---|---|---|---|---|---|---|---|---|---|---|
| ES015 | | 0.703801 | 0.000003 | 0.512879 | 0.000003 | 4.71 | 18.662 | 0.001 | 15.566 | 0.001 | 38.349 | 0.001 | | | | | |
| ES016 | | 0.703785 | 0.000003 | 0.512878 | 0.000002 | 4.68 | 18.657 | 0.001 | 15.565 | 0.000 | 38.347 | 0.001 | | | | | |
| ES017 | | 0.703716 | 0.000003 | 0.512905 | 0.000002 | 5.20 | 18.657 | 0.001 | 15.565 | 0.001 | 38.338 | 0.002 | | | | | |
| ES018B | | 0.703753 | 0.000003 | 0.512875 | 0.000002 | 4.63 | 18.666 | 0.001 | 15.575 | 0.001 | 38.378 | 0.003 | 0.282994 | 0.000007 | 7.85 | 5.62 | |
| ES024B | | 0.703615 | 0.000002 | 0.512971 | 0.000003 | 6.49 | 18.577 | 0.001 | 15.546 | 0.001 | 38.225 | 0.003 | 0.283090 | 0.000007 | 11.25 | 5.35 | |
| *Honduras volcanic front* | | | | | | | | | | | | | | | | | |
| H3B | | 0.703815 | 0.000003 | 0.512999 | 0.000003 | 7.04 | 18.527 | 0.002 | 15.529 | 0.001 | 38.162 | 0.003 | 0.283122 | 0.000010 | 12.36 | | |
| Honduras behind the volcanic front | | | | | | | | | | | | | | | | | |
| H1 | | 0.703743 | 0.000002 | 0.512982 | 0.000002 | 6.72 | 18.593 | 0.001 | 15.539 | 0.001 | 38.221 | 0.003 | 0.283092 | 0.000004 | 11.32 | 5.37 | 0.18 |
| H4B | | 0.703844 | 0.000002 | 0.513002 | 0.000003 | 7.11 | 18.525 | 0.001 | 15.528 | 0.001 | 38.156 | 0.002 | | | | | |
| H5 | | 0.703811 | 0.000002 | 0.512994 | 0.000003 | 6.94 | 18.525 | 0.002 | 15.533 | 0.001 | 38.168 | 0.003 | 0.283145 | 0.000007 | 13.20 | | |
| H9 | | 0.704006 | 0.000003 | 0.512827 | 0.000003 | 3.69 | 18.659 | 0.001 | 15.567 | 0.001 | 38.367 | 0.002 | 0.282976 | 0.000007 | 7.22 | | |
| H13 | | 0.703206 | 0.000003 | 0.512965 | 0.000003 | 6.37 | 18.665 | 0.001 | 15.555 | 0.001 | 38.278 | 0.002 | | | | | |
| H14 | | 0.704078 | 0.000002 | 0.512889 | 0.000002 | 4.89 | 18.668 | 0.002 | 15.578 | 0.001 | 38.406 | 0.003 | 0.282969 | 0.000007 | 6.95 | | |
| H16 | | 0.703985 | 0.000003 | 0.512859 | 0.000002 | 4.32 | 18.681 | 0.001 | 15.580 | 0.001 | 38.421 | 0.004 | | | | | |
| *Honduras backarc* | | | | | | | | | | | | | | | | | |
| H10 | | 0.703089 | 0.000003 | 0.513021 | 0.000003 | 7.47 | 18.630 | 0.001 | 15.550 | 0.001 | 38.227 | 0.002 | 0.283067 | 0.000008 | 10.42 | 5.62 | 0.18 |
| H17A | | 0.702870 | 0.000003 | 0.513062 | 0.000002 | 8.28 | 18.714 | 0.002 | 15.529 | 0.002 | 38.126 | 0.004 | 0.283104 | 0.000006 | 11.74 | | |
| H18A | | 0.702730 | 0.000002 | 0.513050 | 0.000003 | 8.03 | 18.731 | 0.001 | 15.527 | 0.001 | 38.119 | 0.003 | | | | | |
| *NW nicaragua volcanic front* | | | | | | | | | | | | | | | | | |
| P-60 | (**) | 0.703839 | 0.000002 | 0.513084 | 0.000003 | 8.69 | 18.425 | 0.001 | 15.507 | 0.001 | 38.023 | 0.002 | 0.283209 | 0.000005 | 15.44 | 5.59 | 0.11 |
| P-58A | (**) | 0.703872 | 0.000002 | 0.513068 | 0.000003 | 8.38 | 18.464 | 0.001 | 15.518 | 0.001 | 38.091 | 0.002 | 0.283192 | 0.000004 | 14.86 | 5.34 | |
| P-27A | (**) | 0.703909 | 0.000002 | 0.513061 | 0.000002 | 8.26 | 18.475 | 0.002 | 15.519 | 0.002 | 38.099 | 0.005 | 0.283176 | 0.000008 | 14.29 | 4.71 | 0.06 |
| P-13 | (**) | 0.703917 | 0.000002 | 0.513057 | 0.000003 | 8.18 | 18.483 | 0.001 | 15.533 | 0.001 | 38.140 | 0.002 | | | | | |
| P2-16 | (**) | 0.704019 | 0.000003 | 0.513050 | 0.000002 | 8.04 | 18.506 | 0.001 | 15.515 | 0.001 | 38.118 | 0.002 | | | | | |
| P-7A | (**) | 0.704005 | 0.000002 | 0.513060 | 0.000002 | 8.23 | 18.513 | 0.001 | 15.520 | 0.001 | 38.139 | 0.003 | | | | | |
| P-9 | (**) | 0.703971 | 0.000002 | 0.513042 | 0.000003 | 7.88 | 18.532 | 0.001 | 15.534 | 0.001 | 38.188 | 0.002 | 0.283156 | 0.000007 | 13.57 | 5.34 | 0.19 |
| P-43 | (**) | 0.703849 | 0.000002 | 0.513051 | 0.000002 | 8.05 | 18.554 | 0.001 | 15.521 | 0.001 | 38.180 | 0.003 | | | | | |
| P-51 | (**) | 0.703965 | 0.000006 | 0.513067 | 0.000006 | 8.36 | 18.481 | 0.001 | 15.520 | 0.001 | 38.114 | 0.002 | | | | | |
| P-56G | (**) | 0.703941 | 0.000006 | 0.513073 | 0.000004 | 8.48 | 18.493 | 0.001 | 15.525 | 0.001 | 38.131 | 0.002 | | | | | |
| P-4 | (**) | 0.703991 | 0.000006 | 0.513078 | 0.000006 | 8.57 | 18.557 | 0.002 | 15.529 | 0.001 | 38.205 | 0.003 | | | | | |
| P-6 | (**) | 0.703983 | 0.000002 | 0.513066 | 0.000003 | 8.34 | 18.546 | 0.003 | 15.529 | 0.002 | 38.195 | 0.006 | | | | 4.98 | 0.09 |
| P2-3a | (**) | 0.703965 | 0.000003 | 0.513071 | 0.000003 | 8.45 | | | | | | | | | | 5.08 | 0.19 |
| P2-3b | (**) | 0.703978 | 0.000003 | 0.513072 | 0.000002 | 8.47 | 18.538 | 0.002 | 15.522 | 0.002 | 38.171 | 0.005 | | | | | |
| P2-3d | (**) | 0.703994 | 0.000003 | 0.513074 | 0.000003 | 8.50 | 18.533 | 0.002 | 15.526 | 0.002 | 38.172 | 0.005 | 0.283179 | 0.000007 | 14.39 | | |
| P2-11 | (**) | 0.703982 | 0.000005 | 0.513072 | 0.000003 | 8.47 | 18.549 | 0.002 | 15.523 | 0.001 | 38.184 | 0.003 | | | | | |
| P2-13 | (**) | 0.703961 | 0.000009 | 0.513077 | 0.000004 | 8.56 | 18.555 | 0.001 | 15.530 | 0.001 | 38.205 | 0.002 | | | | | |
| P-50 | (**) | 0.703971 | 0.000003 | 0.513057 | 0.000002 | 8.18 | 18.480 | 0.001 | 15.519 | 0.001 | 38.107 | 0.002 | | | | | |
| P-19 | (**) | 0.703864 | 0.000003 | 0.513055 | 0.000002 | 8.13 | 18.514 | 0.003 | 15.518 | 0.002 | 38.133 | 0.006 | | | | | |
| P-40A | (**) | 0.704044 | 0.000007 | 0.513084 | 0.000006 | 8.69 | 18.532 | 0.001 | 15.526 | 0.001 | 38.175 | 0.002 | | | | | |

(*continued on next page*)

Table 2 (*continued*)

| Sample # | | $^{87}Sr/^{86}Sr$ | 2σ | $^{143}Nd/^{144}Nd$ | 2σ | εNd | $^{206}Pb/^{204}Pb$ | 2σ | $^{207}Pb/^{204}Pb$ | 2σ | $^{208}Pb/^{204}Pb$ | 2σ | $^{176}Hf/^{177}Hf$ | 2σ | εHf | $\delta^{18}O_{olivine}$ | 1 σ |
|---|---|---|---|---|---|---|---|---|---|---|---|---|---|---|---|---|---|
| P-42 | (**) | 0.704001 | 0.000002 | 0.513067 | 0.000003 | 8.37 | 18.549 | 0.002 | 15.526 | 0.002 | 38.187 | 0.005 | | | | | |
| P-23 | (**) | 0.703943 | 0.000004 | 0.513063 | 0.000003 | 8.30 | 18.537 | 0.002 | 15.520 | 0.001 | 38.157 | 0.003 | | | | | |
| P-46A | (**) | 0.703936 | 0.000003 | 0.513065 | 0.000002 | 8.32 | 18.550 | 0.001 | 15.523 | 0.001 | 38.180 | 0.002 | | | | | |
| P-47A | (**) | 0.703952 | 0.000002 | 0.513063 | 0.000002 | 8.30 | 18.548 | 0.001 | 15.521 | 0.001 | 38.176 | 0.002 | | | | | |
| P-48B | (**) | 0.703954 | 0.000003 | 0.513065 | 0.000002 | 8.33 | 18.552 | 0.001 | 15.525 | 0.001 | 38.188 | 0.002 | | | | | |
| P-32 | (**) | 0.704046 | 0.000003 | 0.513071 | 0.000003 | 8.44 | 18.557 | 0.001 | 15.527 | 0.001 | 38.202 | 0.003 | 0.283187 | 0.000007 | 14.66 | 5.03 | 0.15 |
| P-34 | (**) | 0.704017 | 0.000002 | 0.513073 | 0.000003 | 8.49 | 18.564 | 0.001 | 15.533 | 0.001 | 38.217 | 0.002 | | | | | |
| *Guatemala basement* | | | | | | | | | | | | | | | | | |
| G 009 L1 | | 0.703699 | 0.000001 | 0.512977 | 0.000003 | 6.61 | 18.588 | 0.001 | 15.536 | 0.000 | 38.231 | 0.001 | 0.283181 | 0.000006 | 14.46 | | |
| G 009 L2 | | 0.704004 | 0.000003 | 0.512947 | 0.000001 | 6.03 | 18.728 | 0.000 | 15.554 | 0.000 | 38.397 | 0.001 | 0.283086 | 0.000004 | 11.12 | | |
| Chor 8A | | 0.703455 | 0.000002 | 0.513017 | 0.000003 | 7.40 | 18.781 | 0.001 | 15.604 | 0.001 | 38.554 | 0.002 | 0.283116 | 0.000004 | 12.15 | | |
| P12 | | 0.704093 | 0.000003 | 0.512764 | 0.000003 | 2.46 | 18.643 | 0.001 | 15.588 | 0.001 | 38.349 | 0.002 | | | | | |
| G3K | | 0.707295 | 0.000002 | 0.512795 | 0.000003 | 3.06 | 18.747 | 0.001 | 15.593 | 0.001 | 38.514 | 0.002 | 0.282927 | 0.000005 | 5.49 | 7.26 (Plag) | |
| M1 | | 0.737244 | 0.000003 | 0.512166 | 0.000003 | -9.20 | 19.006 | 0.001 | 15.699 | 0.001 | 38.803 | 0.002 | | | | | |
| M2 | | 0.742724 | 0.000002 | 0.512131 | 0.000003 | -9.89 | 19.782 | 0.001 | 15.697 | 0.001 | 39.874 | 0.001 | 0.282845 | 0.000007 | 2.60 | | |
| 619 | | 0.723420 | 0.000002 | 0.512219 | 0.000003 | -8.18 | 18.815 | 0.001 | 15.634 | 0.001 | 38.795 | 0.002 | 0.282654 | 0.000006 | -4.19 | | |
| 714A | | 0.734146 | 0.000002 | 0.512158 | 0.000002 | -9.36 | 23.759 | 0.001 | 15.947 | 0.001 | 43.934 | 0.003 | 0.284771 | 0.000006 | 70.69 | | |
| *Cocos Plate sediments* | | | | | | | | | | | | | | | | | |
| 67_0495_009R_02W_73-75 | | 0.707689 | 0.000002 | 0.512716 | 0.000002 | 1.53 | | 18.755 | 0.001 | 15.595 | 0.001 | 38.540 | 0.002 | 0.283074 | 0.000003 | 10.67 | |
| 67_0499_019R_05W_80-82 | | 0.706951 | 0.000002 | 0.512801 | 0.000002 | 3.18 | | 18.727 | 0.000 | 15.581 | 0.000 | 38.491 | 0.001 | 0.283067 | 0.000005 | 10.44 | |
| *Cocos Plate MORB* | | | | | | | | | | | | | | | | | |
| 67_0495_048R_04W_82-84 | | 0.702793 | 0.000003 | 0.513120 | 0.000002 | 9.40 | | 18.476 | 0.001 | 15.502 | 0.001 | 38.012 | 0.003 | 0.283181 | 0.000005 | 14.46 | |
| 206_1256C_10R2_103-105 | | 0.702995 | 0.000002 | 0.513095 | 0.000003 | 8.91 | | 18.478 | 0.009 | 15.510 | 0.008 | 38.086 | 0.019 | 0.283189 | 0.000004 | 14.76 | |
| 206_1256D_74R2_102-111 | | 0.703077 | 0.000002 | 0.513095 | 0.000002 | 8.91 | | 18.513 | 0.005 | 15.502 | 0.005 | 38.110 | 0.011 | 0.283209 | 0.000003 | 15.45 | |

highest $TiO_2$, $Na_2O$, $K_2O$ and $P_2O_5$. Sc and V show a crude decrease and Pb and Sr a crude increase in the most mafic samples going from NW Nicaragua to Guatemala (Fig. 3j–r). The most mafic BVF and BA samples generally extend to lower Sc and V but to higher Rb, Nb and the light rare earth elements (LREE) (Fig. 3j–r) than VF samples with similar MgO contents.

On primitive normal (N) MORB normalized multi-element diagrams (Fig. 4a–d), all VF and BVF samples display enrichment in fluid–mobile large-ion-lithophile elements (LILE; e.g. Ba, K, Pb, Sr) and U, relative to high field strength elements (HFSE; e.g. Nb, Ta, Zr, Hf, Ti) and (LREE; e.g. La, Ce, Nd) reflecting typical subduction-related trace element abundance patterns (e.g. Arculus, 1994; Pearce and Peate, 1995). BVF samples have higher HFSE and REE contents than related VF samples with similar MgO contents (Fig. 3j–r). BA samples from Utila Island, however, do not show enrichments in the LILE relative to the HFSE and have incompatible element characteristics closer to ocean island basalts (OIB) than to the VF and BVF rocks (Fig. 4c).

Systematic variations in trace element compositions and ratios are observed along the volcanic front and between VF, BVF and BA samples. Ratios of LILE elements to HFSE and REE (e.g. Ba/La, U/Th, Ba/Th and to a lesser degree Sr/Ce (not shown here), e.g. Fig. 5) vary systematically along the VF decreasing from NW Nicaragua to NW Guatemala, consistent with the results of previous studies (e.g. Carr et al., 1990, 2007; Carr and Feigenson, 2003; Patino et al., 2000; Sadofsky et al., 2008). Light (L) to Heavy (H) REE ratios (e.g. La/Yb, Fig. 5c), on the other hand, increase northwest along the VF to Guatemala and into the BVF and BA, reflecting both generally lower HREE and higher LREE contents (steeper negative REE patterns) in the Guatemalan lavas (e.g. Fig. 4). The lavas from Central Nicaragua have the highest Ba/La, Ba/Th and U/Th ratios along the entire Central American VF and overlap with those of sediments on the subducting Cocos Plate (Fig. 5a, b, d). BVF and BA samples generally extend to lower Ba/La, Ba/Th (except for El Salvador and one Honduras samples) and U/Th and higher La/Yb ratios than associated VF lavas. Lake Yojoa and Utila Island (BA) rocks extend to the lowest Ba/La, Ba/Th and U/Th and highest La/Yb ratios, overlapping the range observed in OIBs (Fig. 5a, b and d).

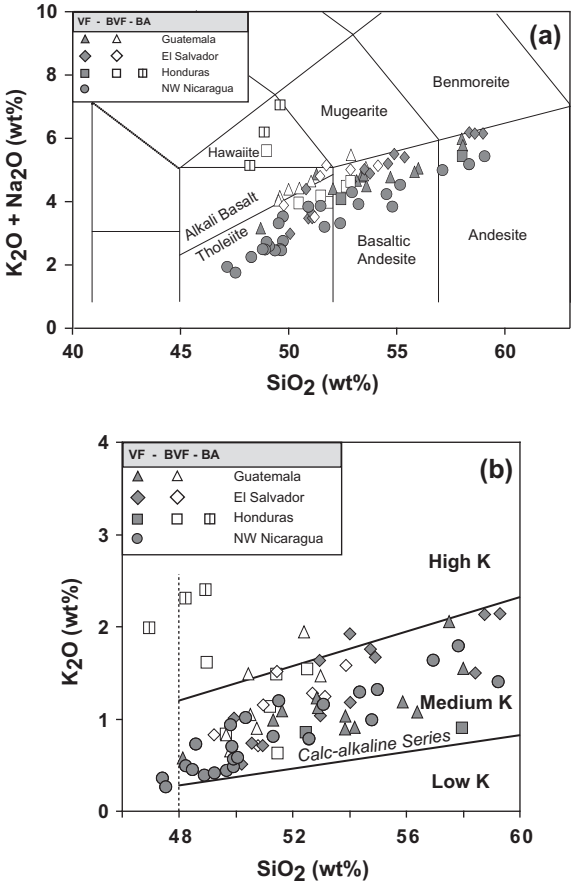


Fig. 2. Major element classification diagrams for northwestern Central American subduction-related volcanic rocks. (a) Total Alkali vs. Silica (TAS) diagram after Le Maitre et al. (2002) with data normalized to 100% on a volatile-free basis for all plots containing major element data. The VF samples range from basalt to andesitic in composition. BVF samples are shifted toward higher alkali contents with the BA samples having the most alkalic (hawaiitic) compositions. Division between alkali basalts and tholeiites is from MacDonald and Katsura (1964). Solid symbols indicate VF and open symbols BVF and BA samples. See Table 1 for geochemical data in this diagram. (b) $SiO_2$ vs. $K_2O$ classification diagram (after Le Maitre et al., 1989). Volcanic rocks (MgO > 2 wt.%) from the volcanic front (VF) plot within the Medium K or calc-alkaline series field, whereas the behind the volcanic front (BVF) samples overlap the VF field and extend into the High K or High-K calc-alkaline series. The back-arc (BA) samples plot within the High K/High-K calc-alkaline field.

### 3.2. Sr–Nd–Pb–Hf–O isotopes

The Sr–Nd–Pb–Hf–O isotope data are presented in Table 2. Although $^{87}Sr/^{86}Sr$ isotopic composition doesn't show a clear systematic variation along the VF, there is a broad decrease from NW Nicaragua to central El Salvador (excluding one sample) and then an overall increase from NW El Salvador to Guatemala (Fig. 6c), similar to what has been observed previously (e.g. Carr and Feigenson, 2003). On the other hand, the $^{143}Nd/^{144}Nd$ and $^{176}Hf/^{177}Hf$ show a systematic decrease and $^{206}Pb/^{204}Pb$ isotope ratios a systematic increase along the VF from NW Nicaragua through Guatemala (e.g. Fig. 6). Oxygen isotope data (i.e. $\delta^{18}O$) of olivines show a broad increase from NW Nicaragua to Guatemala (Fig. 6e), similar to observations by Eiler et al. (2005). BVF samples have similar or lower Sr, Nd, Hf and O, but higher Pb isotope ratios than associated VF samples. BA samples in Honduras have depleted Sr and Nd isotopic compositions that fall within the field for Cocos Plate oceanic crust but slightly lower Hf and higher Pb isotope ratios. The samples from the BA have the least radiogenic $^{87}Sr/^{86}Sr$ and most radiogenic $^{206}Pb/^{204}Pb$ isotope ratios for all NW Central American subduction-related lavas. On an $^{87}Sr/^{86}Sr$ vs. $^{143}Nd/^{144}Nd$ isotope correlation diagram (Fig. 7) for NW Central American

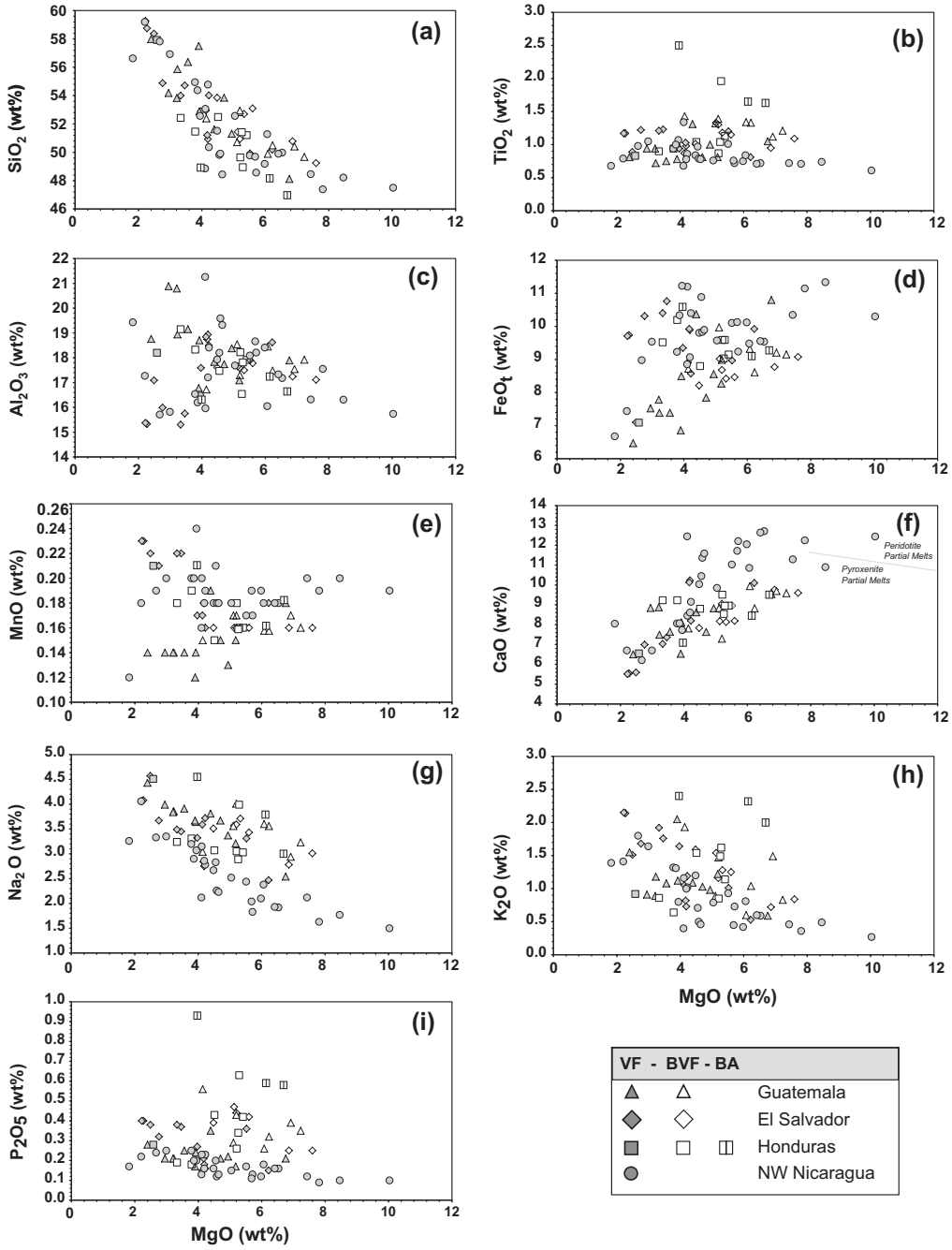


Fig. 3. (a–i) MgO vs. major element oxide variation diagrams for volcanic front (VF) and behind the volcanic front (BVF) and back-arc (BA) mafic volcanic rock samples with MgO > 2 wt.%. (j–r) MgO vs. select trace element variation diagrams for volcanic front (VF) and behind the volcanic front (BVF) and back-arc (BA) mafic volcanic rock samples with MgO > 2 wt.%. Grey line in panel (f) separating pyroxenite from peridotite partial melts after Herzberg and Asimow (2008).

volcanic rocks, BVF and BA samples form a crude negative correlation, extending from the MORB field (Honduras BA samples) towards an enriched component with radiogenic Sr and unradiogenic Nd, characterized by BVF samples from Honduras and Guatemala. The VF samples form a crudely vertical array on this diagram. The Guatemala VF samples overlap the BVF/BA array, but the VF samples from El Salvador and NW Nicaragua plot to the right of the BVF/BA array, having more radiogenic Sr isotope ratios for a given Nd isotopic composition. The Pb isotope data from the NW Central American VF samples form good positive correlations with $r^2 = 0.77$ on the uranogenic Pb isotope diagram (Fig. 8a) and $r^2 = 0.93$ on the thorogenic Pb isotope diagram (Fig. 8b), respectively. On both Pb isotope diagrams, the array extends from the composition of the igneous crust (±sediments) subducting outboard of

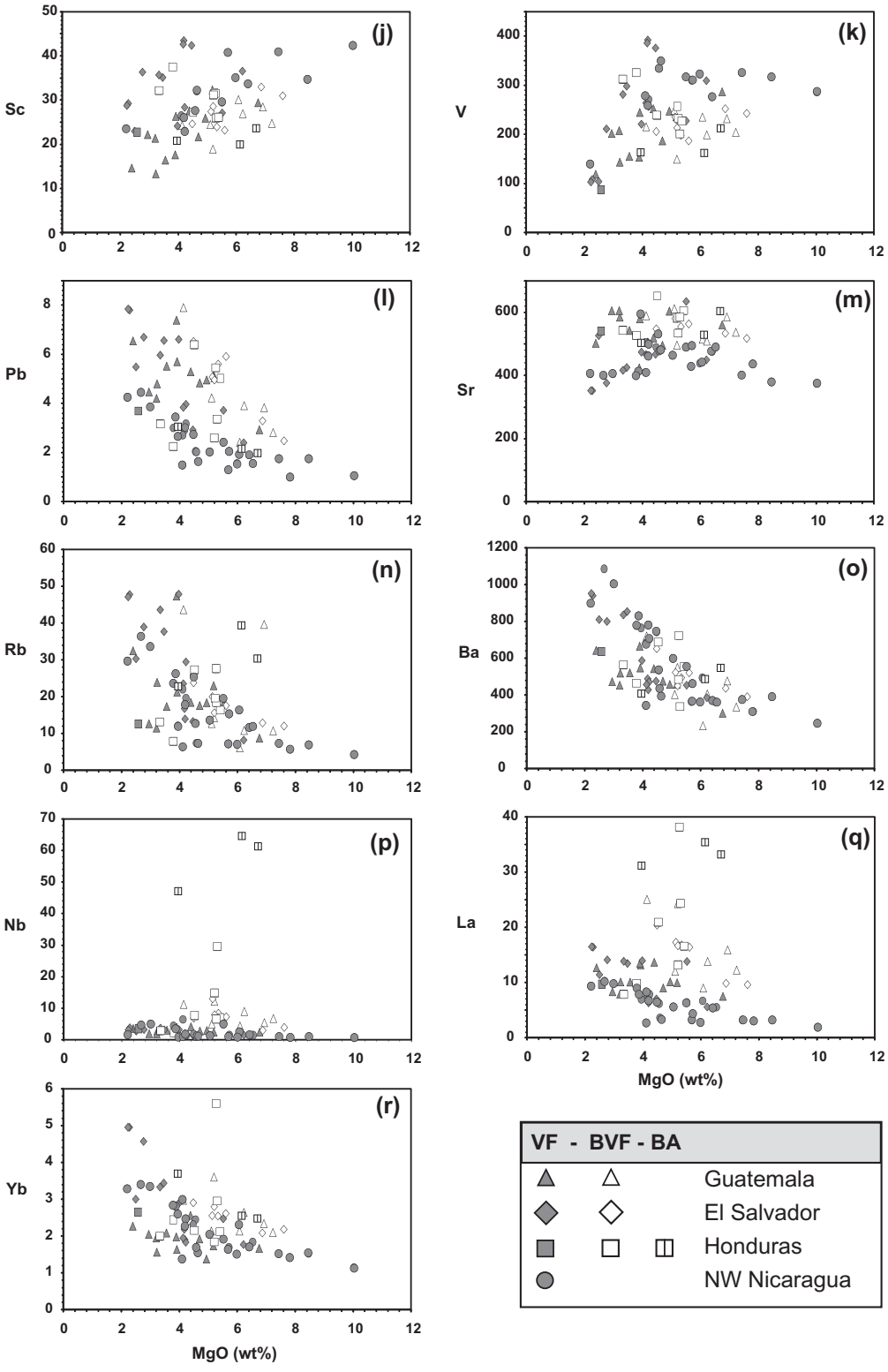


Fig 3. *(continued)*

Nicaragua, as characterized by the composition of a bend-faulted seamount (Werner et al., 2003), into the Cocos Plate sediment field. With the exception of BA samples from Utila (Honduras), the BVF samples overlap the VF trend, extending to compositions with slightly more radiogenic Pb. On $^{207}Pb/^{204}Pb$ vs. Nd and Hf isotope diagrams, NW

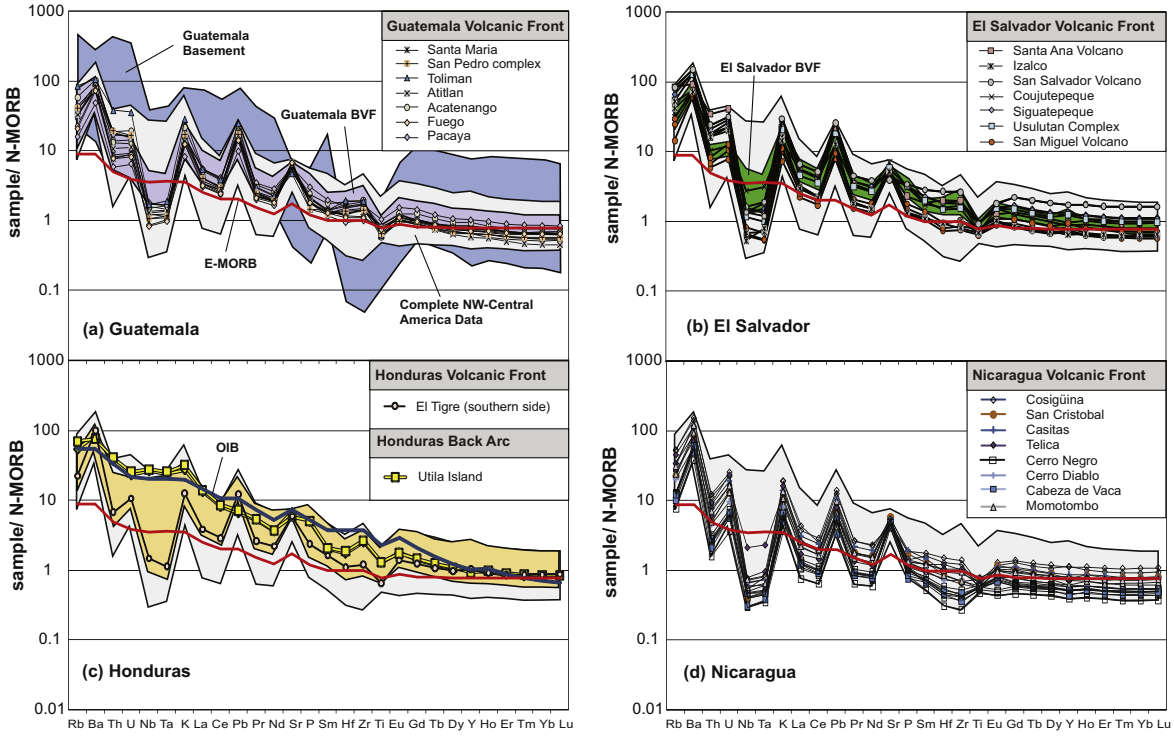


Fig. 4. Primitive N-MORB normalized (after Sun and McDonough, 1989) multi-element diagram of selected volcanic front (VF) samples (MgO > 2 wt%) from Guatemala, El Salvador, Honduras and Nicaragua. The complete range of Central American Arc lava compositions from this study is indicated by underlying grey field, including VF and BVF samples. Colored fields mark BVF sample compositions for respective countries (5a–c). The yellow field (5c) for the Honduras behind the volcanic front (BVF) contains samples from El Tigre to Tegucigalpa. Reference E-MORB (bold red line) and OIB (bold blue line) patterns are after Sun and McDonough (1989). (For interpretation of the references to colour in this figure legend, the reader is referred to the web version of this article.)

Central American VF samples form negative correlations (with $r^2$ of 0.77 and 0.78, respectively), illustrating coupling between Pb and Nd as well as Hf isotopic systems (Fig. 9).

On the $\varepsilon_{Nd}$ vs. $\varepsilon_{Hf}$ diagram (with the epsilon units describing the deviation from the CHUR evolution line in parts per $10^4$ after DePaolo and Wasserburg (1976) and Blichert-Toft et al. (1999) (Fig. 10), the NW Central American volcanic rocks (VF/BVF/BA) form a good positive correlation ($r^2 = 0.89$; VF alone has $r^2 = 0.98$, VF/BVF have $r^2 = 0.94$ and BVF/BA have $r^2 = 0.78$). The BVF/BA samples largely overlap with the VF trend but some samples from Guatemala and especially from Honduras fall below the array with the BA samples deviating the most from the array. It is clear from the Pb vs. Hf and the $\varepsilon_{Nd}$ vs. $\varepsilon_{Hf}$ isotope diagrams that the Cocos Plate sediments cannot serve as the enriched endmember for the VF and the BVF samples. Granitic sample G3K from the Guatemala basement (Chiquimula Pluton), on the other hand, falls on the enriched end of an extension of the NW Central American array.

$\delta^{18}O$ forms crude inverse correlations with Sr (Fig. 11), Nd and Hf and crude positive correlations with Pb isotopic ratios (Fig. 12). $\delta^{18}O$ in the BVF and BA samples (5.3–5.6) are elevated above the range commonly found in olivine from mantle peridotites (5.0–5.2) (Mattey et al., 1994).

## 4. DISCUSSION

As is illustrated on the $^{87}Sr/^{86}Sr$ vs. $^{143}Nd/^{144}Nd$ isotope correlation diagram (Fig. 7), Quaternary volcanism in NW Central America can be divided into three endmember compositional groups. The main characteristics have been summarized in Table 3.

Isotopically volcanic rocks from the NW Nicaragua VF represent a depleted endmember isotopically in the Central American system similar to the subducting Cocos Plate (e.g. bend-faulted seamount sample SO144-1), with the exception of elevated $^{87}Sr/^{86}Sr$. Volcanic rocks from the Guatemalan VF and from BVF centers represent an isotopically enriched endmember. Volcanic rocks from the BA (Yojoa in Honduras and Utila Island in the Caribbean) also represent a depleted endmember isotopically, similar in composition to Pacific MORB. In contrast to the Nicaragua endmember, it also has an unradiogenic Sr isotopic composition.

The incompatible element geochemistry of the Quaternary VF and BVF rocks in NW Central America clearly indicate a subduction zone affinity for these volcanic rocks: relative enrichment of LILEs and Pb (which form peaks on multi-element diagrams; Fig. 4), and relative depletion of HFSE, such as Nb, Ta and Ti (which form troughs on multi-element diagrams), and higher Ba/La, Ba/Th, Ba/Nb,

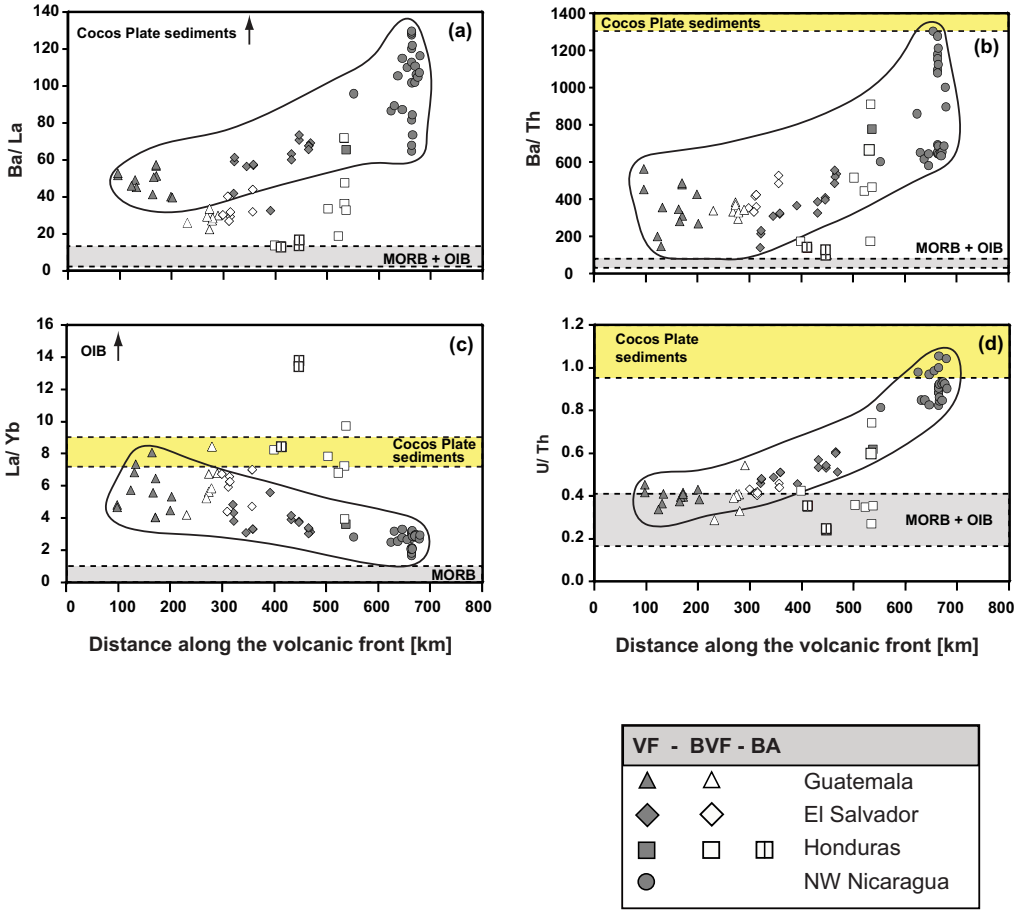


Fig. 5. Distance along the volcanic front vs. selected trace element ratios of fluid mobile to immobile elements (Ba/La, Ba/Th and U/Th) and for more incompatible to less incompatible REE abundance (La/Yb) for mafic northwestern CAVA volcanic rock samples from the VF, BVF and the BA. Distance along the VF in kilometers is calculated from Tacana Volcano near the Guatemalan–Mexican border. Horizontal grey bars indicate typical trace element ratio values for mid-ocean-ridge basalts (MORB), ocean–island–basalts (OIB) and Cocos Plate sediments (consisting of hemipelagic and carbonate sediments) after Hofmann (1988), Sun and McDonough (1989) and Plank and Langmuir (1998).

U/Th and Sr/Ce than commonly found in MORB and OIB. The good correlations between Pb, Nd and Hf isotope ratios further suggest that the geochemistry of these volcanic rocks are largely controlled by two endmembers as defined above for the VF rocks from NW Nicaragua which are isotopically depleted and the VF and BVF rocks from Guatemala which are enriched respectively.

However the incompatible element geochemistry of the BA volcanic rocks is characteristic of intraplate or OIB-type volcanism, i.e. enrichment in moderately to highly incompatible elements with relative enrichment (peak on multi-element diagram; Fig. 4c) in Nb and Ta and relative depletion (trough; Fig. 4c) in Pb. Below we will discuss the origin of these three endmember compositions in Quaternary NW Central American volcanism.

### 4.1. NW Nicaragua VF endmember

The active volcanism in Nicaragua occurs where the fluid/hydrous melt flux from the subducting slab is the highest and focused into a narrow region and the melting column is the longest compared to the rest of the Central America VF (Fig. 15) (e.g. Carr et al., 1990). These factors should result in extensive mantle melting (Plank and Langmuir, 1988; Carr et al., 1990) and effective dilution of fertile pyroxenitic or peridotitic mantle lithologies, possibly existing beneath Nicaragua, with abundant peridotite-derived melts. Indeed, the high CaO at moderately low $SiO_2$ and high $FeO_t$ (Fig. 3) and the near-chondritic Zr/Hf (28–36) in primitive Nicaraguan lavas (this work) and melt inclusions in olivine (e.g. Sadofsky et al., 2008) are fully compatible with peridotite predominantly melting beneath Nicaragua (e.g. Pertermann et al., 2004; Herzberg and Asimow, 2008). The low concentrations of "conservative" elements (Nb, Ta, Zr, Hf, Ti) (Pearce and Peate, 1995) suggest high degrees of peridotite melting beneath Nicaragua estimated to be as high as 25–30% beneath Cerro Negro volcano (e.g. Eiler et al., 2005; Sadofsky et al., 2008). Noticeably, the most primitive (MgO > 5 wt.%) lavas from Nicaragua have low Dy/Yb (1.7–1.8), suggesting no or very

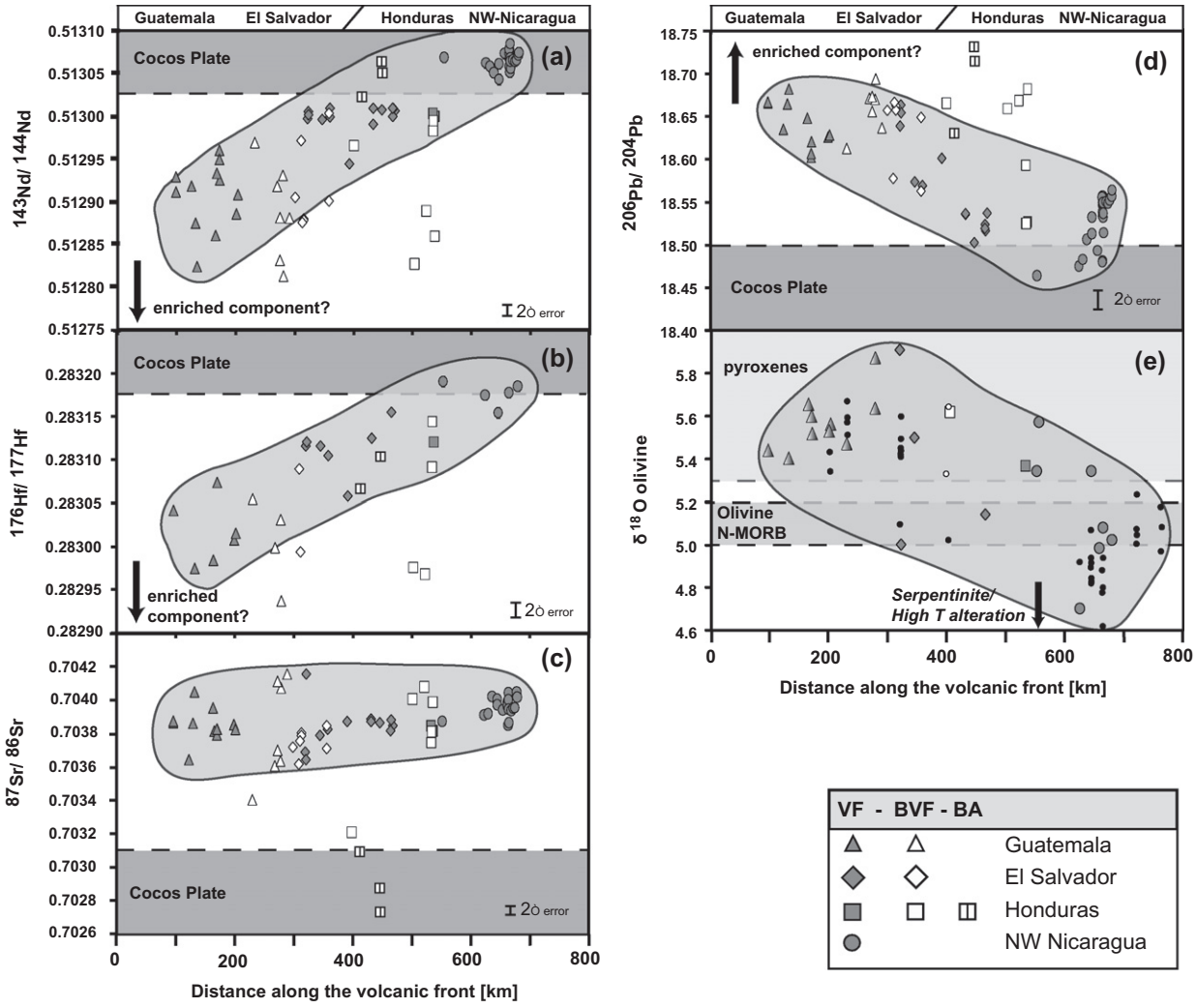


Fig. 6. Distance along the volcanic front vs. $^{143}Nd/^{144}Nd$, $^{176}Hf/^{177}Hf$, $^{87}Sr/^{86}Sr$, $^{206}Pb/^{204}Pb$ and $\delta^{18}O_{olivines}$ for Central American volcanic samples (MgO > 2 wt.%). Corresponding countries are located on top of the diagrams. Solid symbols represent volcanic front and open symbols behind the volcanic front samples respectively. The isotopic composition generally varies systematically along the volcanic front and to a lesser extent into the back arc, ranging between depleted MORB/upper mantle-like isotopic ratios and more enriched isotopic compositions (with the exception of Sr isotopes, which show no systematic variation along the volcanic arc). Gray fields define the volcanic front array. MORB field includes data from DSDP Leg 67 (offshore Guatemala) after Geldmacher et al. (2008), seamount offshore Nicaragua (SO144-1; Werner et al., 2003), IODP site 1256 MORB (Sadofsky et al., 2009) and this study. Small black and white circles in (e) are data from Eiler et al. (2005). Field for $\delta^{18}O$ values for pyroxenites after Pearson et al. (1991). All errors are reported as $2\sigma$ of the mean.

minor amounts of garnet in the source (e.g. Feigenson and Carr, 1993; Blundy et al., 1998).

High ratios of fluid–mobile to less-fluid–mobile incompatible elements, e.g. Ba/La, Ba/Th, Ba/Nb, U/Th and Sr/Ce, in Nicaragua volcanic rocks have been used to argue that the highest flux of subducting slab-derived fluids are being added to the mantle wedge beneath Nicaragua (e.g. Carr et al., 1990; Leeman et al., 1994; Patino et al., 2000; Abers et al., 2003; Eiler et al., 2005; Sadofsky et al., 2008). These ratios are very high in the subducting sediments off Central America (Plank and Langmuir, 1998; Patino et al., 2000) and in the lavas from the central Nicaraguan VF lavas, which extend to values similar to the ones found in the subducting sediments (Fig. 5). In addition, water content in melt inclusions from Central America correlates well with the Ba/La ratio (Wade et al., 2006; Sadofsky et al., 2008). Therefore Ba/La can serve as a proxy for hydrous fluid/melt flux beneath Central America, showing that it is highest beneath volcanoes in central Nicaragua (Cerro Negro).

The reason for this high fluid flux beneath Nicaragua may be related to the serpentinization of the upper mantle of the subducting slab. It has been shown that outer-rise faulting, related to the bending of the plate, outboard of NW Central America extends into the upper mantle (Ranero et al., 2003). Since the upper mantle in the bend-faulted areas has lower seismic velocities than the upper mantle further to the west, it has been proposed that the uppermost

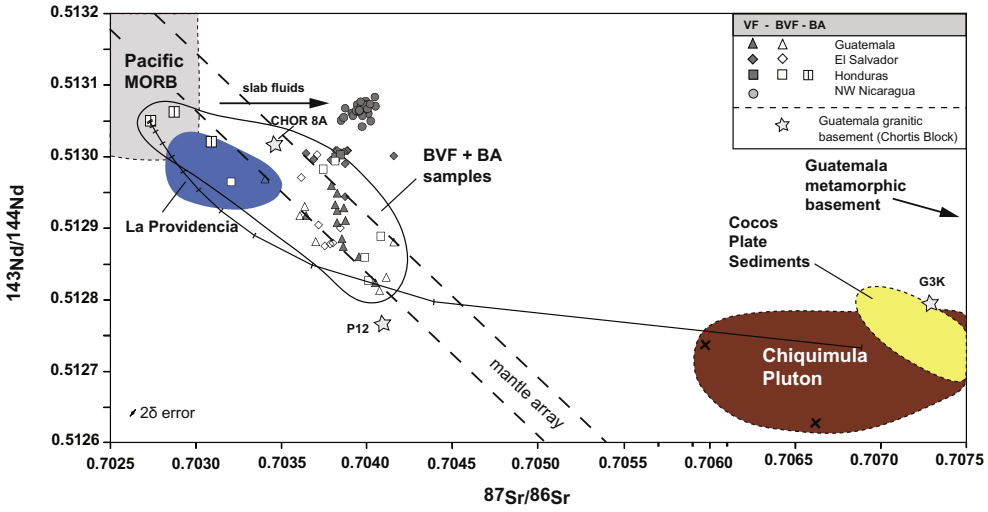


Fig. 7. Sr–Nd isotope diagram for NW Central American volcanics, with VF samples generally forming a crudely positive to vertical array, whereas BVF samples form a negative array. Pacific MORB (after Stracke et al., 2005; Geldmacher et al., 2008; Sadofsky et al., 2009; and this study), Cocos Plate Sediments (Feigenson et al., 2004; Geldmacher et al., 2008; Sadofsky et al., 2009; and this study) and Chiquimula Pluton (after Feigenson et al., 2004) mark potential source component compositions. Black arrow labeled slab fluids indicates Sr isotope enrichment of Nicaraguan samples by slab fluids derived from subducted sediments, seawater-altered oceanic crust and/or serpentinite. The black curve represents a binary mixing line between outboard NW Nicaragua subducting igneous crust (Werner et al., 2003) and an average Chiquimula Pluton (Feigenson et al., 2004; and this study). Used endmember values: SO144-1 (Sr: 106 ppm; Nd: 13 ppm; $^{87}Sr/^{86}Sr$: 0.70268; $^{143}Nd/^{144}Nd$: 0.51311) and G3K avg. (Sr: 39 ppm; Nd: 12 ppm; $^{87}Sr/^{86}Sr$: 0.70730; $^{143}Nd/^{144}Nd$: 0.51280). Tick marks for 1, 5, 10, 20,...,100 percent indicate the amount of granitic pluton assimilated in melt from the mantle wedge without a slab melt component. All errors are reported as $2\sigma$ of the mean.

lithospheric mantle has been hydrated and serpentinized to a depth of ~4 km (Grevemeyer et al., 2007; Ivandic et al., 2008). Although bend-faulting has been mapped along the Cocos Plate outboard of the entire NW Central America (Nicaragua to Guatemala), the steeper subducting angle results in the subducting slab being at the deepest depths beneath the Nicaraguan VF, placing the upper mantle of the down-going plate within the zone of serpentinite dehydration, where the mineral breaks down (Fig. 15). Due to the shallower subduction angle and shallower depths to the subducting plate to the north, the amount of serpentinite dehydration beneath the VF will decrease to the NW beneath El Salvador and Guatemala. The lowest $\delta^{18}O$, well below typical mantle values, in olivine phenocrysts from Nicaragua (see Fig. 6e) are consistent with a greater flux of hydrous fluids from hydrothermally-altered lower oceanic crust and/or upper mantle serpentinite (Eiler et al., 2005). Greater fluid flux beneath Nicaragua will also enhance the degree of melting, contributing to the dilution of Na and other incompatible elements at a given MgO content (e.g. Eiler et al., 2005).

The mobility of trace elements in slab-derived fluids is strongly dependent on temperature (Kessel et al., 2005; Hermann et al., 2006). A quantitative estimate of whether the isotope ratios of incompatible elements in Nicaraguan lavas reflect the composition of mantle source or dominated by slab fluids can be therefore constrained if the temperature of the slab fluid source is known. Sadofsky et al. (2008) published a useful dataset on $H_2O$ and trace element composition of primitive melt inclusions from Cerro Negro volcano in Nicaragua. By using maximum measured $H_2O$/Ce (~10,000) in the melt inclusions and a parameterization relating $H_2O$/Ce in the slab component to its source temperature (Plank et al., 2010), we estimated that the temperature of the fluid source beneath Nicaragua is about 700 °C that is slightly below the wet sediment solidus. At this temperature, the solubility of most trace elements in either sediment- or AOC-derived fluids is low (Kessel et al., 2005; Hermann et al., 2006). By using experimental data from Kessel et al. (2005), we estimate then that at 700 °C Nd and Hf have partition coefficients between fluid and solid well below 0.1 and thus can be considered as very immobile elements. Sr has a partition coefficient of about 0.4 and is a moderately mobile element. A truly fluid–mobile element at these conditions is Pb, which has partition coefficient of ~4 and thus strongly partitions into the fluid phase. The mobility of elements in slab-derived fluids beneath Nicaragua decreases in the order Pb > Sr > Nd ~ Hf which is similar to that inferred for other "cold" arc systems (e.g. Pearce et al., 2007). Based on this analysis, the Hf and Nd isotopic composition should primarily reflect the composition of the mantle wedge with minor contribution from slab fluids, whereas the Sr and Pb isotopic compositions should primarily reflect a large to dominant contribution from the slab fluid to a depleted mantle source.

We now review the isotope data in the order of increasing fluid mobility to better constrain the sources involved in generating the Nicaraguan VF melts. The NW Nicaraguan volcanic rocks have high $^{143}Nd/^{144}Nd$ and $^{176}Hf/^{177}Hf$ ratios, falling within the range observed in Pacific MORB

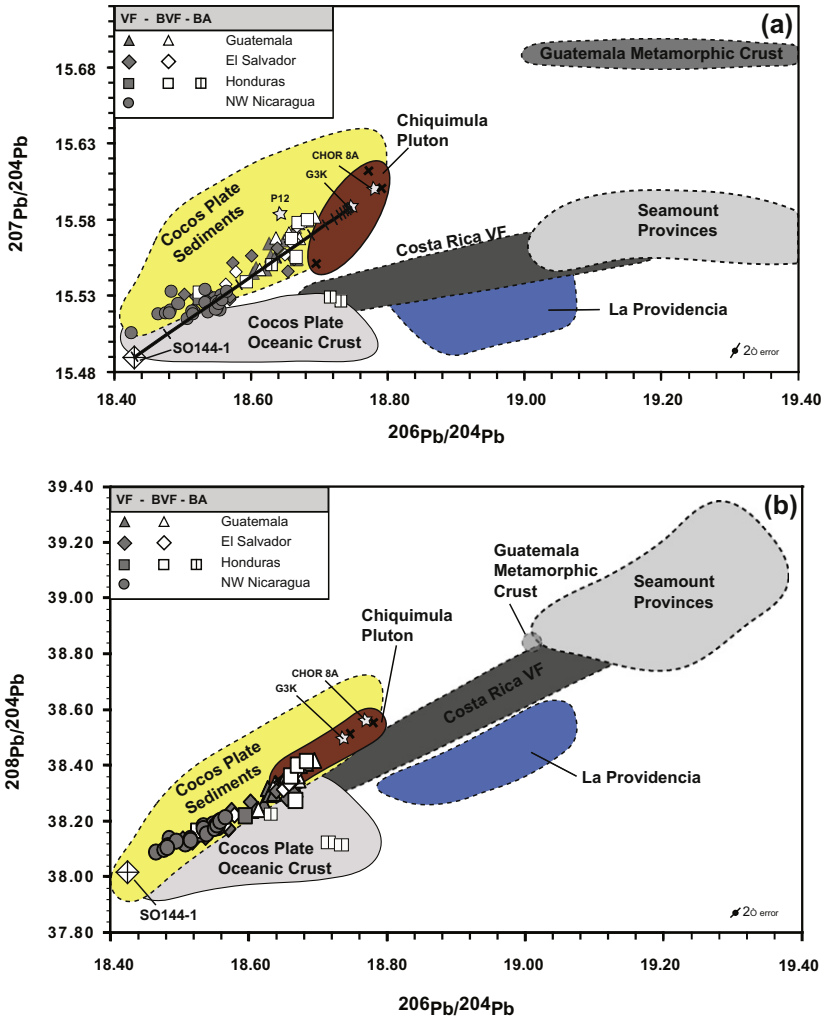


Fig. 8. (a, b) Uranogenic (a) and thorogenic (b) lead isotopic correlation diagram for Central American volcanic rock samples. Northwestern CAVA samples form good linear correlations with $r^2 = 0.77$ ($y = 0.2493x + 10.908$) on (a) for the VF samples alone and $r^2 = 0.86$ ($y = 0.2875x + 10.201$) for VF and BVF samples, excluding back-arc samples from Yojoa and Utila. In both diagrams (a) and (b) Nicaraguan VF samples have the least radiogenic Pb isotopic compositions and overlap with the field for the Cocos Plate. The Guatemalan VF samples and the Guatemala and Honduras BVF samples have the most radiogenic Pb isotopic compositions and overlap the fields for subducting Cocos Plate sediments and Guatemala granitic crust. Subducting crust (SO144-1) offshore NW Nicaragua after Werner et al. (2003). Data for the Chiquimula Pluton is from Feigenson et al. (2004). All errors are reported as $2\sigma$ of the mean. Fields for Costa Rica VF and Seamount Provinces (after Hoernle et al., 2008) indicate that these components cannot generate the observed data array. Solid line in (a) represents a mixing line between SO1441 (Pb: 0.58 ppm; $^{206}Pb/^{204}Pb$: 18.436; $^{207}Pb/^{204}Pb$: 15.499; $^{208}Pb/^{204}Pb$: 38.053) and G3K avg. (Pb: 10.29 ppm; $^{206}Pb/^{204}Pb$: 18.75; $^{207}Pb/^{204}Pb$: 15.59; $^{208}Pb/^{204}Pb$: 38.51). Tick marks for 1, 5, 10, 20, …, 100 percent indicate the amount of outboard NW Nicaragua subducting igneous crust added to the Chiquimula Pluton.

(Fig. 10). Considering that both Nd and Hf are relatively fluid-immobile, the Nd and Hf isotopic compositions are consistent with the mantle wedge beneath Nicaragua having a MORB-like composition. Since a possible minor contribution of Nd and Hf from subducting sediments would cause a decrease in both Nd and Hf isotopic composition, the Nd and Hf isotopic ratios of the Nicaraguan melts represent minimum values for the mantle wedge.

On the Sr vs. Nd isotope correlation diagram, the BVF/BA samples form a negative array, extending the Pacific MORB field to more radiogenic Sr and less radiogenic Nd. The BVF/BA array overlaps and is subparallel to the Sr–Nd isotope mantle array. The Nicaraguan samples show the greatest horizontal deviation, i.e. enrichment in $^{87}Sr/^{86}Sr$, from the BVF/BA (or mantle) array and the amount of deviation/enrichment decreases along the VF to Guatemala. The $\Delta^{87}Sr/^{86}Sr$ represents the difference in $^{87}Sr/^{86}Sr$ ratio between a sample and a point on the best-fit line through the BVF/BA array with the same $^{143}Nd/^{144}Nd$ isotope ratio ($\Delta^{87}Sr/^{86}Sr = {}^{87}Sr/^{86}Sr$ (sample) $-$ (($^{143}Nd/^{144}Nd$ (sample) $- 0.6227$)/$-0.156$) $* 1000$). $\Delta^{87}Sr/^{86}Sr$ forms good positive correlations with ratios of more to less fluid–mobile elements such as Ba/Th, U/Th, Ba/Nb and Ba/La (see e.g. Fig. 13 a and c). These

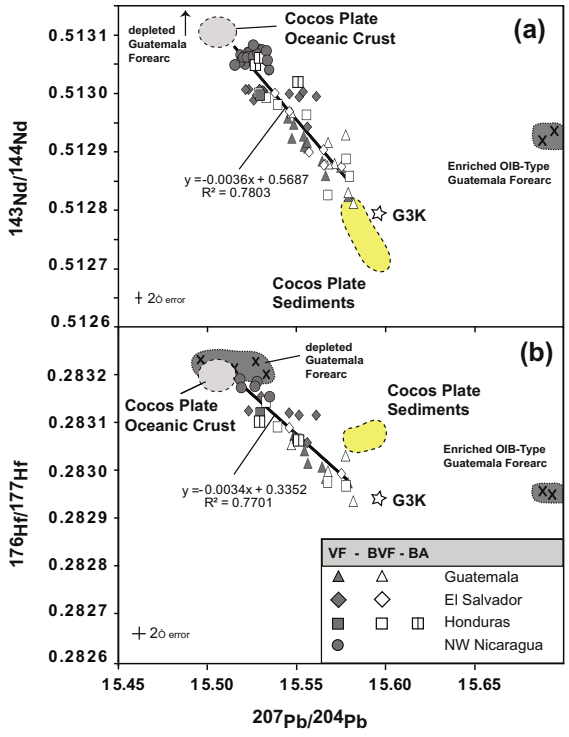


Fig. 9. (a–b). Lead vs. Nd and Hf isotope correlation diagrams for NW CAVA volcanics with MgO > 2%. All samples form negative correlations, ranging from 0.67 to 0.78 for $R^2$ (bold black lines), providing evidence that the Pb isotopic composition is coupled with variations in Nd and Hf isotopic composition. In addition, the Pb vs. Hf isotope correlation diagrams clearly rule out Cocos Plate sediments and enriched OIB-type Guatemalan forearc (Geldmacher et al., 2008), as the enriched endmember for NW Central American volcanism, i.e. Guatemalan VF and Guatemalan and Honduras BVF volcanism. Granitic Guatemalan basement sample G3K however has the appropriate isotopic composition to serve as the enriched endmember. Fields for Cocos Plate sediments and oceanic crust are supplemented by DSDP Leg 67 sample data (offshore Guatemala). Grey oval field indicates Cocos Plate crust subducting offshore NW-Nicaragua (after Hoernle et al., 2008). Additional data are from Werner et al. (2003), Feigenson et al. (2004) and Geldmacher et al. (2008). All errors are reported as 2$\sigma$ of the mean.

correlations are consistent with $\Delta^{87}Sr/^{86}Sr$ reflecting the magnitude of the hydrous fluid/melt flux from the slab, which determines the degree of decoupling of Sr from Nd and Hf isotope ratios, with Sr being derived from a combination of subducted sediments, seawater-altered oceanic crust and sea-water serpentinized upper lithospheric mantle of the incoming slab. Inverse correlations of $\Delta^{87}Sr/^{86}Sr$ with La/Yb and Zr/Hf ratios are likely to reflect differences in degree of melting and source depletion/enrichment (see Fig. 13 b and d). Compared to the chondritic ratio of $34.3 \pm 0.3$ (Münker et al., 2003), the Nicaraguan magmas extend to lower Zr/Hf, reflecting possible source depletion through repeated melting and melt extraction events, and the Honduras, El Salvador and Guatemala lavas to higher Zr/Hf, possibly reflecting source enrichment by small degree melts from a pyroxene-rich source. Therefore the mantle beneath the Nicaragua VF appears to have undergone high degrees of melt extraction and source depletion, whereas the Guatemalan VF has undergone lower extents of melting and possible source enrichment, as is also consistent with the Nd and Hf isotopic data.

The NW Nicaraguan samples have the least radiogenic Pb isotopic compositions, overlapping the compositional fields of the Cocos Plate igneous crust and sediments (Fig. 8). The relatively unradiogenic Pb isotopic compositions of the NW Nicaraguan VF lavas indicate that slab fluids primarily carry Pb from the subducting oceanic crust, possibly with contributions from serpentinites and small amounts of sediment (<1%; Gazel et al., 2009). Considering the highly fluid–mobile behavior of Pb in subduction systems and the high fluid flux to the subarc mantle beneath the Nicaraguan VF, it is not surprising that the subduction input completely dominates the Pb isotopic composition.

In conclusion, the incompatible element and Sr–Nd–Pb–Hf–O isotope geochemistry of the NW Nicaragua lavas appears to be mostly dominated by a largely serpentinite-derived fluid flux from the subducting slab, possibly with small amounts (<1 wt.%) of sediment melts, to a depleted N-MORB type of mantle wedge, resulting in large extents of melting of primarily peridotitic material.

### 4.2. Guatemala VF and BVF endmember

The higher abundances of most incompatible elements, including higher $Na_6$ (Eiler et al., 2005), and higher ratios of more incompatible to less incompatible elements (e.g. La/Yb, La/Sm) could reflect lower degrees of melting and/or a more enriched source for the Guatemala magmas. Lower degrees of melting inferred for Guatemala from inverse modeling of trace element abundances (e.g. Feigenson and Carr, 1993; Eiler et al., 2005; Sadofsky et al., 2008) are also consistent with a more diffusive fluid flux towards the NW, due to the shallower angle of subduction beneath El Salvador, Honduras and Guatemala (e.g. Carr et al., 1990), and with the decreasing thickness of the mantle wedge (i.e. decreasing potential length of the mantle melting column (Fig. 15).

The lavas from Guatemala have lower fluid–mobile to less-fluid–mobile element ratios (e.g. Ba/La, U/Th, Ba/Th, Ba/Nb, Sr/Ce; Fig. 5) and $\Delta^{87}Sr/^{86}Sr$ compared to the NW Nicaragua (Fig. 13). A possible explanation for this difference could be a higher temperature for the slab source beneath Guatemala that should cause less fractionation of the aforementioned element ratios if they originated from the same source as the slab fluids beneath NW Nicaragua (e.g. Kessel et al., 2005; Hermann et al., 2006). As suggested by the melt inclusion data (Sadofsky et al., 2008), the relatively low $H_2O$/Ce (1000–1800) ratios in primitive melts from Guatemala indeed may suggest a higher temperature of ~850 °C in the slab source, which is nearly 150 °C higher compared to NW Nicaragua. The inferred slab temperatures beneath Guatemala are well above the wet sediment solidus (e.g. Plank et al., 2009 and references therein), and therefore the slab component

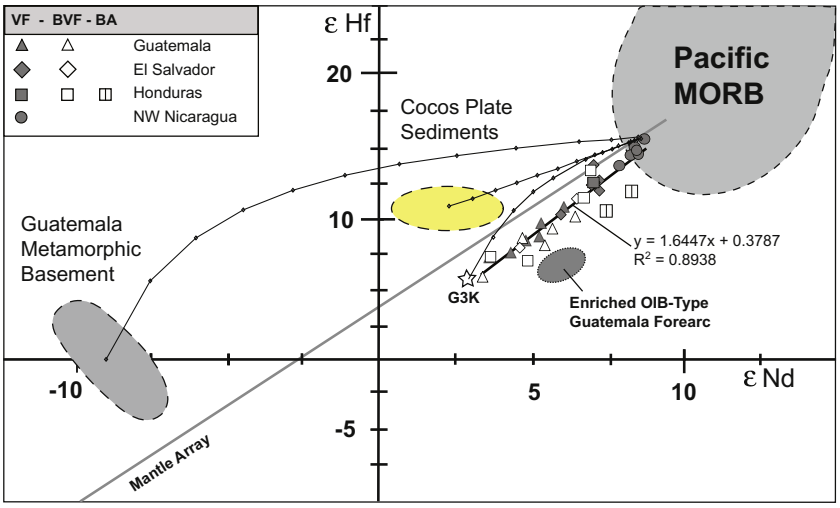


Fig. 10. $\varepsilon_{Nd}$ vs. $\varepsilon_{Hf}$ diagram for Central American volcanic rock samples. Combined VF and BVF samples from the northwestern Central American volcanic arc form a very good positive linear correlation (solid line going through the data with $R^2 = 0.89$). Excluding the BA samples, the positive trend can be defined by two components (SO1441 or P-60 depleted MORB-type composition and G3K enriched type composition) with Nicaraguan samples having the most Pacific MORB-like compositions and Guatemalan samples trending towards an enriched component. Included are binary mixing curves between a Pacific MORB-like component and several selected source components (e.g. Guatemalan metamorphic basement, Cocos Plate sediments). The mantle array line is calculated using $\varepsilon_{Hf} = 1.4\varepsilon_{Nd} + 2.8$ (after J. Blichert-Toft, unpublished compilation). Diagram modified after Geldmacher et al. (2006) with additional fields for Guatemala Basement, Cocos Plate Sediments (DSDP Leg 67 offshore Guatemala) and Guatemala forearc basement (Geldmacher et al., 2008).

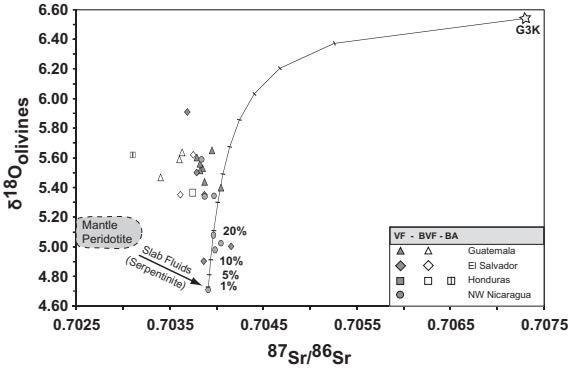


Fig. 11. Correlation of strontium isotope composition vs. $\delta^{18}O_{olivines}$ values for NW Central American volcanics, with VF samples generally forming a steep negative to vertical array. Behind volcanic front samples form a very broad negative array. Curve represents mixing between Chiquimula Pluton (granitic basement) and San Cristobal volcano (asthenospheric mantle wedge source) and shows an assimilation of 45–50% of G3K to generate the trend described by our data. Used endmember values: P-27A (Sr: 531 ppm; O: 502457 ppm; $^{87}Sr/^{86}Sr$: 0.703907; $\delta^{18}O_{olivines}$: 4.71) and G3K avg. (Sr: 39 ppm; O: 559635 ppm; $^{87}Sr/^{86}Sr$: 0.70730; $\delta^{18}O_{olivines}$: 6.54). Note $\delta^{18}O_{olivines}$ value for G3K sample has been calculated from measured $\delta^{18}O_{olivines} - 0.6$. Tick marks indicate the amount of granitic pluton assimilated in melt from the mantle wedge without a slab melt component.

derived at this temperature is expected to be a hydrous melt rich in incompatible trace elements and relatively poor in water.

If the mantle wedge is fluxed with a wet, predominantly sediment-derived slab melt beneath Guatemala and fluids beneath NW Nicaragua, this can explain many geochemical features of the erupted lavas such as overall similarity of the trace element patterns but more pronounced enrichment in the most incompatible elements and lower fluid–mobile to less-fluid–mobile element ratios in Guatemala compared to the NW Nicaragua. Because the productivity of melt-fluxed melting is significantly lower when compared to fluid-fluxed melting (e.g. Eiler et al., 2005), the amount of melt-fluxed induced enriched component in the mantle source of the Guatemala lavas could be relatively large compared to the amount of fluid-fluxed induced depleted component, which results from lower than for NW Nicaragua degrees of melting. This can explain higher $\delta^{18}O$, Sm/Yb and Zr/Hf and a more pronounced sediment-like isotope signature seen in Sr–Nd–Pb–Hf isotope systematics of the lavas from Guatemala.

The enriched Sr, Nd, Hf and Pb isotopic composition of the Guatemala endmember is however not consistent with a major contribution from the subducting plate (sampled at DSDP Site 495 and IODP Site 1256; Geldmacher et al., 2008; Sadofsky et al., 2009) or older accreted arc complexes eroded from the Guatemala forearc by the subduction process (sampled at DSDP Sites 499 and 567; Geldmacher et al., 2008). The Pb vs. Hf (Fig. 9b) and Nd vs. Hf (Fig. 10) isotope correlation diagrams rule out presently subducting Cocos Plate sediments as the enriched Guatemala endmember, as proposed by some studies (e.g. Cameron et al., 2002; Eiler et al., 2005) primarily because the Hf isotopic compositions in the sediments are too high to serve as this endmember. Enriched accreted OIB-type terranes sampled in the forearc can also be ruled out as the enriched Guatemala endmember, because their Pb and Nd isotope ratios relative to Hf isotopic ratios are too high

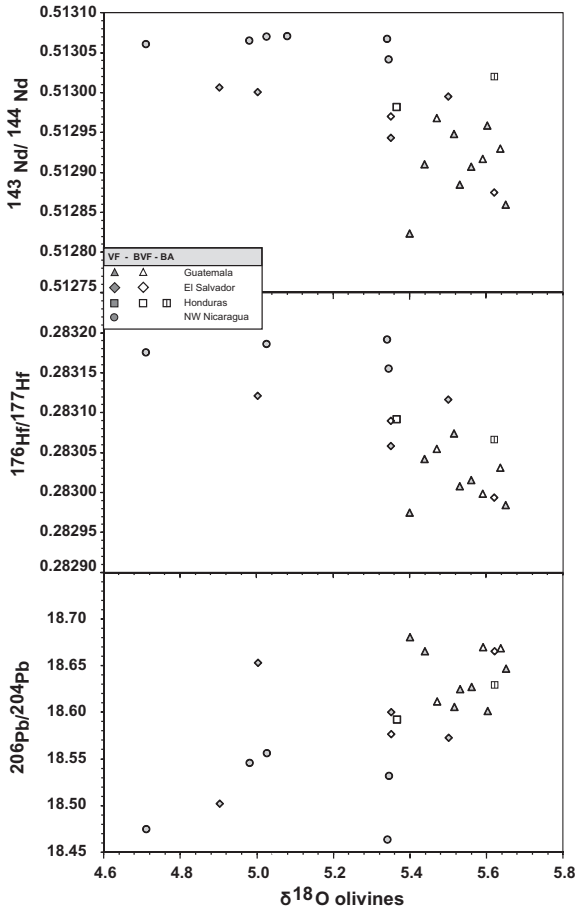


Fig. 12. Correlation of $\delta^{18}O_{olivines}$ values vs. Nd, Hf and uranogenic lead isotope compositions for NW Central American volcanics. All samples form negative correlations in Nd and Hf and positive in $^{206}Pb/^{204}Pb$.

(e.g. Figs. 9 and 10). Therefore the composition of the subduction input (subducting plate and eroded forearc material) cannot explain the combined Nd–Pb–Hf isotopic systematics of the enriched Guatemalan endmember. The source of the enriched component therefore must be in the overriding plate, either within the crust or in the non-convecting lithospheric part of the mantle wedge.

It has previously been proposed that Guatemalan volcanic rocks have been crustally contaminated (e.g. Carr et al., 1990; Walker et al., 1995, 2007, 2009; Patino et al. 2000; Cameron et al., 2002; Carr and Feigenson, 2003; Feigenson et al., 2004; Jicha et al. 2010). Therefore we now review whether the Guatemala basement samples from this and other studies could serve as the possible enriched endmember. Jicha et al. (2010) have proposed up to 20% assimilation of depleted MORB-like ocean crust (for example, in the form of accreted ophiolitic terranes beneath the volcanic arc, e.g. Hoernle et al., 2004; Geldmacher et al., 2008) at Santa Maria to explain a crude correlated decrease in ($^{238}U/^{230}Th$) and $^{87}Sr/^{86}Sr$ isotope ratios. Assimilation of depleted MORB-type crust, however, cannot explain the lower Nd and Hf and higher Pb isotopic compositions in the Guatamala volcanic rocks compared to those further to the southeast, not to mention the enriched incompatible element abundances of the Guatemala volcanic rocks.

We will now evaluate the possible role of assimilation of plutonic and metamorphic basement. To begin with, we will consider dioritic to granodioritic basement samples from the Las Ovejas and Santa Maria areas respectively. Sample Chor 8A from Las Ovejas is too depleted in Sr and Nd isotopic composition to serve as the enriched endmember. Sample P12 from the Las Ovejas area has appropriate Sr and Nd isotopic composition, plotting slightly below the most enriched VF and BVF samples from Guatemala and Honduras (Fig. 7), but the $^{207}Pb/^{204}Pb$ isotope ratio for this sample is too high to serve as the enriched endmember on the uranogenic Pb isotope diagram (Fig. 8). In addition, the Zr/Hf ratios (17–19) of both Las Ovejas samples are too low. The basement samples from the Santa Maria Volcano (G009 L1 and L2) also do not serve as appropriate endmembers, because their Nd is too radiogenic, Pb not radiogenic enough and the Zr/Hf is again too low (13–25).

Phyllite samples (M1, M2) from the metamorphic Chortis Block basement behind the VF in Guatemala have very radiogenic Sr and Pb and unradiogenic Nd and thus could serve as the enriched endmember in these isotopic systems (data from this study and Feigenson et al., 2004). This basement, however, can be ruled out, because it plots above the mantle array on the $\varepsilon_{Nd}$ vs. $\varepsilon_{Hf}$ diagram. The northwestern Central American VF and BVF rocks, however, form a positive correlation below the Nd–Hf mantle array, which has a slightly steeper slope than the mantle array and thus projects to an enriched component beneath the mantle array. Furthermore, mixing between the most depleted sample (with the most radiogenic Nd and Hf) from the Nicaraguan VF with the Guatemalan metamorphic basement forms a convex (or concave down) mixing curve, which does not go through the NW Central American data array (see Fig. 10). The Zr/Hf ratios of these samples are also too low (27–28) to serve as the enriched endmember. Mylonitic gneiss rocks from the Maya Block (619 and 714A), on the other side of the plate boundary from the NW Central American arc rocks, also do not have appropriate Nd-Hf and Pb isotopic compositions (Table 2), and their Zr/Hf ratios (17–24) are also too low to serve as the enriched endmember, not to mention the difficulty of getting this material across the plate boundary to the source of the subduction-zone volcanism on the Chortis Block.

Interestingly, only granitic sample G3K from the Chiquimula Intrusive Complex behind the Guatemalan VF on the Chortis Block has a Sr–Nd–Pb–Hf–O isotopic composition that could serve as the enriched endmember (Figs. 8–11). Chiquimula samples G1 (granite) and G2 (granodiorite) also have appropriate Sr–Nd–Pb isotopic compositions (Feigenson et al., 2004), but no Hf isotope data exist for these samples. There are, however, a number of problems with explaining the enriched Guatemala endmember with assimilation of granitic basement by melts with similar compositions to the BA lavas, presumed to reflect the composition of the mantle wedge beneath NW Nicaragua. In order to model a mixing curve in the Sr–Nd isotope system from the most depleted BA sample (least radiogenic

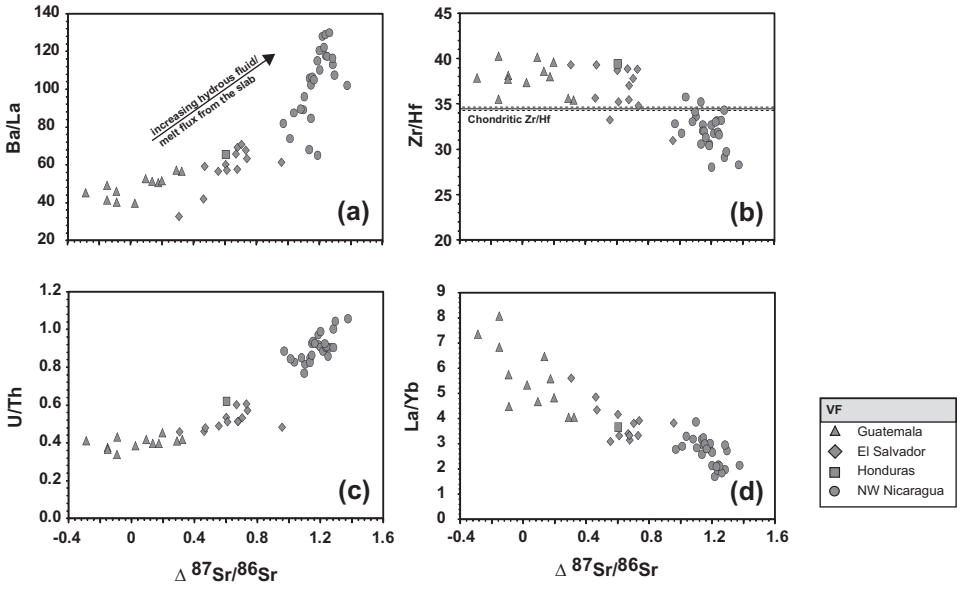


Fig. 13. (a–d) Fluid flux variation diagram using $\Delta^{87}Sr/^{86}Sr$ vs. selected fluid–mobile to less-fluid–mobile element ratios (Ba/La, U/Th), La/Yb and Zr/Hf from Central American volcanic rock samples from the volcanic front. The $\Delta^{87}Sr/^{86}Sr$ value ($\Delta$ value: $^{87}Sr/^{86}Sr$ (sample) $-$ (($^{143}Nd/^{144}Nd$ (sample) $-$ 0.6227)/$-$0.156) $*$ 1000) is based on the horizontal deviation from a best-fit line through the BVF/BA (or mantle) array on the Sr vs. Nd isotope correlation diagram (Fig. 8). Line for Chondritic Zr/Hf ratio after Münker et al. (2003).

Table 3
Endmember compositional main characteristics: major elements (>2MgO wt.%); Trace elements and ratios, and isotopic ratios.

| # | Location | Content | Major* | Traces | Isotopes |
|---|---|---|---|---|---|
| 1 | NW Nicaragua VF | High | FeOt, CaO, MnO | Sc, V, Ba/La, Ba/Th, Ba/Nb, U/Th, Sr/Ce | $^{87}Sr/^{86}Sr$, $^{143}Nd/^{144}Nd$ and $^{176}Hf/^{177}Hf$, |
| | | Low | SiO2, TiO2, Na2O, P2O5, K2O | Pb, Sr, Nb, Ta, LREE, La/Yb, Sm/Yb, Zr/Hf | $\delta^{18}O$ and Pb isotope ratios |
| 2 | Guatemala VF and BVF | Higher | $SiO_2$, $TiO_2$, $Na_2O$, $P_2O_5$, $K_2O$ | Pb, Sr, Nb, Ta, LREE, La/Yb, Sm/Yb, Zr/Hf | $\delta^{18}O$ and Pb isotope ratios |
| | | Intermediate | | | $^{87}Sr/^{86}Sr$ |
| | | Lower | $FeO_t$, CaO, MnO | Sc, V, Ba/La, Ba/Th, Ba/Nb, U/Th, Sr/Ce | $^{143}Nd/^{144}Nd$ and $^{176}Hf/^{177}Hf$, |
| 3 | BA volcanics from Honduras | High | $TiO_2$, $Na_2O$, $P_2O_5$, $K_2O$ | Moderately to highly incompatible trace element abundances (except Pb), ratios of more to less incompatible elements (e.g. La/Yb and La/Sm, Sm/Yb), Zr/Hf, | $^{143}Nd/^{144}Nd$ and $^{206}Pb/^{204}Pb$ |
| | (Yohoa and Utila) | Low | $SiO_2$, CaO | LILE vs. HFSE and REE ratios (e.g. Ba/La, Ba/Th, Ba/Nb, U/Th, Sr/Ce) | $^{87}Sr/^{86}Sr$, $^{207}Pb/^{204}Pb$ and $^{208}Pb/^{204}Pb$ |

* Differences in major elements are relative to a specific MgO content.

Sr and radiogenic Nd isotope ratios, similar to the Nd isotopic composition of the NW Nicaragua VF lavas) to an average Chiquimula Pluton (Feigenson et al., 2004; and this study) that goes through the BVF/BA array and the Guatemala VF samples more than 60 wt.% assimilation is required which is hardly compatible with the mafic composition of many Guatemala lavas (Fig. 7). On the Nd vs. Hf isotope diagram (Fig. 10), the backarc samples from Honduras do not lie on the array formed by the VF and BVF data, indicating that the backarc mantle in Honduras does not have the same Hf isotopic composition as the depleted NW CAVA VF and BVF endmember. Since Nd and Hf behave conservatively in the NW Nicaragua melts, we assume that the sample with the most radiogenic Nd and Hf from NW Nicaragua reflects the mantle wedge composition beneath NW Nicaragua. Assimilation of G3K granite by melts with the depleted Nicaragua endmember composition produces a convex (concave down) mixing

curve that doesn't go through the data, due to the higher Nd/Hf in G3K (16.9), as compared to the depleted Nicaragua endmember (P-58A = 5.5). Accessory titanium oxide phases in the granitoid e.g. rutile, could fractionate the Nd/Hf ratio but the partition coefficient for hafnium ($D_{Hf}$) is much greater than one (Green and Pearson, 1986; Foley et al., 2000). Therefore, rutile in the residuum would increase the Nd/Hf ratio in the granitic melt, which would generate an even more convex (concave down) curve on the Nd vs. Hf isotope plot. Furthermore, a basalt from Guatemala with the most enriched (lowest) Nd and Hf isotope ratios would require nearly 100% assimilation, which is not consistent with the basaltic (rather than granitic) whole rock composition. Finally, the Zr/Hf ratio (27) of G3K is also too low to be the enriched endmember.

The oxygen isotope data are also inconsistent with assimilation of granitic material. Mixing correlations between the Nicaragua samples with the lowest $\delta^{18}O$ and G3K cannot explain the crude negative trend on the Sr vs. O isotope correlation diagram formed by the northwestern Central American VF rocks and do not go through most of the VF or any of the BVF samples with elevated $\delta^{18}O$ greater than commonly observed in mantle peridotites (i.e. >5.2; Fig. 12). The oxygen isotope data for the Guatemala VF and the BVF rocks also do not allow such a large contribution from granitic rocks, with $\delta^{18}O$ values for the granitic basement of ~6.5. Assuming the lowest $\delta^{18}O$ value of 4.7 for the NW Nicaragua VF source, 50% and 60% assimilation of G3K is required to explain the highest values in El Salvador VF and the Guatemala BVF. Since oxygen is a major element in silicate rocks, lower degrees of melting will not change the oxygen content of the melt sufficiently to substantially decrease the amount of assimilation (e.g. Bindeman, 2008). In conclusion, although granitic sample G3K has the appropriate Nd–Pb–Hf isotopic composition to serve as the enriched endmember for northwestern Central America, it does not have the appropriate major and trace element composition to serve as the enriched Guatemalan endmember.

Since the Chiquimula granitic sample (G3K) has the appropriate Nd–Pb–Hf isotopic composition to serve as the enriched endmember, further consideration of this pluton, however, could provide insights into the enriched Guatemala endmember. The Chiquimula plutonic complex consists of gabbroic through granitic rocks, which yield a whole-rock Rb/Sr age of 50 ± 9 Ma and an initial $^{87}Sr/^{86}Sr$ of ~0.706 (Clemons and Long, 1971), close to the value measured for sample G1 of 0.70596 (Feigenson et al., 2004). On the other hand, a biotite whole-rock Rb/Sr isochron from a granitic sample produced an age of 95 ± 1 Ma (two sigma), whereas a K/Ar age of 83.9 ± 1.7 Ma was obtained on "the same material" (Clemons and Long, 1971). Assuming an initial $^{87}Sr/^{86}Sr$ of 0.706 and using the Rb and Sr concentrations measured by ICP-MS, which generate a very high $^{87}Rb/^{86}Sr$ ratio of 9.56, we obtained an age of 9.5 Ma for granitic sample G3. Assuming an age of 50 Ma, the initial $^{87}Sr/^{86}Sr$ of 0.70050 is clearly too low. Alternatively, assuming an initial $^{87}Sr/^{86}Sr$ identical to the BVF sample with the most radiogenic Sr (0.70415), sample G3K would have an age of 23 Ma. Therefore, either the G3 granite is relatively young (⩽23 Ma), or the sample has not served as a closed system for Rb and/or Sr (both highly mobile elements during weathering), since the formation of the granite. Although the Rb–Sr system is very sensitive to age corrections for sample G3K, corrections for radiogenic ingrowth for the other isotopic systems are relatively minor, even if an age of 50 Ma is assumed. The above discussion serves to illustrate that radiogenic ingrowth of $^{87}Sr$ has played an important role in the evolution of Chiquimula Pluton, and until we have reliable age data for each sample, we will not be able to determine the initial $^{87}Sr/^{86}Sr$ ratios. The measured $^{87}Sr/^{86}Sr$ ratios of the samples (0.70596–0.70729), however, represent maximum initial values and thus maximum source ratios. On the other hand, assuming that parent–daughter ratios for the Sm–Nd, Lu–Hf and (U–Th)/Pb systems were not substantially higher in the source of the Chiquimula Pluton, the Nd, Hf and Pb isotopic compositions could reflect the source composition.

As discussed above, the present subduction input can be ruled out as the source of the Quaternary northwestern Central American enriched endmember. As is illustrated by the Chiquimula plutonic rocks, an enriched component, with an isotopic composition appropriate for the enriched Guatemala endmember, is present within the overriding plate in NW Central America. These granitic crustal rocks, however, do not have the appropriate major and trace element compositions to serve as the enriched endmember. In order to reconcile this discrepancy, we propose that an appropriate enriched endmember for Guatemala magmas could be a present in the lithosphere, representing the mafic counterparts of the granites.

We propose that the parental magmas for the Chiquimula Pluton and other plutonic rocks in NW Central America froze and formed pyroxene-rich cumulates (Pearson et al., 1991) in the lithospheric mantle or possibly in the lower crust. Although the major oxide and compatible trace element contents have been affected by fractional crystallization, correlations of $Na_2O$ and CaO with both Nd and Pb isotope ratios in the most mafic (MgO > 5 wt.%) VF and BVF samples (Fig. 14) indicate that the variations in major oxides are at least partly related to differences in source composition. The generally lower CaO, FeO, Sc and V and the higher Na2O and possibly in part $SiO_2$ in the most mafic Guatemala samples with similar MgO (>5 wt.%) to the Nicaragua VF samples could reflect a greater proportion of pyroxenite contributing to these melts (e.g. Herzberg and Asimow, 2008; Fig. 3). A greater contribution from pyroxenite (or generally speaking from a pyroxene-rich mafic source) could also explain the correlations in radiogenic isotope ratios with Dy/Yb and Zr/Hf (Fig. 14) and the substantially higher Zr/Hf (up to 52) and mantle-normalized $(Sm/Yb)_n$ ratios (1.5–2.6) in the Guatemala endmember and BA samples compared to both the chondritic value Zr/Hf (~34) and relatively low $(Sm/Yb)_n$ (1.2–1.7) of the Nicaraguan lavas (Pertermann et al., 2004). Although high Zr/Hf and Sm/Yb ratios in Guatemala can be likely explained by low degree melting of garnet peridotite with high clinopyroxene/garnet ratio (e.g. Huang and Frey, 2005), we do not favor peridotite as the

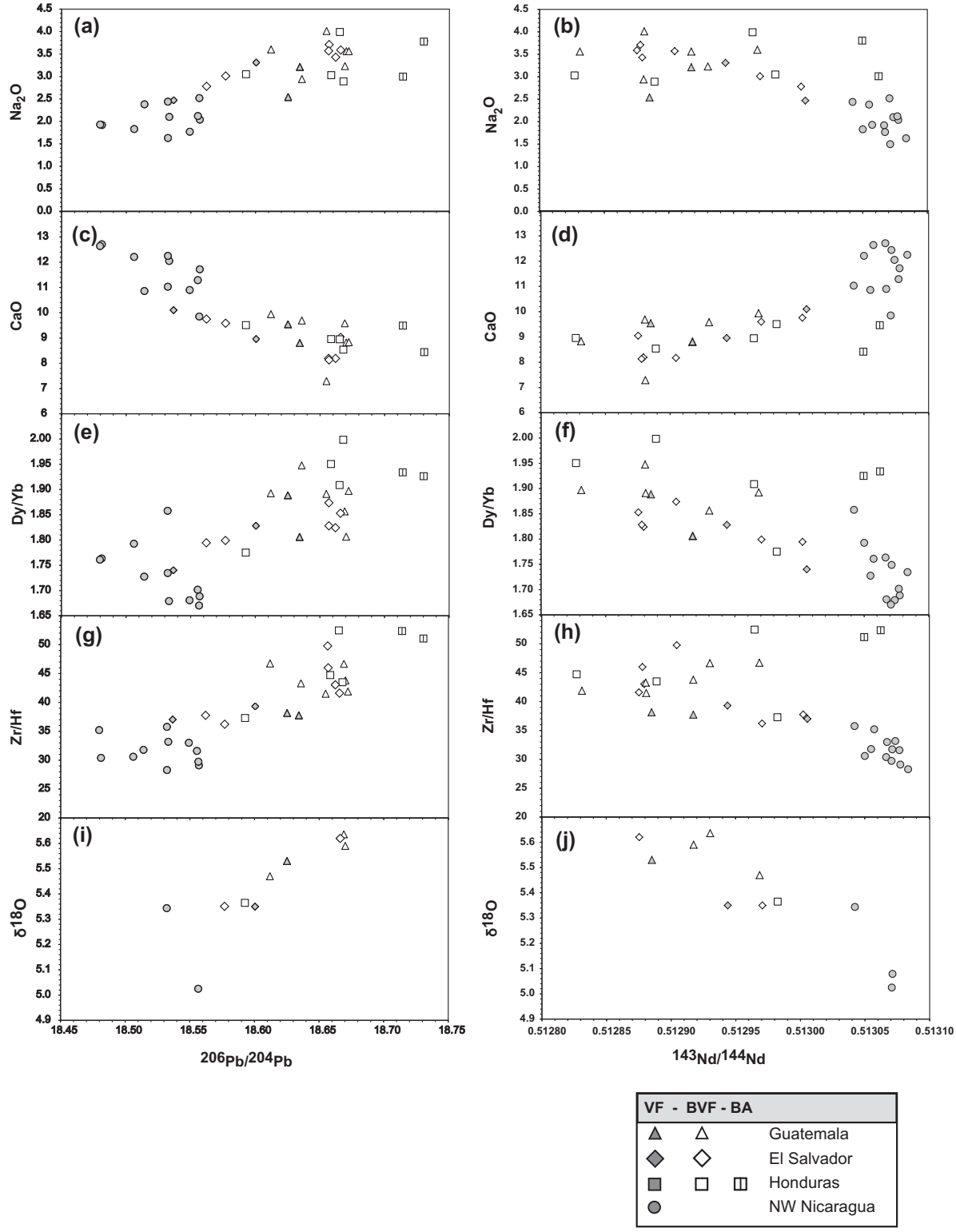


Fig. 14. Pb and Nd isotope ratios vs. $Na_2O$ (a, b), CaO (c, d), Dy/Yb (e, f), Zr/Hf (g, h) and $\delta^{18}O$ (i, j). The VF and BVF samples form a good positive correlation between Nd isotope ratio and CaO and good negative correlations with $N_2O$, Dy/Yb, Zr/Hf and $\delta^{18}O$. All the NW CAVA samples form a good negative correlation between Pb isotope ratios and $Na_2O$, Dy/Yb, Zr/Hf and $\delta^{18}O$ and a good negative correlation with CaO. These correlations are consistent with the enriched source being pyroxenitic/eclogitic and the depleted source being peridotitic.

source of the enriched Guatemala component. In order to preserve the isotopic signature for millions of years, the source needs to be in the lithosphere. If the melts were derived from a garnet peridotite, the lithosphere would have

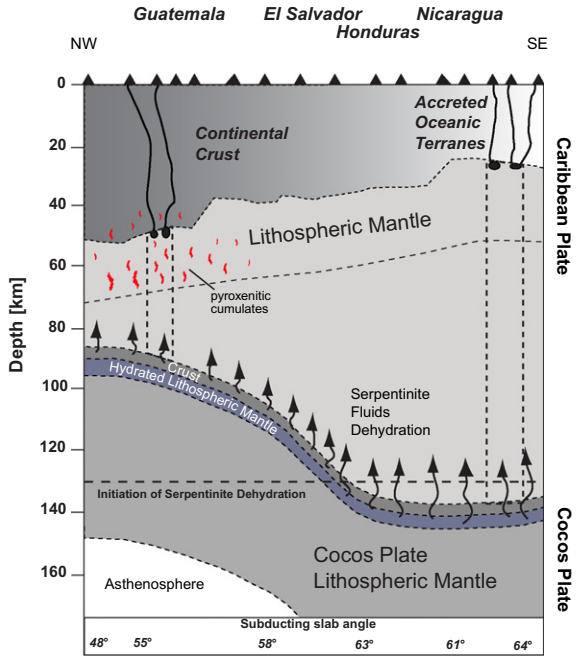


Fig. 15. Model showing the partial melting of pyroxenitic cumulates or reaction pyroxenites in the lithospheric mantle beneath Guatemala as a source for the arc volcanism in NW-CAVA. The schematic profile parallel to the volcanic front from Guatemala to NW Nicaragua as marked by red box in Fig. 1, illustrates the increasing crustal thickness and decreasing depth to the subducting slab surface going north from beneath Nicaragua to Guatemala. As a result, the thickness of the mantle wedge (and possible mantle melting columns) decreases to the NW. Data for crustal thickness after Carr (1984) and MacKenzie et al. (2008). Transition zone between continental and oceanic crust is still unspecified but presumably occurs between NW Nicaragua and Honduras/El Salvador based on the change in isotopic composition along the VF. Values for subducting slab angle and averaged depth to the top of the subducting plate are from Syracuse and Abers (2006). The dashed line at ~130 km represents the beginning of serpentinite mineral breakdown after Rüpke et al. (2004). The thickness of hydrated lithospheric mantle is from Grevemeyer et al. (2007) and Ivandic et al. (2008) and beneath Nicaragua from MacKenzie et al. (2008).

to extend to at least 70–80 km depth, where the transition from the spinel to the garnet stability field in peridotite occurs (Hirschmann and Stolper, 1996). If the lithosphere extends to 80 km depth, the thickness of the convecting mantle wedge below the Guatemala volcanic front would be reduced to less than 10 km. Garnet, however, is stable to shallower depths in pyroxenite than peridotite (e.g. Hirschmann and Stolper, 1996), making garnet pyroxenite a more likely source for the enriched endmember. Thus the Guatemalan VF and BVF lavas reflect a mixture of minor amounts of melts from hot garnet peridotite in the mantle wedge with melts from garnet pyroxenite in the lithosphere or lower crust, which can also explain the relatively heavy oxygen isotope composition of the Guatemala magmas (Figs. 11 and 12). The high oxygen isotope ratios do not generally occur in mantle peridotites, but are well within the range of reported compositions of pyroxenite veins ($\delta^{18}O = 5.3–6.1‰$ Pearson et al., 1991).

Although the thickness of the lithosphere beneath northwestern Central America is not well-constrained, thinner crust and much greater depth to the slab surface beneath Nicaragua strongly indicate that interaction of primary magmas with lithosphere will play a more important relative role beneath the northwesternmost part of the Central American arc (Guatemala) than beneath Nicaragua (Fig. 15).

In conclusion, we favor the partial melting of a mafic "counterpart" of the granite i.e. pyroxenite/eclogite veins/dikelets in the lithosphere to generate the necessary enriched isotopic compositions and major and trace element concentrations for the enriched Guatemala endmember basaltic rocks.

### 4.3. Honduras BA endmember

The BA samples from Utila Island and Yojoa in Honduras are alkalic (hawaiitic) in composition with similar major element compositions to alkalic ocean–island–basalt (OIB) type rocks with similar MgO contents. These samples have the highest $TiO_2$, $K_2O$, $P_2O_5$, lowest $SiO_2$ and similar $Al_2O_3$, $FeO_t$, MnO, CaO and $Na_2O$ contents when compared to the BVF rocks with a similar MgO content. The incompatible element characteristics of the BA volcanics are similar to those commonly observed in OIBs, with their multi-element patterns showing relative enrichment in Nb and Ta, relative depletion in Pb and no pronounced peaks at fluid–mobile incompatible elements, in contrast to the VF and most BVF samples. An OIB-type source is also consistent with the low Ba/La and U/Th and high La/Yb ratios.

In contrast to the enriched incompatible element abundances, the Sr–Nd–Hf isotopic compositions of the BA samples are depleted, falling at the enriched end of the Pacific MORB field. The Pb isotopic composition of the Utila and La Providencia, also in the Caribbean offshore of Nicaragua, samples, however, are anomalous and fall below the VF/BVF data array on Pb isotope and the Nd vs. Hf isotope diagrams. On the Pb isotope diagrams, these samples plot near the radiogenic end of the field for Cocos Plate Oceanic Crust, exhibiting relatively high $^{206}Pb/^{204}Pb$ but low $^{207}Pb/^{204}Pb$ and $^{208}Pb/^{204}Pb$. Interestingly, the samples with the highest $^{206}Pb/^{204}Pb$ but relatively low $^{207}Pb/^{204}Pb$ and $^{208}Pb/^{204}Pb$ from the Cocos Plate are the samples that appear to have gained uranium through seafloor alteration processes (e.g. Hart and Staudigel, 1982; Hauff et al., 2003). Although Pb is relatively immobile during low temperature seafloor alteration, the elevated $^{206}Pb$ results from radiogenic ingrowth of $^{206}Pb$ by relatively recent $^{238}U$ enrichment. $^{207}Pb$ is derived from $^{235}U$, which has largely been exhausted by radioactive decay since the formation of the Earth due to its relatively short half-life of 0.7 Ga compared to the age of the Earth. Due to the small amount of $^{235}U$ relative to $^{238}U$, the $^{207}Pb$ is not significantly affected by relatively recent U enrichment. Since $^{208}Pb$ is derived from $^{232}Th$ and Th is relatively immobile during seafloor alteration processes, the composition of $^{208}Pb$ will

also not be significantly affected by low temperature seafloor alteration. Therefore altered seafloor can evolve high $^{206}Pb$ within relatively short time scales of 10–100s of millions of years, while $^{207}Pb$ and $^{208}Pb$ show relatively little ingrowth over these time scales (e.g. Thirlwall, 1997). The high $Na_2O$, Dy/Yb and Zr/Hf and the low CaO in the most mafic (MgO > 5 wt.%) samples (Fig. 14), similar to those for the BVF samples, again points to a pyroxenitic/eclogitic source. In summary, we interpret the OIB-like major and trace element compositions of the Utila samples, combined with their depleted Sr, Nd and Hf and relatively depleted Pb isotopic compositions, to reflect derivation through decompression melting of back-arc mantle containing recycled oceanic crust in the form of eclogite/pyroxenite.

The BVF samples show less pronounced subduction-zone incompatible element signatures than the VF samples, displaying less pronounced Nb and Ta troughs and less pronounced peaks at fluid mobile elements (and lower fluid–mobile to less-fluid–mobile element ratios). In Honduras some of the multi-element patterns approach those of ocean–island–basalt (OIB) – type rocks, displaying neither relative Nb and Ta depletion (a trough at these elements in the incompatible element patterns) nor relative Pb enrichment (a peak in the patterns). Therefore the incompatible elements of the BVF rocks suggest that an OIB-like component, similar to that sampled at Utila and La Providencia, is in the mantle wedge located beneath the BVF localities also. This component however seems to be largely absent in the mantle beneath the VF or is sufficiently diluted at large degrees of melting, such that it is not readily recognized in the geochemistry of the volcanic front samples.

## 5. CONCLUSIONS

We used major and trace elements and Sr–Nd–Pb–Hf–O isotopic compositions from mafic volcanic front (VF), behind the volcanic front (BVF) and back-arc (BA) lava and tephra samples from NW Nicaragua, Honduras, El Salvador and Guatemala to further constrain the sources for NW Central American Arc volcanism. We distinguished three geochemically distinct endmember components for the prevalent volcanism in NW Central America:

(1) The NW Nicaragua VF endmember, characterized by high $FeO_t$ and low $SiO_2$, extremely high fluid–mobile-element contents (e.g. LILE) but low N-MORB-like fluid–immobile-element contents (e.g. REE and HFSE), low $\delta^{18}O$ and enriched (radiogenic) Sr isotope ratios, but depleted (unradiogenic) Pb and (radiogenic) Nd and Hf isotopic compositions. In order to explain these geochemical characteristics, we propose, as have other published studies (Rüpke et al., 2004; Syracuse et al., 2008), that a very steep slab dip results in serpentinite dehydration and a high flux of low-temperature (~700 °C) water-rich fluid and possibly small amounts of sediment melts (Gazel et al., 2009) into the asthenospheric wedge beneath Nicaragua. This primarily hydrous fluid has high contents of fluid–mobile elements such as Sr, Pb, K, U and Ba and high fluid–mobile to fluid-immobile element ratios, such as Ba/La, Pb/Nd and Pb/Ce ratios. Sediment melts could also contribute to high mobile to immobile element ratios, since such ratios are also high in sediments. The low (lower than commonly found in the upper mantle) $\delta^{18}O$ is derived from hydrothermally-altered parts of the oceanic crust and underlying (serpentinized) uppermost mantle. The high Sr concentrations and isotope ratios are ultimately derived from seawater-altered ocean crust and serpentinized upper mantle and from sediments of the incoming plate. The elevated Pb abundance (compared to MORB) in the Nicaraguan arc magmas is dominated by Pb leached from the subducting ocean crust by the serpentinite-derived fluids with minor amounts of Pb being contributed by subducting sediments and the overriding plate. The radiogenic Nd and Hf isotopic compositions of the Nicaraguan lavas are largely derived from the mantle wedge, with the addition of small amounts possibly from fluid from the subducting plate. In summary, the trace element and Sr–Nd–Pb–Hf isotope ratios of the Nicaraguan lavas appear to be dominated by a largely serpentinite-derived fluid flux from the subducting slab that has variably interacted with subducting AOC and sediments to a depleted N-MORB type of mantle wedge, resulting in large degrees of melting of primarily peridotitic material.

(2) The enriched Guatemala VF and BVF endmember, characterized by lower $FeO_t$, CaO, MnO, Sc and V and higher $SiO_2$ and $Na_2O$ at a given MgO composition than in Nicaraguan VF lavas, high Zr/Hf and more to less relatively immobile incompatible element ratios (e.g. La/Yb and La/Sm), elevated $\delta^{18}O$ and enriched Sr, Nd, Hf and Pb isotopic composition. A granitic sample from the Guatemala basement has an appropriate isotopic composition to serve as the enriched endmember. A very large ($\geqslant$40–50%) amount of assimilation of the granitic basement is however required to explain the most enriched compositions of the Guatemala VF and BVF lavas, which is not consistent with the mafic major element and trace element compositions of these lavas. In addition, assimilation of granitic crust by mantle wedge melts should form a convex (concave down) mixing array and not the observed linear array. Assimilation of granitic material with a composition similar to sample G3K can also not explain the higher $\delta^{18}O$ coupled with lower Sr isotopic composition of the Guatamalan VF and the BVF samples. On the other hand, the low CaO, FeO, Sc and V, the high $Na_2O$, Zr/Hf, Sm/Yb and elevated $\delta^{18}O$ are consistent with melting of mafic garnet-bearing pyroxene-rich material (perhaps pyroxenitic/eclogitic material) (e.g., Bindeman et al., 2005). We therefore propose that parental magmas for the granitic basement in NW Central America crystallized pyroxenitic cumulates in the lithospheric mantle (and possibly lower crust) that were subsequently melted during Quaternary subduction-related volcanism to generate

the enriched Guatemala endmember. The presence of the enriched Guatemala endmember correlates with the increased crustal thickness and most likely reflects more extensive interaction of magmas with enriched lithosphere formed through ancient arc volcanism.

(3) The Honduras and Caribbean BA endmember is characterized by alkalic lavas with OIB-type trace element compositions and relatively depleted (E)-MORB-type isotopic compositions. We propose that the BA lavas originate via low-degree decompression mantle melting in the back-arc and likely sample young recycled oceanic crust present in the form of ecologite/pyroxenite in the upwelling largely peridotitic mantle.

Mixing between these three distinct types of magmas can generate the observed along- and across-arc variations in incompatible trace element and Sr–Nd–Pb–Hf–O isotope ratios.

## ACKNOWLEDGEMENTS

We would like to thank Carlos Pullinger, Dolores Ferres, Walther Hernandez from SNET, Eddi Sanchez and Otoniel Mathias from INSIVUMEH and Amilcar S. Hernandez from UNAH for field assistance. We thank S. Hauff, J. Fietzke and D. Rau for analytical assistance. We are grateful to M. Carr and U. Martens for generously providing Guatemalan basement samples. We are grateful to M. Jackson, T. Rooney and an anonymous reviewer for their constructive comments that helped improve the manuscript. This publication is contribution no. 146 of the Sonderforschungsbereich 574 "Volatiles and Fluids in Subduction Zones" of Kiel University. INB thanks NSF Grant 0844772 for support.

## REFERENCES

Abers G., Plank T. and Hacker B. R. (2003) The wet Nicaraguan slab. *Geophys. Res. Lett.* **30**.

Abers G. A., Fischer K. M., Auger L., Syracuse E., Rychert K., Protti J. M., Gonzales V. and Strauch W. (2007) Imaging the arc source in Central America: The TUCAN broadband seismic experiment. *Geopys. Res. Abstr* **9**.

Arculus R. J. (1994) Aspects of magma genesis in arcs. *Lithos* **33**, 189–208.

Auboin J., Azéma J.-C., Carfantan A., Demant A., Ranging C., Tardy M. and Tournon J. (1982) The middle american trench in the geological framework of central america. *DSDP Initial Rep.* **67**, 747–755.

Auger L. S., Abers G., Fischer K., Protti M., Gonzalez V. and Strauch W. (2006) Crustal thickness variations beneath the central American arc. *Am Geophys Union, Fall Meeting 2006* (abstract).

Bindeman I. (2008) Oxygen isotopes in mantle and crustal magmas as revealed by single crystal analysis. *Rev. Mineral. Geochem.* **69**, 445–478.

Bindeman I. N., Eiler J. M., Yogodzinski G. M., Tatsumi Y., Stern C. R., Grove T. L., Portnyagin M., Hoernle K. and Danyushevsky L. V. (2005) Oxygen isotope evidence for slab melting in modern and ancient subduction zones. *Earth Planet. Sci. Lett.* **235**, 480–496.

Blichert-Toft J. and Albarède F. (1997) The Lu–Hf isotope geochemistry of chondrites and the evolution of the mantle–crust system. *Earth Planet. Sci. Lett.* **148**, 243–258.

Blichert-Toft J., Frey F. A. and Albarède F. (1999) Hf isotope evidence for pelagic sediments in the source of Hawaiian basalts. *Science* **285**, 879–882.

Blundy J. D., Robinson J. A. C. and Wood B. J. (1998) Heavy REE are compatible in clinopyroxene on the spinel lherzolite solidus. *Earth Planet. Sci. Lett.* **160**, 493–504.

Cameron B. I., Walker J. A., Carr M. J., Patino L. C., Matias O. and Feigenson M. D. (2002) Flux versus decompression melting at stratovolcanoes in southeastern Guatemala. *J. Volcanol. Geoth. Res.* **119**, 21–50.

Carr M. J. (1984) Symmetrical and segmented variation of physical and geochemical characteristics of the Central American volcanic front. *J. Volcanol. Geoth. Res.* **20**, 231–252.

Carr M. J. and Feigenson M. D. (2003) Volcanism and geochemistry in Central America: progress and problems. *Geophys. Monogr.* **138**, 153–174.

Carr M. J., Feigenson M. D. and Bennett E. A. (1990) Incompatible element and isotopic evidence for tectonic control of source mixing and melt extraction along the Central American arc. *Contrib. Mineral. Petrol.* **105**, 369–380.

Chan L.-H. and Kastner M. (2000) Lithium isotopic compositions of pore fluids and sediments in the Costa Rica subduction zone: implications for fluid processes and sediment contribution to the arc volcanoes. *Earth Planet Sci. Let.* **183**, 275–290.

Chan L. H., Leeman W. P. and You C.-F. (1999) Lithium isotopic composition of Central American Volcanic Arc lavas: implications for modification of subarc mantle by slab-derived fluids. *Chem. Geol.* **160**, 255–280.

Chan L.-H., Starinsky A. and Katz A. (2002) The behavior of lithium and its isotopes in oilfield brines: evidence from the Heletz-Kokhav field. *Israel. Geochim. Cosmochim. Acta* **66**, 615–623.

Chan L.-H., Leeman W. P. and Plank T. (2006) Correction to "lithium isotopic composition of marine sediments". *Geochem. Geophys. Geosyst.* **7**, Q08004. doi:10.1029/2006GC001380.

Clemons R. E. and Long L. E. (1971) Petrologic and Rb-Sr Isotopic Study of the Chiquimula Pluton, Southeastern Guatemala. *Geol. Soc. Am. Bull.* **82**, 2729–2740.

DeMets C. (2001) A new estimate for present-day Cocos-Caribbean plate motion: implications for slip along the Central American volcanic arc. *Geophys. Res. Lett.* **28**, 4043–4046.

DePaolo D. J. and Wasserburg G. J. (1976) Inferences about magma sources and mantle structure from variations of $^{143}Nd/^{144}Nd$. *Geophys. Res. Lett.* **3**(743), 249–252.

Donnelly T. W., Horne G. S., Finch R. C. and López-Ramos E. (1990) Northern Central America; The Maya and Chortis blocks. In *The Geology of North America; The Caribbean Region* (eds. J. E. Case and G. Dengo). The Geological Society of America, Boulder/Colorado, pp. 37–76.

Eiler J. M., Crawford A., Elliott T., Farley K. A., Valley J. W. and Stolper E. M. (2000) Oxygen isotope geochemistry of oceanic-arc lavas. *J. Petrol.* **41**, 229–256.

Eiler J. M., Carr M. J., Reagan M. and Stolper E. (2005) Oxygen isotope constraints on the sources of Central American arc lavas. *Geochem. Geophys. Geosyst.* **6**, Q07007. doi:10.1029/2004GC000804.

Feigenson M. and Carr M. J. (1993) The source of Central American lavas: inferences from geochemical inverse modeling. *Contrib. Mineral. Petrol.* **113**, 226–235.

Feigenson M. D., Carr M. J., Maharaj S. V., Juliano S. and Bolge L. L. (2004) Lead isotope composition of Central American volcanoes: influence of the Galapagos plume. *Geochem. Geophys. Geosyst.* **5**, Q06001. doi:10.1029/2003GC000621.

Foley S. F., Barth M. G. and Jenner G. A. (2000) Rutile/melt partition coefficients for trace elements and an assessment of the influence of rutile on the trace element characteristics of

subduction zone magmas. *Geochim. Cosmochim. Acta* **64**, 933–938.

Garbe-Schönberg C.-D. (1993) Simultaneous determination of thirty-seven trace elements in twenty-eight international rock standards by ICP-MS. *Geostand. Newsl.* **17**, 81–97.

Gazel E., Carr M. J., Hoernle K., Feigenson M. D., Szymanski D., Hauff F. and Bogaard P. v. d. (2009) Galapagos-OIB signature in southern Central America: mantle refertilization by arc-hot spot interaction. *Geochem. Geophys. Geosyst.* **10**, Q02S11, doi:10.1029/2008GC002246.

Geldmacher J., Hoernle K., Klügel A., Bogaard P. v. d., Wombacher F. and Berning. B. (2006) Origin and geochemical evolution of the Madeira-Tore Rise (eastern North Atlantic). *J Geophys Res* **111**, B09206.

Geldmacher J., Hoernle K., Klugel A., van den Bogaard P. and Bindeman I. (2008) Geochemistry of a new enriched mantle type locality in the northern hemisphere: implications for the origin of the EM-I source. *Earth Planet. Sci. Lett.* **265**, 167–182.

Govindaraju K. (1994) Compilation of working values and sample descriptions for 383 geostandards. *Geostand. Newsl.* **18**, 158 pp.

Green T. H. and Pearson N. J. (1986) Ti-rich accessory phase saturation in hydrous mafic-felsic compositions at high P, T. *Chem. Geol.* **54**, 185–201.

Grevemeyer I., Ranero C. R., Flueh E. R., Kläschen D. and Bialas J. (2007) Passive and active seismological study of bending-related faulting and mantle serpentinization at the Middle America trench. *Earth Planet. Sci. Lett.* **258**, 528–542.

Hart S. R. and Staudigel H. (1982) The control of alkalies and uranium in seawater by ocean crust alteration. *Earth Planet. Sci. Lett.* **58**, 202–212.

Hauff F., Hoernle K., Boogard P. v. d., Alvarado G. E. and Garbe-Schönberg D. (2000) Age and geochemistry of basaltic complexes in Western Costa Rica: contributions to the geotectonic evolution of Central America. *Geochem. Geophys. Geosyst.* **1**. doi:10.1029/1999GC000020.

Hauff F., Hoernle K. and Schmidt A. (2003) Sr–Nd–Pb composition of Mesozoic Pacific oceanic crust (Site 1149 and 801, ODP Leg 185): implications for alteration of ocean crust and the input into the Izu–Bonin–Mariana subduction system. *Geochem. Geophys. Geosyst.* **4**. doi:10.1029/2002GC000421.

Herzberg C. and Asimow P. D. (2008) Petrology of some oceanic island basalts: PRIMELT2.XLS software for primary magma calculation. *Geochem. Geophys. Geosyst.* **9**, Q09001. doi:10.1029/2008GC002057.

Hermann J., Spandler C., Hack A. and Korsakov A. V. (2006) Aqueous fluids and hydrous melts in high-pressure and ultra-high pressure rocks: implications for element transfer in subduction zones. *Lithos* **92**, 399–417.

Hirschmann M. M. and Stolper E. M. (1996) A possible role for garnet pyroxenite in the origin of the "garnet signature" in MORB. *Contrib. Mineral. Petrol.* **124**, 185–208.

Hoernle K. and Tilton G. (1991) Sr–Nd–Pb isotope data for Fuerteventura (Canary Islands) basal complex and subaerial volcanics: applications to magma genesis and evolution. *Schweiz. Mineral. Petrogr. Mitt.* **71**, 3–18.

Hoernle K. and Hauff F. (2007) Oceanic igneous complexes. In *Central America: Geology, Resources and Hazards* (eds. J. Bundschuh and G. E. Alvarado). Taylor & Francis/Balkema, London, pp. 523–547.

Hoernle K., Hauff F. and Bogaard P. v. d. (2004) 70 m.y. history (139–69 Ma) for the Caribbean large igneous province. *Geology* **32**, 697–700.

Hoernle K., Abt D. L., Fischer K. M., Nichols H., Hauff F., Abers G. A., van den Bogaard P., Heydolph K., Alvarado G., Protti M. and Strauch W. (2008) Arc-parallel flow in the mantle wedge beneath Costa Rica and Nicaragua. *Nature* **451**, 1094–1097.

Huang S. and Frey F. A. (2005) Recycled oceanic crust in the Hawaiian Plume: evidence from the temporal geochemical variations within the Koolau Shield. *Contrib. Mineral. Petrol.* **149**, 556–575.

Ivandic M., Grevemeyer I., Berhorst A., Flueh E. R. and McIntosh K. (2008) Impact of bending related faulting on the seismic properties of the incoming oceanic plate offshore of Nicaragua. *J. Geophys. Res.* **113**.

Jicha B. R., Smith K. E., Singer B. S., Beard B. L., Johnson C. M. and Rogers N. W. (2010) Crustal assimilation no match for slab fluids beneath Volcan de Santa Maria, Guatemala. *Geology* **38**, 859–862.

Jochum K. P. and Jenner G. (1994) Trace element analysis of Geological Survey of Japan silicate reference materials: comparison of SSMS with ICP-MS data and a critical discussion of compiled values. *Fresenius J. Anal. Chem.* **350**, 310–318.

Kessel R., Schmidt M. W., Ulmer P. and Pettke T. (2005) Trace element signature of subduction-zone fluids, melts and supercritical liquids at 120–180 km depth. *Nature* **437**, 724–727.

Leeman W. P. (1996) Boron and other fluid–mobile elements in volcanic arc lavas: implications for subduction processes. *Geophys. Monogr.* **96**, 269–276.

Leeman W. P., Carr M. J. and Morris J. D. (1994) Boron geochemistry of the Central American Volcanic Arc: constraints on the genesis of subduction-related magmas. *Geochim. Cosmochim. Acta* **58**, 149–168.

Ligorria J. P. and Molina E. (1997) Crustal velocity structure of southern Guatemala using refracted and Sp converted waves. *Geofísica Int*.

MacKenzie L., Abers G. A., Fischer K. M., Syracuse E. M., Protti J. M., Gonzalez V. and Strauch W. (2008) Crustal structure along the southern Central American volcanic front. *Geochem. Geophys. Geosyst.* **9**, 1–19.

Mattey D., Lowry D. and MacPherson C. (1994) Oxygen isotope composition of mantle peridotite. *Earth Planet. Sci. Lett.* **128**, 231–241.

Meschede M. (1998) The impossible Galápagos connection: geometric constraints for a near-American origin of the Caribbean plate. *Geol. Rundsch.* **87**, 200–205.

Morris J. D., Leeman W. P. and Tera F. (1990) The subducted components in island arc lavas: constraints from Be isotopes and B-be systematics. *Nature* **344**, 31–36.

Münker C., Pfander J. A., Weyer S., Buchl A., Kleine T. and Mezger K. (2003) Evolution of planetary cores and the earth–moon system from Nb/Ta systematics. *Science* **301**, 84–87.

Narcía-Lopez R., Castro R. and Rebollar C. J. (2004) Determination of crustal thickness beneath Chiapas, Mexico using S and Sp waves. *Geophys. J. Int.* **157**, 215–228.

Patino L. C., Carr M. J. and Feigenson M. D. (2000) Local and regional variations in Central American arc lavas controlled by variations in subducted sediment input. *Contrib. Mineral. Petrol.* **138**, 265–283.

Pearce J. A. and Peate D. W. (1995) Tectonic implications of the composition of volcanic arc magmas. *Annu. Rev. Earth Planet. Sci.* **23**, 251–285.

Pearce J. A., Kempton P. D. and Gill J. B. (2007) Hf–Nd evidence for the origin and distribution of mantle domains in the SW Pacific. *Earth Planet. Sci. Lett.* **260**, 98–114.

Pearson D. G., Davies G. R., Nixon P. H., Greenwood P. B. and Mattey D. P. (1991) Oxygen isotope evidence for the origin of pyroxenites in the Beni Bousera peridotite massif, North Morocco: derivation from subducted oceanic lithosphere. *Earth Planet. Sci. Lett.* **102**, 289–301.

Pertermann M., Hirschmann M., Hametner K., Günther D. and Schmidt M. W. (2004) Experimental determination of trace element partitioning between garnet and silica-rich liquid during anhydrous partial melting of MORB-like eclogite. *Geochem. Geophys. Geosyst.* **5**. doi:10.1029/2003GC000638.

Plank T. and Langmuir C. H. (1988) An evaluation of the global variations in the major element chemistry of arc basalts. *Earth Planet. Sci. Lett.* **90**, 349–370.

Plank T. and Langmuir C. H. (1998) The chemical composition of subducting sediment and its consequences for the crust and mantle. *Chem. Geol.* **145**, 325–394.

Protti M., Güendel F. and McNally K. (1995) Correlation between the age of the subducting Cocos plate and the geometry of the Wadati-Benioff zone under Nicaragua and Costa Rica. In *Geologic and Tectonic Development of the Caribbean Plate Boundary in Southern Central America* (ed. P. Mann). Gelogical Society of America, Boulder, Colorado, pp. 309–326.

Ranero C. R. and Huene von R. (2000) Subduction erosion along the middle America convergent margin. *Nature* **404**, 748–752.

Ranero C. R., Morgan J. P., McIntosh K. and Reichert C. (2003) Bending-related faulting and mantle serpentinization at the Middle America trench. *Nature* **425**, 367–373.

Rüpke L. H., Morgan J. P., Hort M. and Connolly J. A. D. (2004) Serpentine and the subduction zone water cycle. *Earth Planet. Sci. Lett.* **223**, 17–34.

Sadofsky S., Portnyagin M., Hoernle K. and van den Bogaard P. (2008) Subduction cycling of volatiles and trace elements through the Central American volcanic arc: evidence from melt inclusions. *Contrib. Mineral. Petrol.* **155**, 433–456.

Sadofsky, S., Hoernle, K., Duggen, S., Hauff, F., Werner, R., and Garbe-Schönberg, D. (2009) Geochemical variations in the Cocos Plate subducting beneath Central America: implications for the composition of arc volcanism and the extent of the Galápagos Hotspot influence on the Cocos oceanic crust. doi:10.1007/s00531-007-0289-5.

Sun S.-S. and McDonough W. F. (1989) Chemical and isotopic systematics of oceanic basalts: implications for mantle composition and processes. In *Magmatism in the Ocean Basins* (eds. A. D. Saunders and M. J. Norry). Blackwell, London, pp. 313–345.

Syracuse E. M. and Abers G. A. (2006) Global compilation of variations in slab depth beneath arc volcanoes and implications. *Geochem. Geophys. Geosyst.* **7**, Q05017. doi:10.1029/2005GC001045.

Syracuse E. M., Abers G. A., Fischer K., MacKenzie L., Rychert C., Protti M., Gonzalez V. and Strauch W. (2008) Seismic tomography and earthquake locations in the Nicaraguan and Costa Rican upper mantle. *Geochem. Geophys. Geosyst.* **9**, 1–22.

Thirlwall M. F. (1997) Pb isotopic and elemental evidence for OIB derivation from young HIMU mantle. *Chem. Geol.* **139**, 51–74.

Todt W., Cliff R. A., Hanser A. and Hofmann A. W. (1996) Evaluation of a 202Pb–205Pb double spike for high-precision lead isotope analysis. In *Earth Processes: Reading the Isotopic Code* (eds. A. Basu and S. Hart). AGU Geophysical Monograph, Washington, DC, pp. 429–437.

Valley J. W., Kitchen N., Kohn M. J., Niendorf C. R. and Spicuzza M. J. (1995) UWG-2, a garnet standard for oxygen isotope ratios: strategies for high precision and accuracy with laser heating. *Geochim. Cosmochim. Acta* **59**, 5223–5231.

Vannucchi P., Galeotti S., Clift P. D., Ranero C. R. and Von Huene R. (2004) Long-term subduction–erosion along the Guatemalan margin of the Middle America Trench. *Geology* **32**, 617–620.

Vanucchi P., Scholl D. W., Meschede M. and McDougall-Reid K. (2001) Tectonic erosion and consequent collapse of the Pacific margin of Costa Rica: combined implications from ODP Leg 170, seismic offshore data and regional geology of the Nicoya Peninsula. *Tectonics* **20**, 649–668.

Wade J. A., Plank T., Melson W. G., Soto G. J. and Hauri E. H. (2006) The volatile content of magmas from Arenal volcano, Costa Rica. *J. Volcanol. Geoth. Res.* **157**, 94–120.

Walker J. A., Carr M. J., Patino L. C., Johnson C. M., Feigenson M. D. and Ward R. L. (1995) Abrupt change in magma generation processes across the Central American arc in southeastern Guatemala: flux-dominated melting near the base of the wedge to decompression melting near the top of the wedge. *Contrib. Mineral. Petrol.* **120**, 378–390.

Walker J. A., Mickelson J. E., Thomas R. B., Patino L. C., Cameron B., Carr M. J., Feigenson M. D. and Edwards R. L. (2007) U-series disequilibria in Guatemalan lavas, crustal contamination and implications for magma genesis along the Central American subduction zone. *J. Geophys. Res.* **112**.

Werner R., Hoernle K., Barckhausen U. and Hauff F. (2003) Geodynamic evolution of the Galapagos hot spot system (Central East Pacific) over the past 20 m.y.: Constraints from morphology, geochemistry, and magnetic anomalies. *Geochem. Geophys. Geosyst.* **4**, 1108. doi:10.1029/2003GC000576.

*Associate editor:* Shichun Huang